AQUIFER GEOMETRY AND STRUCTURAL CONTROLS ON GROUNDWATER POTENTIAL IN MOUNT ELGON AQUIFER, TRANS-NZOIA COUNTY, KENYA.

OGUT JULIUS ODIDA

I56/79737/2012

A dissertation submitted to the Department of Geology in partial fulfillment of the requirements for the Degree of Master of Science in Geology (Applied Geophysics) of the University of Nairobi.

Department of Geology

School of Physical Sciences

College of Biological and Physical Sciences

University of Nairobi

OCTOBER 2015

Declaration

I hereby declare that this is my original work and has not been submitted by any other person, form or institution for award.

SIGNATURE: …….. Date…….

Mr. Ogut Julius Odida,
M.Sc. Student in Applied Geophysics,
Department of Geology, School of Physical Sciences, CBPS,
University of Nairobi.

This dissertation has been submitted for examination with our knowledge as university supervisors

Signature…… Date…….

Prof. Daniel O. Olago,
Associate Professor,
Department of Geology, School of Physical Sciences, CBPS,
University of Nairobi.

Signature…… Date……

Dr. Edwin W. Dindi,
Senior Lecturer,
Department of Geology, School of Physical Sciences, CBPS,
University of Nairobi.

Signature…… Date…….

Dr. Zachariah N. Kuria,
Senior Lecturer,
Department of Geology, School of Physical Sciences, CBPS,
University of Nairobi.

Declaration of Originality Form

UNIVERSITY OF NAIROBI

This form must be completed and signed for all works submitted to the University for Examination.

Name of Student: Julius Odida Ogut

Registration Number: I56/79737/2012

College: Biological and Physical Sciences

Faculty/School/Institute: School of Physical Sciences

Department: Geology

Course Name: M.Sc. in Geology (Applied Geophysics)

Title of the work: Aquifer Geometry and Structural Controls on Groundwater Flow, Trans-Nzoia County, Kenya.

DECLARATION

1. I understand what Plagiarism is and I am aware of the University's policy in this regard.

2. I declare that this project (Thesis, project, essay, assignment, paper, report, etc) is my original work and has not been submitted elsewhere for examination, award of a Degree or publication. Where other people's work or my own work has been used, this has properly been acknowledged and referenced in accordance with the University of Nairobi's requirements.

3. I have not sought or used the services of any professional agencies to produce this work.

4. I have not allowed, and shall not allow anyone to copy my work with the intention of passing it off as his/her own work.

5. I understand that any false claim in respect of this work shall result in disciplinary action, in Accordance with University Plagiarism Policy.

Signature:

Date: 5th September, 2015

Dedication

This work is dedicated to my mother, Nora from whom I derive my motivation every day.

Acknowledgements

Completion of this work is attributable to assistance and support received from various sources. Special thanks to Almighty God for protection; guidance and grace that enabled me cope up with academic life challenges. Sincere gratitude is to the University of Nairobi, Geology Department. More so, I express my deepest appreciation to DSGRE and IGAD-INWRMP, through Prof. Daniel O. Olago who sponsored my research project. Special thanks to my supervisors: Prof. Daniel O. Olago, Dr. E. Dindi, and Dr. Z.N. Kuria for the support and continued guidance they offered me from the onset of the research to the final completion of this dissertation. I extend my humble appreciation to Mr. Michael Mwania from Ken-Gen and Miss. Susan Kiemi for their technical assistance in numerical modeling of the electrical resistivity data. Lastly, I appreciate my family for their support and parental guidance. Every time I spent with them motivated me and gave me a reason to look forward. This list is not exhaustive and anyone who contributed to my work is highly appreciated.

Abstract

Mount Elgon Aquifer is a trans-boundary aquifer shared between Kenya and Uganda. The aquifer originates from Mt. Elgon which is a solitary extinct volcano that straddles the Kenya-Uganda border. The geological formations in the area are Mozambique Mobile Belt overlain by Neogene volcanics and recent Soils. The enclosing coordinates of the study area are 34°40'E to 35° 05'E to the east and 0° 05'N to 1° 1.5'N to the north. There have been pronounced boreholes failures in the Mt. Elgon aquifer on the Kenyan side. This research tries to resolve the aquifer geometry of Mt. Elgon Aquifer, structural influence of groundwater flow and effects of geological formations on borehole potentials. Hydrogeological surveys were done from the slopes of Mt. Elgon to the Lowlands of Kitale. It involved sending a direct current into the ground to deduce vertical and lateral changes in lithology and refining the resulting field data to deduce aquifer geometry and structural influences of groundwater flow. Existing borehole data were used to calculate the aquifer transmissivity and potential yields. A total of thirty three (33) Vertical electrical soundings were done parallel to geological strikes while three horizontal electrical profiling were done transverse to geological strike. Existing borehole data were further analyzed using surfer and Arc-GIS to deduce influence of major geological formations to borehole potential yields. The Aquifer geometry varies consistently from Mt. Elgon slopes toward the lowlands and the plains. The probed depth at the mountain slopes showed no metamorphic characteristics. The metamorphic become shallower as the volcanic thins down slope and towards the plains. A volcanic window and metamorphic ridge are observed northwards of the study area. From the potentiometric surface map, north-south trending fractures and fissures influence groundwater flow within the Mozambique Mobile Belt rocks. Aquifer Transmissivity map shows a water divide that separates the Nyanza and Turkana drainage basins. Koibotoss, Koykoy and Endebess bluffs are related to higher aquifer transmissive zones. The research shows that Mt. Elgon Aquifer is a potential groundwater zones but good understanding of geology and structural patterns is inevitable for successful borehole siting in the area.

Contents

LIST OF FIGURES

LIST OF PLATES

LIST OF TABLES

Abbreviations and acronyms

ADC	Agricultural Development Corporation
DC	Direct Current
DSGRE	Development of Shared Groundwater Resources
ERT	Electrical Resistivity Tomography
HEP	Horizontal Electrical Profiling
M^3/h	cubic meters per hour
MMB	Mobile Mozambique Belt
NEMA	National Environmental and Management Authority
NGO	Non Governmental Organization
NRBMI	Nzoia River Basin Management Initiative
INWRMP	International Water Resources Mapping Programme
ITCZ	Inter Tropical Convergence Zone
IGAD	Inter Governmental Authority on Development
IUCN	International Union for Conservation of Nature
KNBS	Kenya National Bureau of Standards
KSC	Kenya Seed Company
KWS	Kenya Wildlife Service
Q	Yield of an aquifer
S	Storativity
T	Transmissivity
VES	Vertical Electrical Sounding
WRMA	Water Resources Management Authority
WRL	Water Rest Level also referred to as static water level
WSL	Water Strike Level
Yr^{-1}	Per year

1 CHAPTER ONE: INTRODUCTION

1.1 Introduction

Mt. Elgon aquifer is a trans-boundary aquifer that is shared between Kenya and Uganda. Mount Elgon is a solitary extinct Pliocene shield volcano with one of the largest craters in the world, about 8 km in width, located in the western part of Kenya and bisected by the Kenya Uganda border (Mugagga and Bunyinza, 2013; Rannveig and Bernardas, 2012; GOK, 2012; Knapen *et. al.*, 2005: Petursson *et al*., 2006). Mt. Elgon rises to a height of 4320m and forms part of the East African volcanic rings associated with the Great Rift Valley System (Mugagga and Bunyinza, 2013; Knapen *et al.*, 2005; Hetzel and Strecker, 1993). The research area lies in Trans Nzoia County within the Mount Elgon Aquifer region (Figure 1.1), and it is situated in the western part of Kenya. The Trans-Nzoia County headquarters (Kitale) is approximately 380km from Nairobi.

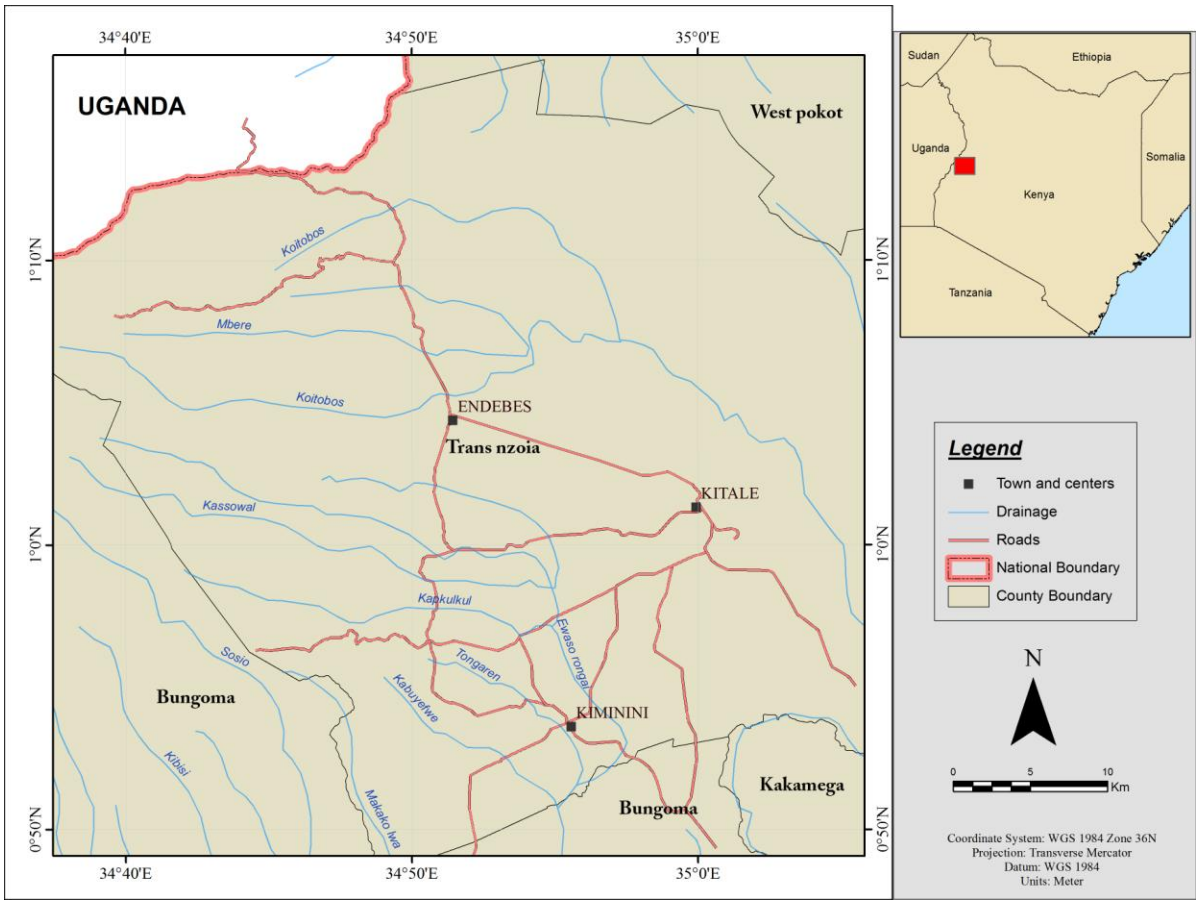

Figure 1.1: General location of the study area

1.2 Scope of the Project

This dissertation is a study of the aquifer geometry, structural influence of groundwater flow, and geological formations and how they influence on borehole potential yields in Trans Nzoia County of Mount Elgon Aquifer. The study area consists of Achaean as the oldest rocks, followed by Mobile Mozambique Belt (MMB), Neogene volcanic and the youngest are Pleistocene to Recent soils. Geophysical study, Vertical Electrical Sounding (VES) and Horizontal Electrical Profiling (HEP) was undertaken, data analyzed by IPI2Win and Surfer 9 to deduce aquifer geometry and vertical structures. The piezometric surfaces were computed using the existing borehole data and a potentiometric map drawn to show groundwater flow directions. The map was then overlain on the structural map to visualize the structural controls of groundwater flow. Finally, aquifer transmissivity was calculated and a transmissivity map constructed that was overlain on the geological map to visualize how the geological units affect borehole potential yields and subsequent borehole failure in Trans Nzoia area of Mt. Elgon Aquifer.

1.3 Overview of Methodological Approach

The first phase of geophysical research work was done in October-November 2014during the short rain season and the second phase was done in March 2015 during a dry period just before the onset of the long rain seasons. Direct Current (DC) electrical resistivity was undertaken with electrode spacing of 500m from the array centre for VES. The geophysical parameters measured were aquifer thickness and geo-electric layer resistivity. HEP was undertaken with a potential electrode spacing of 33.3m and current electrode spacing 100m. The current penetration depth was 100m below ground level (bgl).

Existing borehole data were collected from Water Resources Management Authority (WRMA): Kapenguria and Kitale offices. The borehole data were used to calculate the aquifer transmissivity (T) and derive the piezometric surface. Borehole total depth and water rest levels were verified using a water dipper. An aquifer transmissivity map was then drawn and contoured using Surfer 9 and Arc-GIS software. The resulting map was overlain on the geological map to establish aquifer potential yield on different geological units. The piezometric map was also constructed and then overlain on the structural map to visualize the relation of borehole potential yields and the subsurface structures.

1.4 Literature Review

The Mt. Elgon Aquifer and its environs have not been much studied since the area is well endowed with sufficient surface water resources (Kipkorir and Towett, 2013). Groundwater occurs at the contact between the Mobile Mozambique Belt (MMB) rocks and the volcanics (Murray-Hughes, 1933). Searle (1952) noted that other water bearing zones are the weathered crystalline MMB rocks, individual volcanic layers, and fissures within the MMB. This was further supported by Batte *et al.* (2008) who used VES as an exploration technique to site borehole points in the fractured crystalline MMB aquifers of eastern Uganda. They realized that the occurrence of groundwater was highly localized in MMB terrains. They also determined that some aquifer zones occurred in narrow buried valleys of coarse sand and gravel in some areas of the metamorphic rocks. Kuria (2013) identifies Mt. Elgon Aquifer as extending from the mountain to the Kitale plains and Suk Lowlands on the Kenyan side. The aquifer has very high groundwater potential zones in volcanic areas with transmissivity values ranging from100 m^2/day to 1600 m^2/day. The highest potential zones were in the north (including the area of study) than in the south. Kuria (2013) further deduced that the piezometric surface of the area ranged from 1196.8m-2048.9m above mean sea level (Figure 2.5, page 22).

Nzoia escarpment was considered as a fault feature, but had no evidence of faulting apart from the long straight feature that was previously published by Glenday and Parkinson (1926) and Murray-Hughes (1933). Miller (1956) later observed series of quartzite and semi-pelitic gneisses that dipped at 005° in the upper part of Kapolet Valley. This probably is the true dip of gneisses forming the escarpment which increases to about 040° downwards west of Kaibotoss (Miller, 1956). Dixey (1948) noted that Nzoia Escarpment forms part of the pre-Miocene peneplain of the Trans-Nzoia County and has a slight southerly tilt, with the principal drainage system of River Nzoia flowing southwards to Lake Victoria. The maximum elevation appears to lie along an east-west line, which forms a watershed between the Nyanza drainage area and that of the Lake Turkana area. North of this line, the Kitale plain dips gently northwards to the Trans-Nzoia escarpment. In the northern part of the Plain the north-flowing streams have incised the MMB rocks to a considerable depth, giving rise to steep-sided V-shaped valleys with many prominent interlocking spurs (Dixey, 1948). Searle (1952) observed shallow anticlinal and synclinal folds pitching southerly at the foot of Trans-Nzoia escarpment which agreed with previous works of

Dixey (1948) and Glenday and Parkinson (1926).

Glenday and Parkinson (1926) observed that quartz schist was the main rock outcropping on the Trans-Nzoia escarpment with presence of rare and small flakes of white mica and pale green kyanite as inclusions. The inclusions in quartz are arranged in parallel rows and dipped 0° and 020° at Kadongele. The trend of this MMB rocks run almost parallel to those observed by Miller (1956). Nephelinites and augites seemed to be characteristic of more recent extrusions of Mount Elgon. Searle (1952) in his geological mapping of the area north west of Kitale Township noted that volcanic rocks dominated the mountain area while the basement were observed away from the mountain towards the Kitale Plains.

Kitutu *et al.* (2009) noted influence of soil properties on landslide occurrences in Bududa district: Eastern Uganda realized that soil texture had significance influence on landslides. The landslides in the eastern zone of Mt. Elgon were dependent on soil texture, depth to the bedrock, land use and slope shape. The buried soil profiles in the western side were due to different landslide events. They concluded that landslides in western zone were due to soil horizon stratification that favored water stagnation in the lower horizons.

1.5 Problem Statement

Due to increasing population in Trans Nzoia County, the available surface water sources are over strained hence not enough to meet the demand of both domestic, industrial and livestock consumption. This has led the inhabitants to seek alternatives since rainfall, though regular, cannot sustain industrial purposes in the study area (Kipkorir and Towett, 2013). This therefore leads to exploitation of groundwater reserves which are not easily affected by pollution and respond slowly to climate changes as opposed to surface water (Kipkorir and Towett, 2013). Boreholes that have been sunk on the Kenyan side within the volcanic rocks yield between $5m^3$/hr and $25m^3$/hr., while areas within the Precambrian metamorphic and igneous rocks yield very little groundwater, between $1.5m^3$/hr to $6.0m^3$/hr. (National Water Master Plan, 1992). The study therefore attempts to provide an evidence-based context within which sustainable development of groundwater resources can be undertaken.

1.6 Aim and Objectives

The aim of the research is to focus and determine the reasons for the pronounced borehole failure in the Mt. Elgon Aquifer in the Kenyan side.

The objectives of this research are to:

1) Determine the aquifer geometry of Mt. Elgon Aquifer in the specified study area.

2) Establish the structural influence on groundwater flow and aquifer potential yields in the study area.

3) Evaluate the influence of different geological formations to groundwater potential in the study area.

1.7 Justification and Significance of the Research

There have been pronounced boreholes failures in Trans-Nzoia County especially within the MMB rocks on the Kenyan side (National Water Master Plan, 1992). Understanding and predicting subsurface flow and transport is important for better management of groundwater (Overmeeren, 1981). The aquifer geometry, structural geological influences of groundwater flow patterns are important in borehole siting to minimize losses incurred in borehole drilling and development.

1.8 Output

The expected outputs were:

Hydrogeological profiles showing aquifer geometry and characteristics in the specified study area.

Groundwater flow maps showing alignment, concentration of flow paths and structural influence on the flow patterns.

Groundwater distribution, geo-electrical models and potential maps in the area.

2 CHAPTER TWO: STUDY AREA

2.1 Location and Description

Trans-Nzoia is located approximately 380km northwestern part of Kenya from Nairobi between River Nzoia and Mt. Elgon. Trans-Nzoia County is about 2500km^2 while the project area is about 2000km^2. The study area within Trans Nzoia County stretches from 34°40'E to 35° 05'E to the east and 0° 05'N to 1° 1.5'N to the north. (Figure 2.1). Trans-Nzoia County is situated between River Nzoia and Mt. Elgon and borders the Republic of Uganda to the North West.

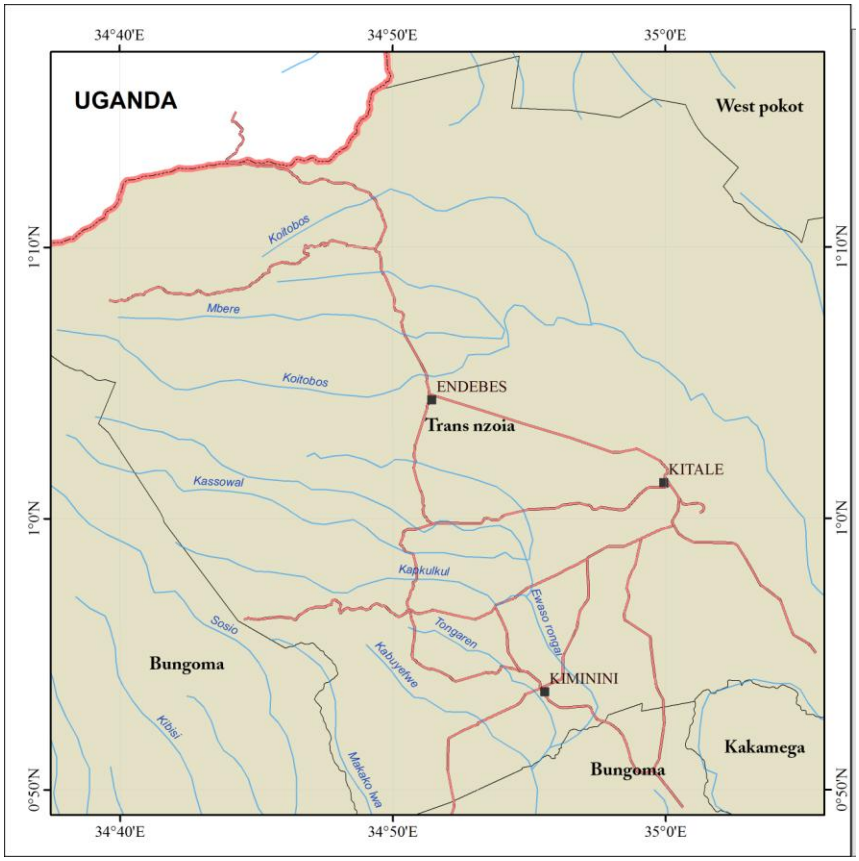

Figure 2.1: Location and extent of the Study area

2.2 Climate

The climate in Trans-Nzoia County is highland equatorial with an annual rainfall of 700 to 2100 mm and a mean daily temperature that can vary between 10°C to 37°C (Kagai, 2011; NEMA 2009). The mean annual temperature in the County is 18.6°C and the mean annual rainfall is 1296 mm yr^{-1} (NEMA, 2009). The area being within the Inter Tropical Climatic Zone (ITCZ) experiences four seasons annually. The long rain seasons normally stretch from March to May

and the short rains from October to November (Kipkorir *et al.,* 2007). Dry seasons occur in the months of January to February and June to September (NRBMI, 2011). The highest precipitation rates are received on the western slopes of the Cherengany Hills and Mt. Elgon (NEMA, 2009). Many of such showers originate over the forest below Kaibuch and proceed in a south-westerly direction to Kitale, which account for higher rainfall in Kitale areas (Kipkorir *et al.,* 2007). The principal climatic difference between the Kitale plains and the West Suk Lowlands lies in the relative humidity which is greater over the Kitale area than over the lowlands, and is due to the difference in altitude between these two levels (Searle, 1952). There is more rainfall in the foothill zone of Mount Elgon, with an average of 1270mm the minimum recorded being 1016mm and the maximum 1549mm (Kipkorir *et al.,* 2007).

2.3 Vegetation

Mt. Elgon area has variable vegetation ranging from grass savanna on the lowlands to montane forest and bamboo on Mt. Elgon slopes (Figure 2.2). Mt. Elgon area rises to an alpine belt (White, 1983). To the south of the mountain slopes, there are *Prunus africana* and *Podocarpus milanjianus* that pass into bamboo zone. On the northern side towards Suk lowlands, dry montane forest support growth of species such as *Juniperus procera, Podocarpus gracilior, Ilex mitis, Olea europaea* ssp. *africana, Euclea divinorum* and *Olinia usambarensis.* Open woodland is dominated by *Senecio elgonensis* below 3900m (White, 1983). Afro Alpine heath and moorland at the peak of the mountain, forest at high altitudes are followed by Savanna like communities derived from forest. There is a vast occurrence of Combretaceous Savanna on the lowlands surrounding the mountain (White, 1983).

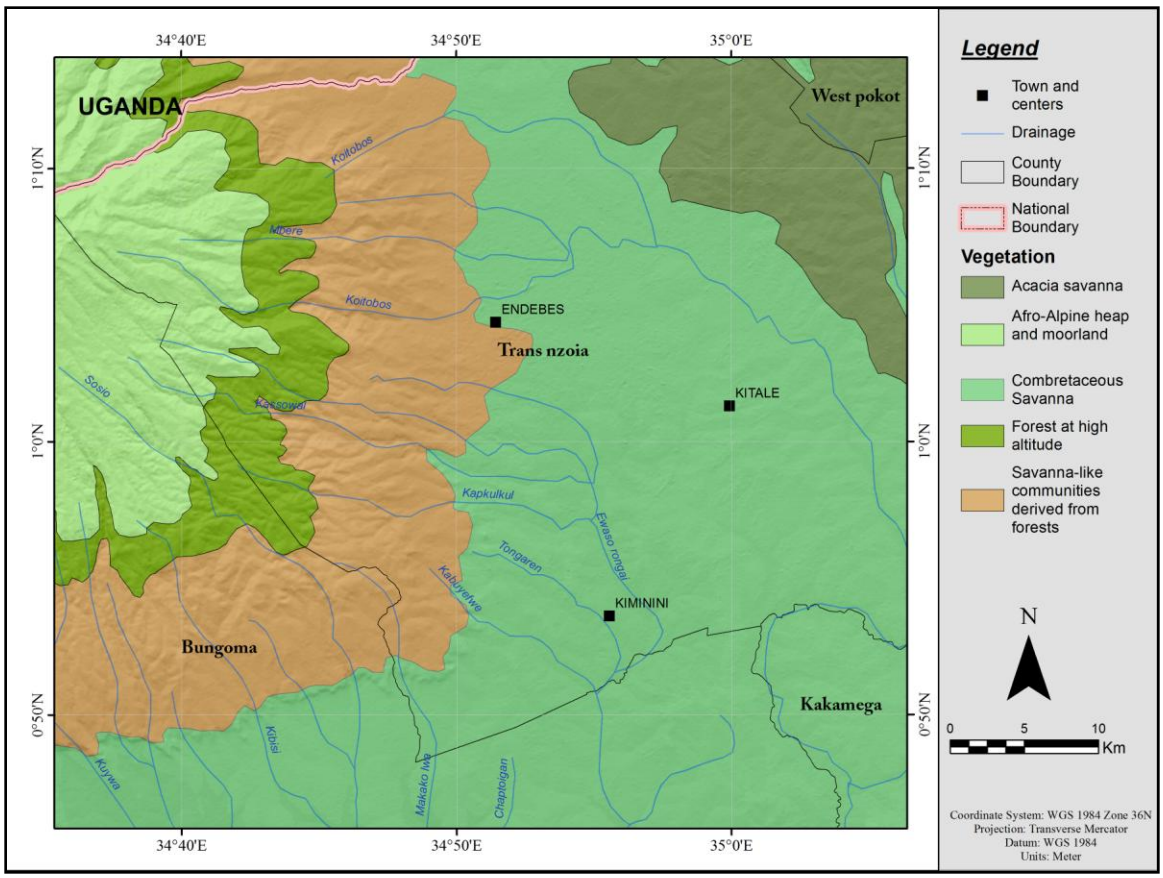

Figure 2.2: Vegetation map of the study area (Modified from White *et al.*, 1983)

2.4 Land Use

Land use on the lower slopes of Mt. Elgon is intensive with cultivation of maize as the dominant crop **(**IUCN, 2006). Adjacent to the Mt Elgon forest are smallholder farmers who largely practice mixed farming but also depend on the forest for their livelihood. In Kenya, some large-scale farms are owned and cultivated by Agricultural Development Corporation (ADC), Kenya Seed Company, East African Seed Company and several large-scale farmers. Common crops grown are maize (*Zea mays*), beans (*Phaseolus vulgaris*), potatoes (*Solanum tuberosum*), sweet potatoes (*Ipomoea batatas*), sorghum (*Sorghum bicolor*), cassava (*Manihot esculenta*) and finger millet (*Eleusine coracana*) (Kagai, 2011). Trans Nzoia County is one of the most important maize production areas in Kenya.

The practice of agro-forestry is common with trees like Sesbania (*Sesbania grandiflora*), Calliandra (*Calliandra calothyrsus*) and certain timber and fruit trees are planted together with crops or along the farm borders (Haldin *et al.*, 2000) (Plate 2.1). The potential of Trans Nzoia County

to produce food is large, but many farmers are still experiencing food insecurity (Kagai, 2011).

Plate 2.1: Planted vegetation in the study area

There are also some large-scale irrigated flower farms and green houses (Plate 2.2). Horticultural products like vegetables, fruits, nuts, and flowers are produced for both local market and for export (Kagai, 2011). Additional source of food and income is dairy farming which is widely practiced in Trans Nzoia County (Kagai, 2011). Other crops grown include beans, Irish potatoes and vegetables. On the Kenyan side, some parts of the forest have been opened up to the local community for cultivation under the Plantation Establishment Livelihood Improvement Scheme (PELIS) system. Agricultural encroachment on the forest continues even as the Kenya Forest Service and Kenya Wildlife Service continue to act against such actions (Larsen *et al*., 2008). Beans are the annual crop and have grown between February and March and are harvested during the rainy season in Trans Nzoia (Cooper and Law, 1978).

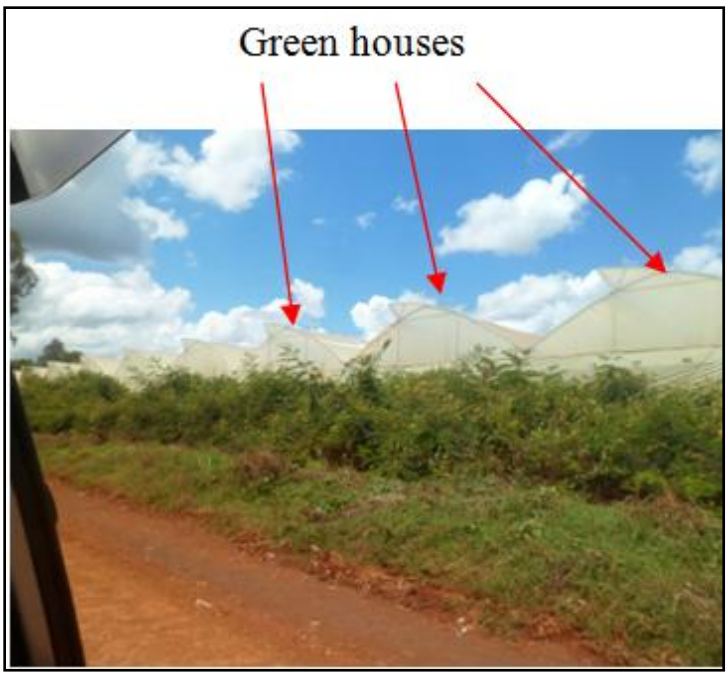

Plate 2.2: Photo showing greenhouses belonging to Andesen Flowers Ltd along Endebess-Suam Road

2.5 Physiography and Drainage

The main physiographical feature in Trans Nzoia area is the Trans-Nzoia upland including the Mt. Elgon slopes to the west, the Suk Lowlands to the north and the Kitale Plains at the centre (Figure 2.2). Trans-Nzoia upland is hemmed to the west by Mt. Elgon and to the east by Cherangany Hills (Murray-Hughes, 1933). The topography is dominated by the tributaries of the Nzoia River (Hess, 2010). Large areas which are either swampy or seasonally waterlogged are associated with river valleys such as the Koitoboss, Nai and the Saiwa swamps, north of Kitale Township. On the southern side of the watershed the drainage is mainly easterly, but to the east of Kitale it flows in a south-easterly direction (Searle, 1952). The Kitale plain, which forms part of the pre-Miocene peneplain of the Trans-Nzoia County (Dixey, 1948), has a slight Southerly tilt, with the principal drainage system flowing towards Lake Victoria. The maximum elevation appears to lie along an east-west line corresponding to latitude 01° 10' N (Dixey, 1948), which forms a watershed between the Nyanza drainage area and that of the Lake Turkana area. North of this line, the Kitale plain dips gently Northwards to the Trans-Nzoia escarpment (Figure 2.2).

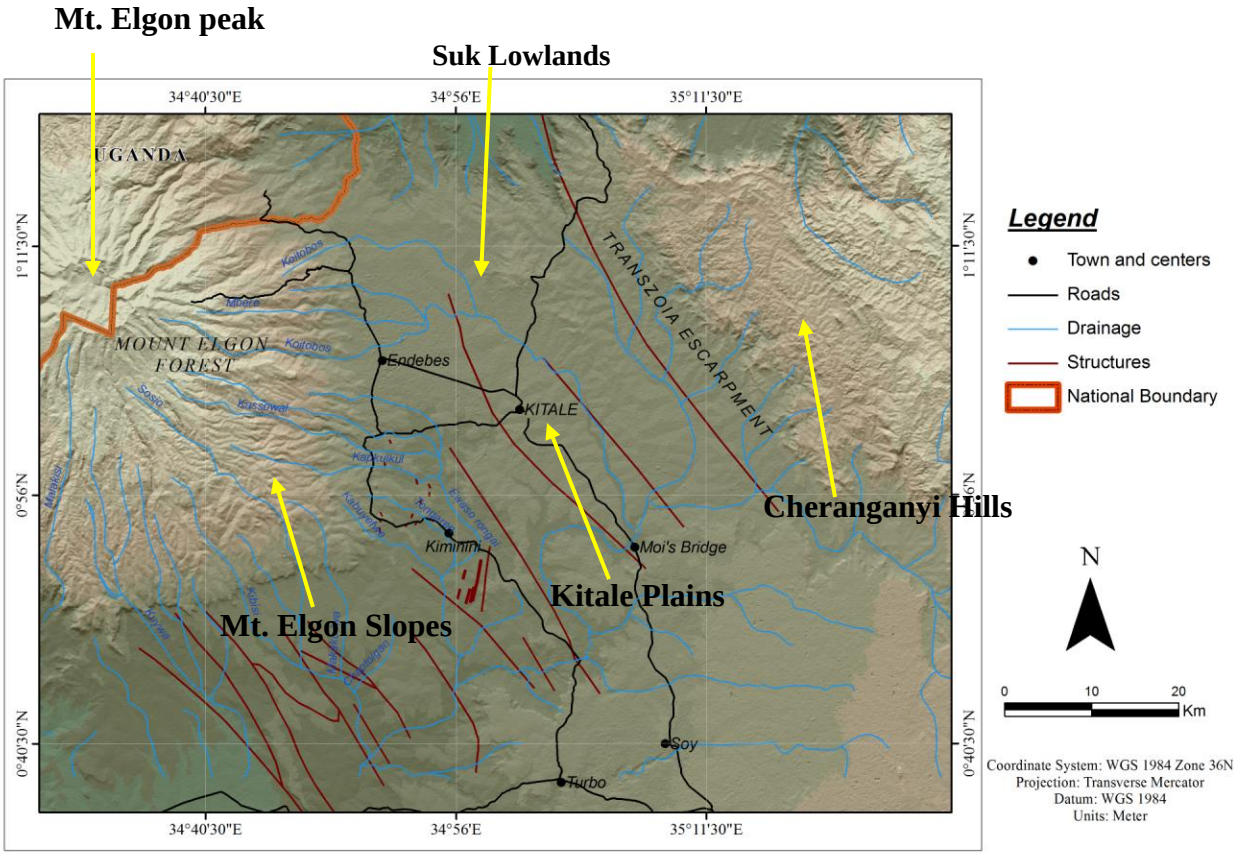

Figure 2.2: Physiographical and structural features of Trans Nzoia County and its environs

The Mt. Elgon Aquifer system is an important catchment area providing water for both domestic and industrial use, as well as feeding into Lake Kyoga in Uganda via River Mpologoma and Lake Turkana in Kenya via Rivers Suam and Bukwa while River Nzoia flows southwards to Lake Victoria (GOK and UNESCO, 2012). The principal river of the Kitale Plain is the Koitoboss which rises at the foot of Koitoboss Peak. All streams between Endebess Bluff and the Chepchoina River are tributary to it (Searle, 1952). The southern watershed separating the Koitoboss tributaries from those of the Rongai River runs in an east-west direction roughly parallel to the Endebess road (Figure 2.2). The other major river in the area is River Suam that originates from Mt. Elgon slopes. River Kaptega is its main tributary. They flow northwards and join River Turkwel which drains in Lake Turkana. River Nzoia originates from the Mount Elgon area and flows southwards to Lake Victoria while River Sipi originates from the North Eastern part of Mt. Elgon and flows towards the Nile Basin (Rannveig and Bernardas, 2012).

2.6 Geology, Hydrogeology and Structures

2.6.1 Regional Geology of the Area

The study area comprises of rocks of the MMB, the Neogene lavas of Mt. Elgon volcanic and the recent lateritic and black cotton soils (Figure 2.3). The MMB rocks in the study area consist mainly of quartzite and schist derived from argillaceous and arenaceous sediments which were transformed by metamorphism and recrystallization into quartz and feldspar-rich rocks with much muscovite, biotite, and hornblende minerals (Searle, 1952). Further south of study area and around Kiminini, there are Kavirondian rocks which are sedimentary in origin. These rocks are unfossiliferous and probably of Pre-Cambrian age (Combe, 1950; Gibson, 1954). The main members of this unit are conglomerates, mudstone and grits while pebbly grits and sandy mud-stones make up the subordinate with different sequence of deposition (Miller, 1956).

The Mount Elgon Neogene Lavas comprise of a great mass of agglomerate, breccias and tuff with intercalated bands of lava, the whole having been ejected from a vent during Neogene periods. The boulders of lava in the agglomerate are composed of nephelinites that contained minerals such as olivine, augite, magnetite, ilmenite and perovskite similar to the lava flows themselves (Searle, 1952). Surrounding the caldera produced round the vent are lavas and breccias of phonolitic-nephelenites in which aegirine-augite and orthoclase appear. The floor of the caldera, lying over 300 meters below the caldera rim and beyond, is composed of volcanic ash, the last eruptive material ejected from the volcano (Miller, 1956).

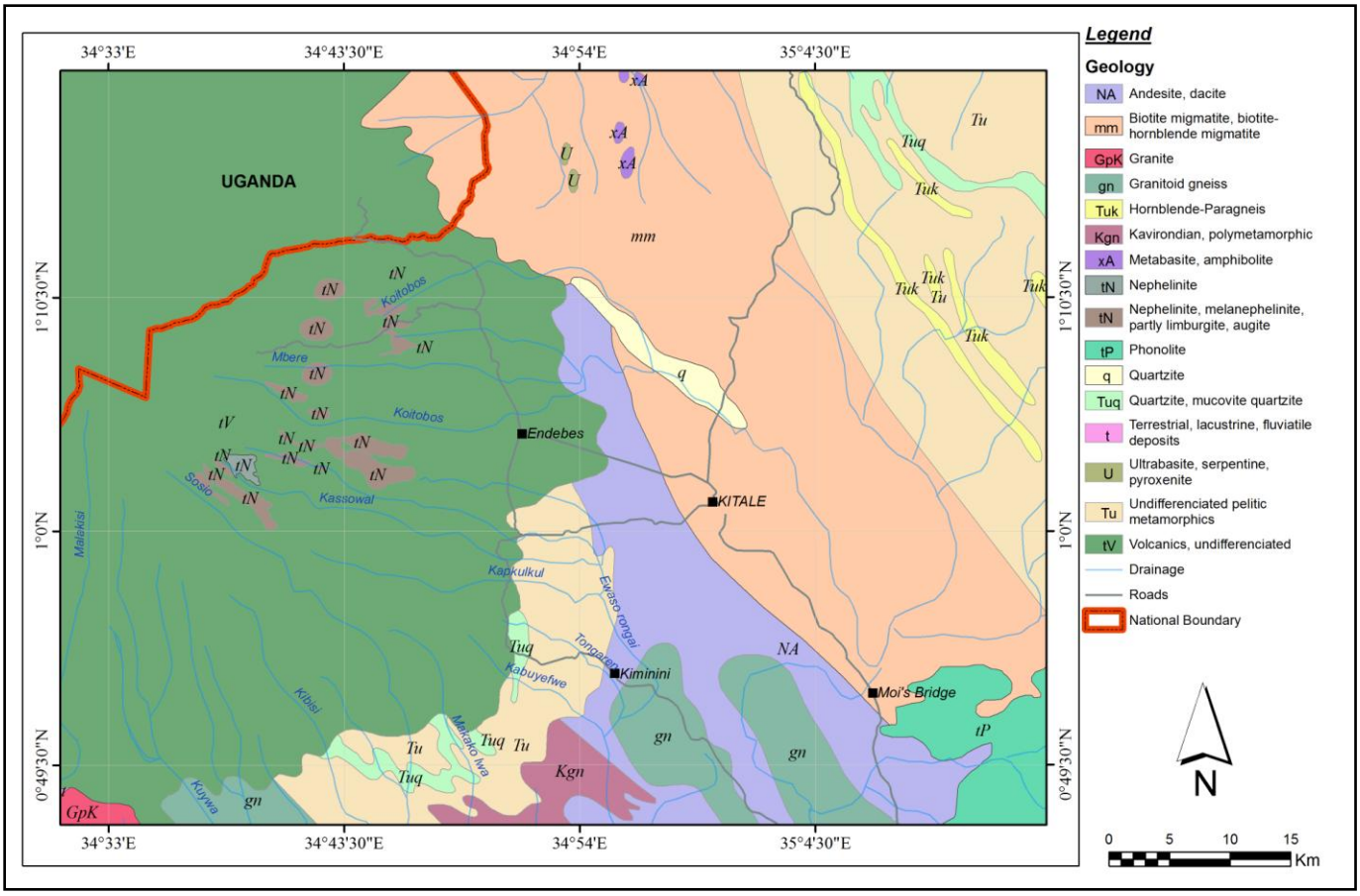

Figure 2.3: Geological map of Trans Nzoia area and its environs

2.6.2 Detailed Geology of the study area

2.6.2.1 Mobile Mozambique Belt (MMB) Rocks

MMB rocks in the Trans Nzoia area consist of metamorphic rock that resulted mainly as the effect of pressure, and consequent rise in temperature. In Trans Nzoia area, the rocks mainly pelitic schist and gneisses, metamorphosed semi pelitic sediments. Main minerals include quartz, feldspar, muscovite, biotite, and hornblende (Glenday and Parkinson, 1926; Gibson, 1950).

2.6.2.1.1 Pelitic Schists and Gneisses

These rocks are the predominant types in Trans-Nzoia area and include muscovite-quartzite, mica schist and hornblende schist. The outcrops occur to the west of Kitale toward Kwanza, Kolongolo, Muungano and northwards to Kacheliba. Biotite-schists were closely associated with the asbestos deposits in some areas forming an outer rim to the zoned bodies. Muscovite-schists

containing about 60 percent muscovite and 40 percent kaolinized feldspar and quartz were also fairly observed in the region (Searle, 1952).As observed during the research, the schists occur within the metamorphic succession, but showed considerable distortion (Plate 2.3). Inclusions within the muscovite include rutile, zircon and apatite (Miller, 1956). Chlorite-schists were noticeably rare in the area as a whole, but may occur only in close contact with the zoned asbestos bodies of which they form part; talc-schists in the area were also a product of the metasomatism of the ultramafic igneous intrusions (Glenday and Parkinson, 1926).The hornblende schists and migmatites occur to the north east and to the west of Kiminini. The outcrops are fine grained, dense, glistening black rocks which outcropped only over narrow widths, suggesting dyke-like forms (Searle, 1952).

Plate 2.3: Photo showing Pelitic schist and gneiss around Muungano, south of Saboti town.

2.6.2.1.2 Metamorphosed Semi-Pelitic Sediments

These gneisses are formed by the metamorphism of sandy shales and argillaceous sandstones and are represented in the area by biotite gneisses, feldspar-porphyroblast gneisses and the banded microcline augen gneisses (Searle, 1952; Miller, 1956). This was observed around Sabata and Kiminini to the south of the study area. The semi pelitic sediments are good indicators of groundwater occurrence and flow due to their porosity and permeability within their individual grains and foliation planes (Plate 2.4).

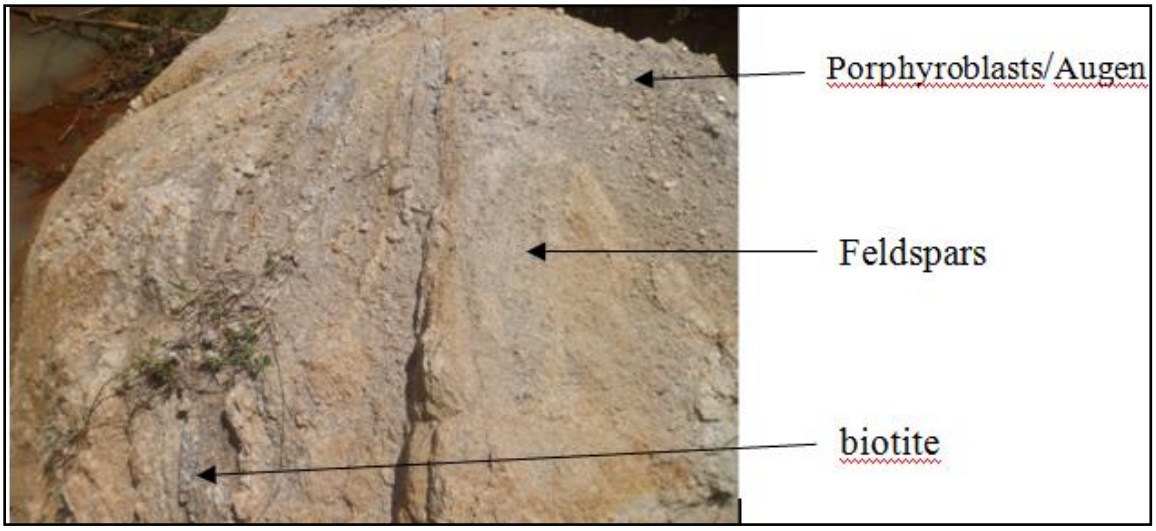

Plate 2.4: Photo showing Augen Gneiss outcrop in Sabata area

2.6.2.2 The Neogene Volcanics of Mt Elgon

The study area falls in what is referred in the geological reports as the Lower Pyroclastics Series (Gibson, 1950; Miller, 1956). The contact between the pyroclastics rocks of Mount Elgon and the MMB rocks runs approximately north-south across the Kitale Plains and crosses the Kitale-Endebess road about 20 kilometres from Kitale. North of this road there are no sharply defined morphological features separating the volcanic rocks from the MMB rocks (Searle, 1952; Miller, 1956) and only a change in soil type, from the black cotton reddish-brown volcanic soil to lighter colored sandy MMB soils, is visible. Huge boulders of agglomerates and phonolites occur around Mt. Elgon National Park (Plate 2.6). Other observable volcanic flows are compact trachytic tuffs (Plate 2.5).

Neogene lavas of Mt Elgon are largely composed of the huge mass of agglomerates, breccia and tuffs with intercalated bands of lava the whole having been ejected from a vent during Neogene times. The boulders of lava in the agglomerates are composed of nephelinites that contain mafic material such as olivine, augite and magnetite. Surrounding the caldera are lavas and breccias of phonolitic-nephelinites in which aegirine augite and orthoclase appear round vent. The floor of the caldera, lying over 300 metres below the caldera rim, is volcanic ash that mark the last eruptive material ejected from the volcano. Isolated occurrences of nephelinite are found capping hills in the Suk plains. Though the vents through which these lavas were extruded have not been

discovered, a volcano plug has been found at Sagat Hill containing agglomerates with associated nepheline-syenite-porphyry intrusions and dykes.

Plate 2.5: Plate showing trachytic tuff in Gituamba Area, South west of study area

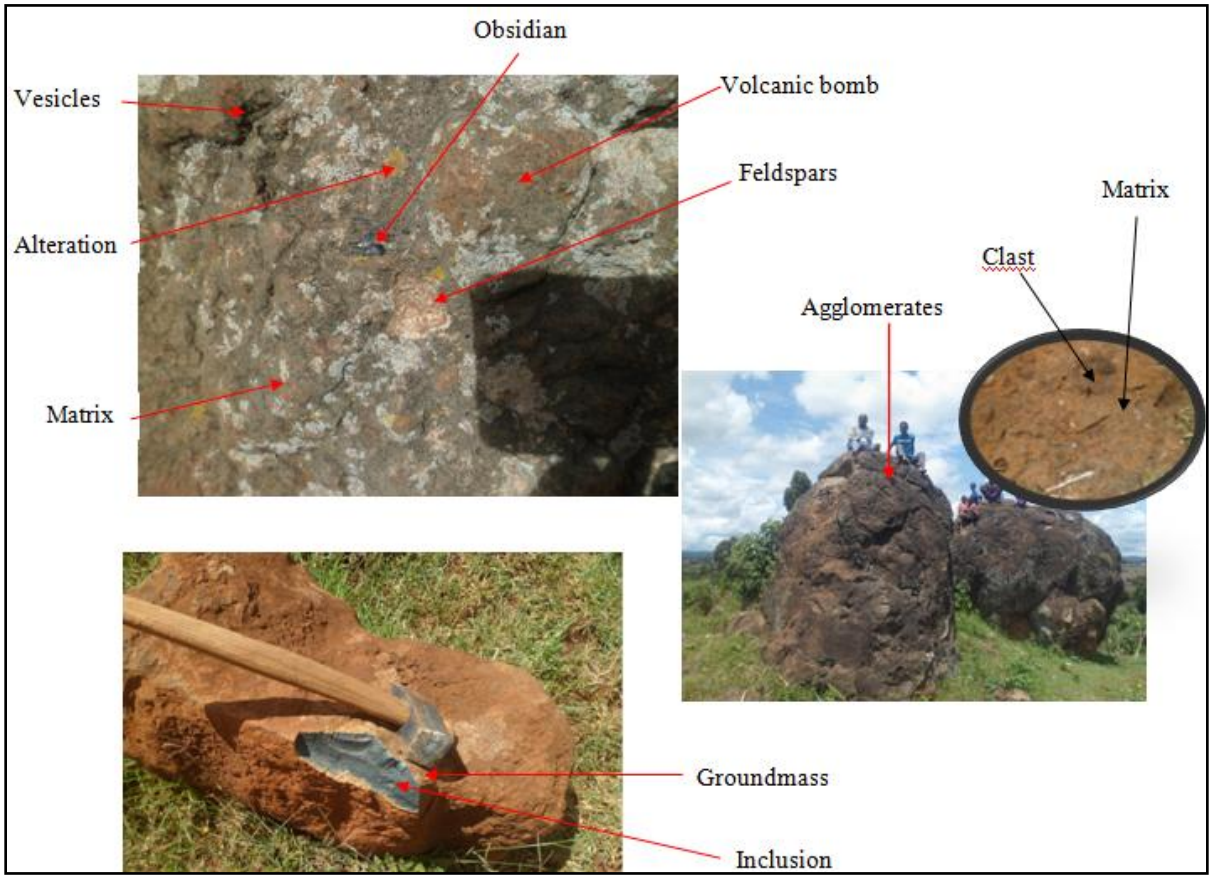

Plate 2.6: Photo showing phonolite and agglomerate boulder outcrop around Saboti.

2.6.2.3 Pleistocene to Recent Deposits

Road sections around Kitale showed irregular bedded layers of coarse pebbles, coarse sands, fine sands and silts. These Pleistocene sediments formed part of old river terraces deposited during the period of glaciations of Mount Elgon when abundant water from the melting glaciers not only incised deep gorges through the volcanic rocks (Miller, 1956) but on reaching the flat Kitale Plains, spread out into broad torrential rivers, of which the limits are shown by the outcrop of black cotton soil (Searle, 1952).

2.6.2.4 Soils

The dominant soil type in Kitale area is Ferralsols (Ui17). Soils in the study area are well drained, very deep, and red to dark red (Sombroek *et al*., 1982). Underlying MMB rocks are predominantly gneisses (Figure 2.4). The soil cover is reddish brown to grey in colour and support large scale farming of maize and coffee and other natural and planted trees (Kipkorir *et al*., 2007). There is a close relationship of ferralsols and cambisols (Ui13) which are formed from disintegration of granitic rocks. The granites give rise to coarse light brown, sandy, soils more subject to soil erosion than the more clayey varieties, while the diorites, syeno-diorites and syenites, having a greater proportion of mafic minerals, give darker red brown, more clayey, types (Huddleston, 1946). North of Kitale along Kitale-Endebess road, buff or light brown sandy soils are observed which are produced by the breakdown of undifferentiated MMB rocks and bright red clayey soils by the mudstones (Miller, 1956; Sombroek *et al*, 1982). The soils are denoted by B8 (Solonetz) and B9 (Gleysols) as shown in Figure 2.4, and are imperfectly to poorly drained. They are calcareous, moderately sodic and the deeper soils are saline (Sombroek *et al.*, 1982). Nitosols (Ui1) are observed at the transition between the MMB rocks and the volcanic. These soils are well drained, deep and dark red.

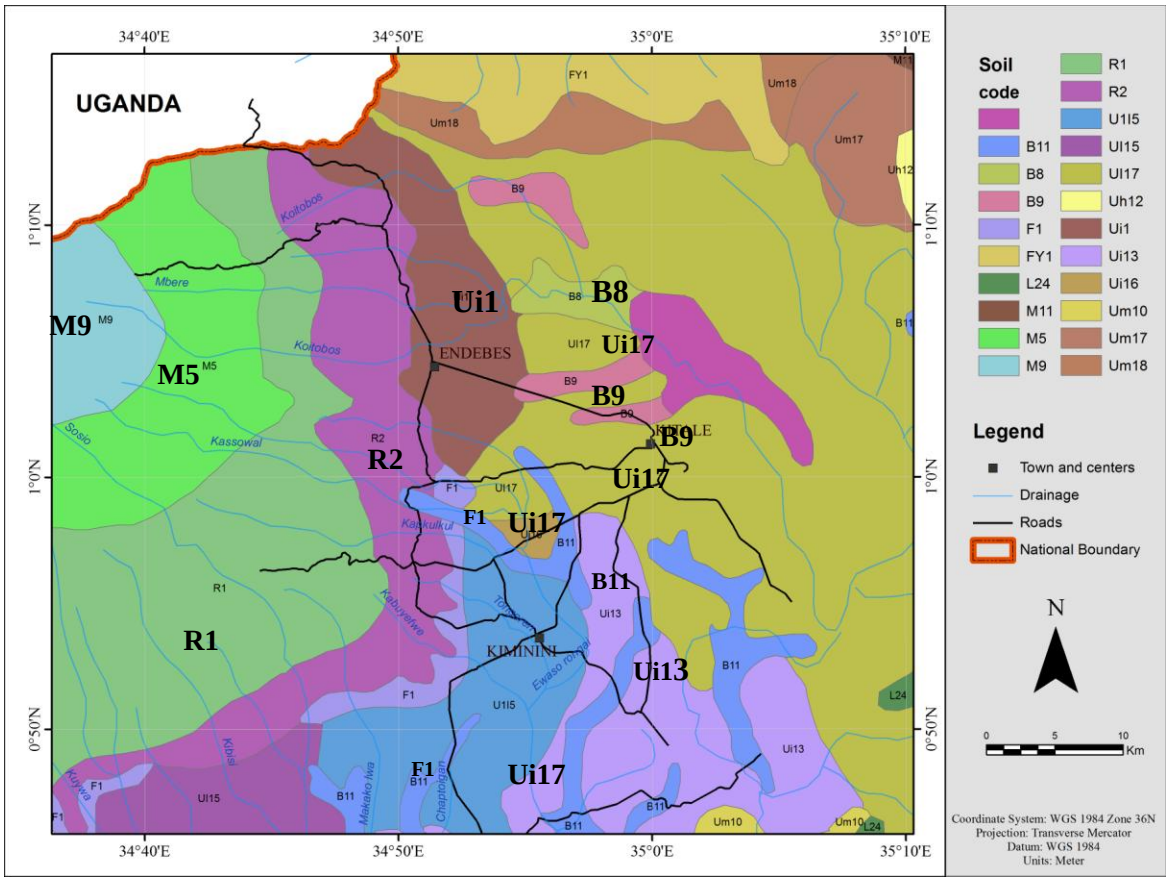

Figure 2.4: Soil map of the study area (modified from Sombroek *et al.*, 1982)

Histosols (M9), cambisols (M5), andosols (R1) and nitosols (R2) are volcanic soils that are observed on the top ridges of Mt. Elgon. Histosols and cambisols are originated from olivine basalts and ashes. The soils are shallow and moderately to well drained.

Andosols and nitosols are found on the ridges of Mt. Elgon and are well drained, deep and dark to reddish brown.

2.6.3 Structures

Geological structures in Trans Nzoia area are associated with MMB rocks, volcanic rocks and depositional features of the two geological units. Major structures that influence the hydrogeology and hydrology are discussed below.

2.6.3.1 Folds

Miller (1956) noted that the semi pelitic and calcareous gneisses granulites between Trans Nzoia and Kobinet – Kasiongul escarpments all dipped generally to the north east, but the calcareous

granulites west of Kiptaburr probably lie in the core of a fold that is overturned to the west. If viewed from close proximity, this fold would be anticlinal with its fold axis to the West of Kapsait (Murray-Hughes, 1933) with open anticline and syncline pitching in opposite directions to the north-east of Kapenguria. Gibson (1950) described similar east-west trends in the Mozambique system of the Broderick Falls area and considered them to be due to the superimposition of the post Kavirondian folding of original Mozambique system structures.

2.6.3.2 Foliation and lineation

The primary foliations in the study area include the bedding planes and igneous layering. Development of mineral grains in a preferred orientation within the secondary foliation either by rotation of the mineral grains or recrystallisation results into secondary foliations such as cleavage (Fletcher, 1978). The MMB rocks in the area are highly foliated with observable schistosity, trending approximately N15°W. Large lenticels of pure quartz lie in the foliation planes as was evident on the outcrops along the river and road cuttings in Birunda and Nabiswa areas in Kiminini (Plate 2.7).

The evident lineation is due to alignment of the biotite and muscovite mineral grains (Fletcher, 1978). These structures tend to control groundwater flow since the layers may have different rock properties hence easily weathered and eroded leaving behind a conduit for groundwater flow (Miller, 1956).

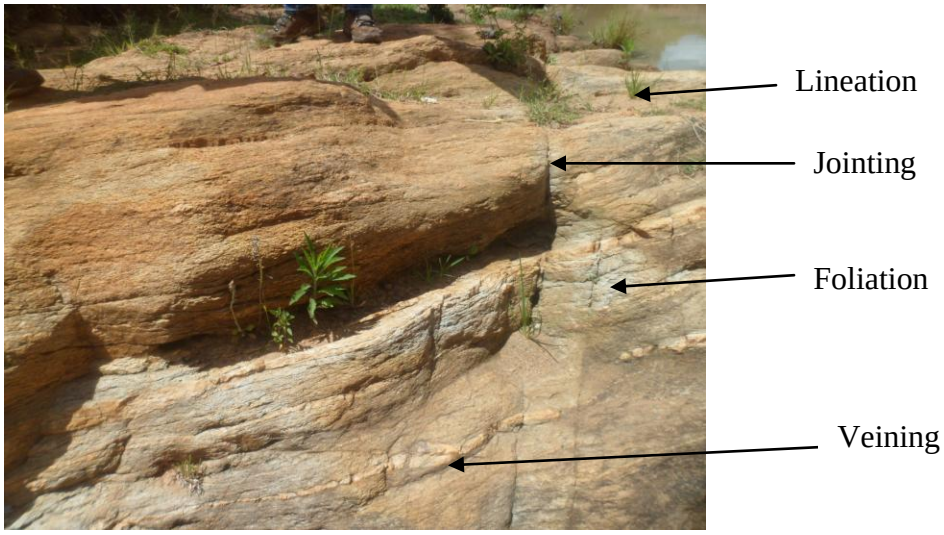

Plate 2.7: Foliation, Lineation in a MMB rock outcrop

2.6.3.3 Fault

In the upper part the Trans Nzoia Escarpment (Figure 2.2), there is a series of quartzites and semi-pelitic gneisses dipping 005°. This may be considered the true dip of the gneisses forming this escarpment. The lowest quartzites on being traced from the river to Kirk's farm South West of Kaibotoss, increases its angle of dip to 040° (Murray-Hughes, 1933). Tilau and other small hills overlooking Trans Nzoia plain formed by this lowest quartzite at Kaiboss. The feature is maintained to the south east after the quartzites lensed out confirming that Trans Nzoia Escarpment is a fault line feature (Miller, 1956).

2.6.4 Hydrology and Hydrogeology

The volcanics, mostly the agglomerates and pyroclasts are porous and permeable. The percolated water at the MMB - volcanic contact flows to the surface as observed along road and river cuttings. The abundance of surface water resources (permanent rivers) and the expense involved in the development of groundwater wells has resulted in reduced groundwater utilization (Miller, 1956, Kipkorir and Towett, 2013). Surface water flow is influenced mostly by the regional structural trends and the Neogene volcanic flows. River Kaptega (Plate 2.8), a tributary of Suam River flows in a northerly direction and joins River Turkwel further north. The aquifer system in the upper catchment comprises of various geological formations. In the Mt. Elgon region, it includes decomposed Neogene volcanic phonolites and agglomerate tuffs, supporting good inter-granular and fracture-flow aquifers with yields from $5m^3$/hr. to over 20 m^3/hr. The aquifers in the lower catchment comprise of weathered MMB rocks. These areas have lower potential yields and aquifers are confined mainly in the fracture zones.

Plate 2.8: River Kaptega running flowing northwards

A number of water wells and shallow boreholes were observed both in the metamorphic and volcanic terrains. Those in the volcanic terrain dried up during the dry seasons while those existing on the metamorphic terrain were considerably productive during the rainy and dry seasons. An example of productive borehole was observed in Mubere Primary School with a total drilled depth of 25m (Plate 2.9).

Plate 2.9: Borehole point at Mubere Primary School

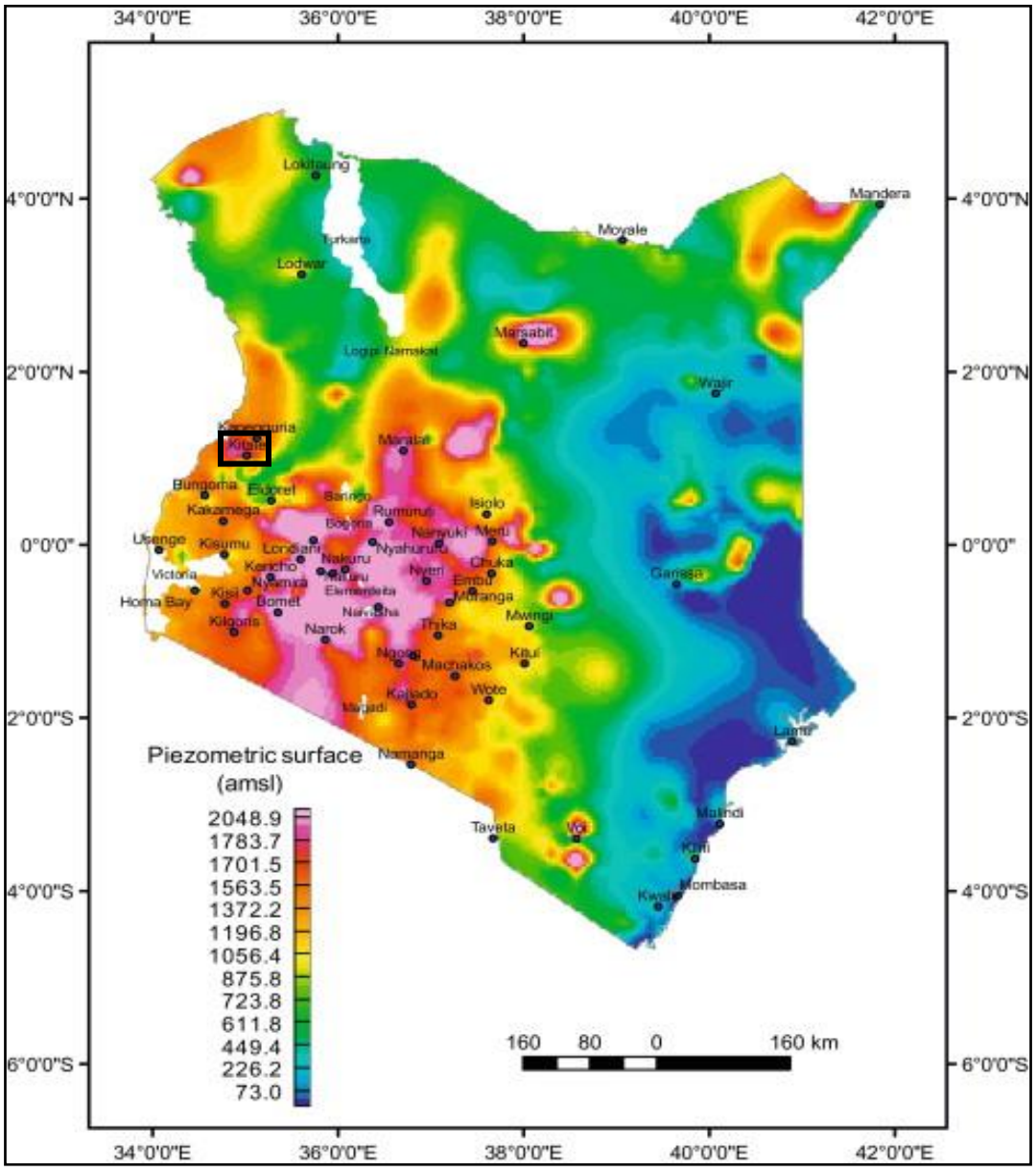

Figure 2.5: Piezometric surface map of Kenya showing the groundwater flow mechanism. The black rectangle shows the position of the study area, (after Kuria, 2013).

From the Figure 2.5, groundwater potential is high around Mt. Elgon area. The higher potential zones are due west of Kitale town.

3 CHAPTER THREE: METHODOLOGY

3.1 Basic Principles

3.1.1 Electrical Resistivity

Direct Current (DC) electrical resistivity method is one of the most commonly used exploration techniques to delineate aquifer composition, groundwater, bed-rock, fresh and salt intrusion (Robinson and Coruh, 1988; Burger, 1992; Telford *et al*. 1990). The ground resistivity is related to various geological parameters such as the mineral and fluid content, porosity, degree of water saturation in the rock as well as water salinity in the rocks (Grant and West, 1965). Electrical current may be propagated in rocks and minerals in three different ways: Electronic (ohmic), electrolytic and dielectric induction (Telford *et al*., 1990). The electronic/ohmic is the most common one in materials that contain free electrons like metals, minerals and some rocks. The DC electrical resistivity method in general involves passing current (I) into the ground through a pair of current electrodes (AB) and measuring the potential drop (ΔV) through a pair of suitably implanted potential electrodes and (MN) (Lowrie, 2007) (Figure 3.1).

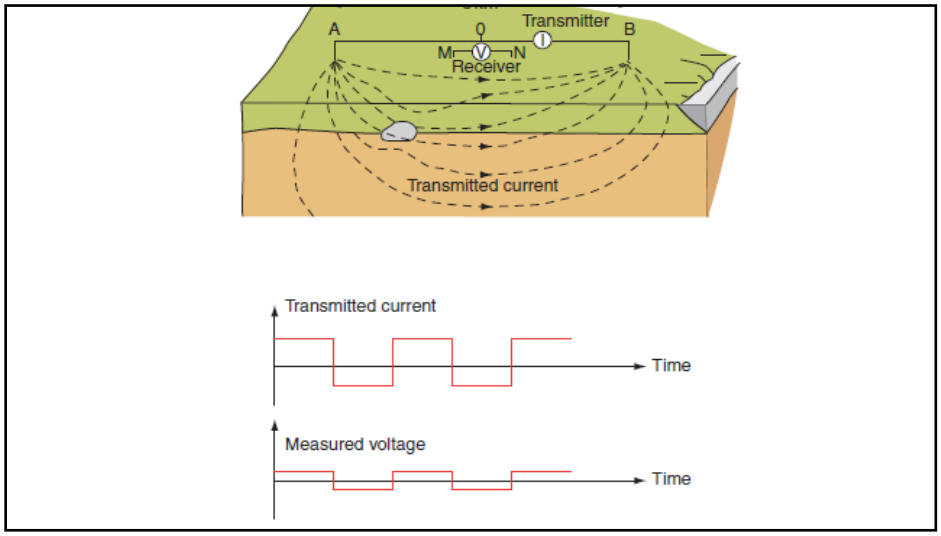

Figure 3.1: Schematic representation of electrical resistivity transmitted current and measured voltage (Hersir and Bjornsson, 1991).

The resistivity is defined as the ratio of the magnitudes of electric field and current density (Hugh and Roger, 1996; Hersir and Bjornsson, 1991).

ρ= E/J…….. ……..... (3.1)

The electrical resistivity (**ρ**) is the quotient between the potential difference (∂V) and the current (I) through the substance which has a cross-sectional area (A) of one meter squared and one meter in length (Figure 3.2) (Telford *et al*, 1990; Hersir and Bjonsson, 1991).

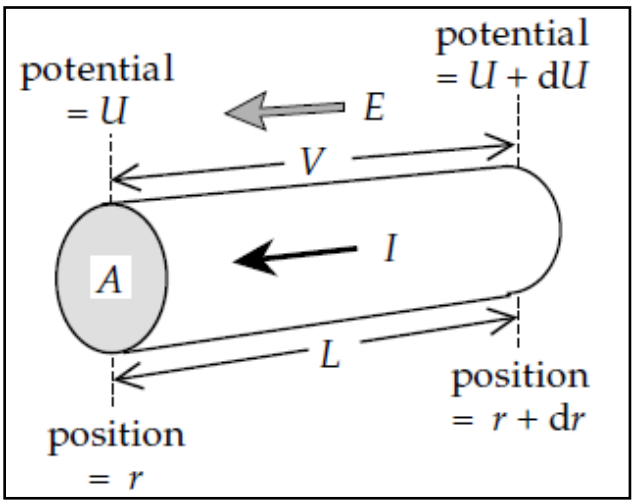

Figure 3.2: Parameters used to define Ohms law for a straight conductor.

Associated strength in the field, *E*at any given position in a material is proportional to the current density, *J* (Paransis 1997). The proportionality constant, ρ, depends on the material and is called the particular resistivity for a specific material, computed in Ωm. Electrical field strength, E at a point in a material is directly proportional to the current density, J (Ohm's Law)**.**

$E = \rho j$……(3.2)

Electric field, $E = -\frac{\partial V}{\partial r} = \frac{V}{L}$……(3.3)

Current density, $j = \frac{Current}{Area} = \frac{I}{A}$……(3.4)

Where:

J is the current density (A/m^2)

E is the electric field (V/m)

A is the cross sectional area

I is the current

L is length of the material

r is the original position of the particle

r+∂r r is the final position of the particle

∂V is the potential difference

∂r is the small change in length

3.1.1.1 Vertical Electrical Sounding

Consider an arrangement consisting of a pair of current electrodes and a pair of potential electrodes (Figure 3.3). The current electrodes A and B act as source and sink, respectively

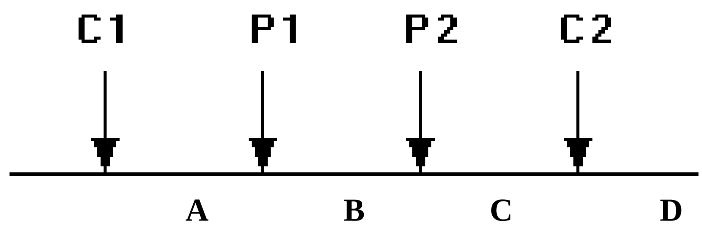

Figure 3.3: Conventional array with four electrodes to measure the subsurface resistivity.

At the detection electrode C the potential due to the source A is

$$+\rho I / [2\pi r_{AC}] \qquad (3.5)$$

While the potential due to the sink B is $-\rho I / [2\pi r_{AC}]$ (Lowrie, 2007)………………..... (3.6)

The combined potential at C is $U_C = \frac{\rho I}{2\pi}\left(\frac{1}{r_{AC}} - \frac{1}{r_{CB}}\right)$……………………………....... (3.7)

Similarly, the resultant potential at D is

$$U_D = \frac{\rho I}{2\pi}\left(\frac{1}{r_{AD}} - \frac{1}{r_{DB}}\right) \qquad (3.8)$$

Where,

r_{AC}, r_{CB}, r_{AD}, r_{DB} is the distances from the array centre to the electrodes

The potential difference measured by a voltmeter connected between C and D is obtained by subtracting equation 3.8 from equation 3.7

$$\Delta V = \frac{\rho I}{2\pi}\left[\underbrace{\left(\frac{1}{r_{AC}} - \frac{1}{r_{CB}}\right) - \left(\frac{1}{r_{AD}} - \frac{1}{r_{DB}}\right)}_{G}\right] \qquad (3.9)$$

Making ρ the subject of the formula,

$$\rho = \frac{2\pi \Delta V}{IG} \qquad (3.10)$$

$$\rho = \left(\frac{2\pi}{G}\right) \times \left(\frac{\Delta V}{I}\right) \ldots \ldots \ldots \ldots \ldots \ldots \ldots (3.11)$$

But $\left(2\pi/_{G}\right)$ is a constant, k. The substantial formula for apparent resistivity reduces to

$$\rho = \kappa \frac{\Delta V}{I} \ldots \ldots \ldots \ldots \ldots \ldots \ldots (3.12)$$

Where:

I=current.

ΔV= potential difference.

ρ = resistivity.

k = is the geometric factor for the electrode array in use and obtained by:

$$\kappa = \frac{2\pi}{l}(L^2 - l^2) \text{ (Lowrie, 2007)} \ldots \ldots \ldots \ldots \ldots \ldots (3.13)$$

Where:

L is the current electrode separation AB/2 in metres.

l is the potential electrode separation MN/2 metres.

From equation 3.12, apparent resistivity varies by altering the geometrical arrangement of the four electrodes, VES, or on moving them on the ground without altering their geometry, HEP. Electrical current in geological materials is usually carried by either free electrons or ions in the solid or by motion of ions in connate water (Greenhalgh, 2009). Electrical resistivity surveys have been used for many decades in hydrogeological, mining and geotechnical investigations. More recently, it has been used for environmental surveys (Loke, 2004). Subsurface information about the geometry of an aquifer can be achieved either by core drilling or geophysics (Overmeereen, 1981). Apart from core drilling, geophysics methods are the only and most reliable means for getting the information about the subsurface (Adiat *et al.,* 2009). Common causes of resistivity anomalies are faults, dykes, water content and lava flows.

Deep electrical sounding can provide valuable information about the internal structure of the Earth's crust and mantle (Lowrie, 2007). Electrical surveys may be based on natural sources of potential and current. More commonly, they involve the detection of signals induced in subsurface conducting bodies by electric and magnetic fields generated above ground. Investigations in this category include resistivity and electromagnetic methods (Flathe, 1963). These techniques have long been used in commercial geophysical surveying. In recent years, they have also be-

come important in the scientific investigation of environmental problems. Useful relations for describing and characterizing resistivity of rocks have been well documented in relevant literature (Domenico, 1977; Griffiths and King, 1981; Dobrin and Savit, 1988; Keary and Brooks, 1991).

3.1.1.1.1 Current

Hugh and Roger (1996) noted that current is the net charge flowing through a cross sectional area A per unit time. If a net charge **δQ** flows through an area in a time **δt**, the current **I** through the area is;

$$I = \delta Q/\delta t = {}^{\delta Q}/_{\delta t} = nqV_d\, A \quad \text{..... (3.14)}$$

Where:

n= charged particles per unit volume (concentration).

q= charge.

v_d= drift velocity.

A= cross sectional area.

Although we refer to the direction of current as from the above equation, current is not a vector quantity. In a current carrying wire, the current is always along the length of the wire whether the wire is straight or curved. No single vector could describe motion along a curved path; hence current is a scalar quantity (Hugh and Roger, 1996). The SI unit of current is Ampere which is defined as one coulomb per second.

3.1.1.1.2 Conductivity

Electrical conductivity in matter in solid or liquid state transpires by the mobility of electrons and ions of groundwater contained in pores of the rocks and along surface layers at the contact of rock and solution (Hersir and Bjornsson, 1991).

The reciprocal of the material resistivity will give the required material conductivity whose equation is given as follows:

$$\frac{1}{\rho} = \sigma = J/E \quad \text{..... (3.15)}$$

J is the current density (A/m^2).

E is the electric field (V/m).

There are four basic curve types obtained during VES surveys: K, H, A and Q types. The type K curve rises to a maximum then decreases, indicating that the intermediate layer has higher resistivity than the top and bottom layers. The types H curve falls to a minimum then increases again since the intermediate layer is a better conductor than the top and bottom layers. The type A curve may show some changes in gradient but the apparent resistivity generally increases continuously with increasing electrode separation, indicating that the true resistivities increase with depth from layer to layer. The type Q curve exhibits the opposite effect; it decreases continuously along with a progressive decrease of resistivity with depth (Lowrie, 2007).

The apparent resistivity curve for a three-layer structure generally has one of four typical shapes, determined by the vertical sequence of resistivities in the layers (Lowrie, 2007; Grant and West, 1965). These theoretical curves, calculated for a particular four-electrode array, take into account the change in depth penetration when current lines cross the boundary to a layer with different resistivity (Telford *et al.*, 1990). The electrical boundary conditions require continuity of the component of current density **J**, normal to the interface and of the component of electric field **E** tangential to the interface. At a boundary the current lines behave like optical or seismic rays, and are guided by similar laws of reflection and refraction (Moon *et al.*, 2006).

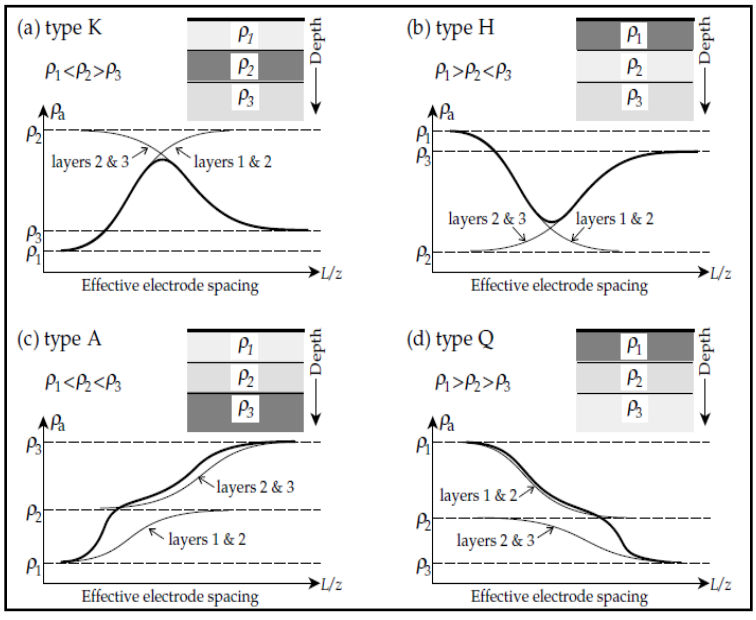

Figure 3.4: Different curves expected in a VES (Lowrie, 2007).

3.1.1.2 Horizontal Electrical Profiling (HEP)

In the Wenner configuration (Figure 3.3) the current and potential electrode pairs have a common mid-point and the distances between adjacent electrodes are equal, so that $r_{AB} = r_{BC} = r_{CD} = a$, and $r_{AC} = r_{BD} = 2a$ (Telford *et al.*, 1990).

$$\rho = 2\pi \frac{V}{I}\left\{\left(\frac{1}{a} - \frac{1}{2a}\right) - \left(\frac{1}{2a} - \frac{1}{a}\right)\right\}^{-1} \quad \text{..... (3.16)}$$

$$\rho = 2\pi a \frac{\Delta V}{I} \quad \text{..... (3.17)}$$

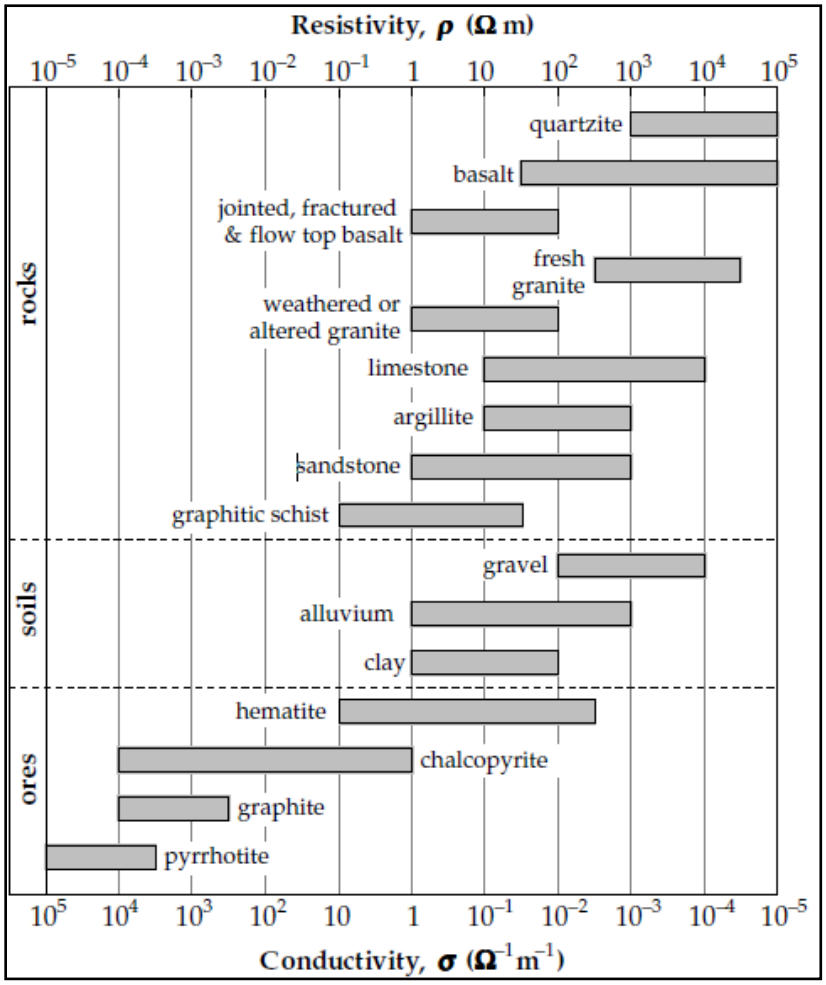

Figure 3.5: Ranges of electrical resistivity for some common rocks, soils and ores (Telford *et al.*, 1990).

3.1.2 Aquifer Potential yield

An imaginary or hypothetical surface of the piezometric pressure or hydraulic head throughout all or part of a confined or semi-confined aquifer; analogous to the water table of an unconfined

aquifer. An imaginary surface representing the total head in an aquifer; that is it represents the height above a datum plane at which the water level stands in boreholes penetrating the aquifer. The piezometric surface provides an indication of the direction of groundwater flow and is used to determine hydraulic gradients. The piezometric levels were then computed to establish the aquifer potential yields in different geological units. Water Rest Level (WRL) was subtracted from ground elevation to give the piezometric surface above mean sea level.

In confined aquifers, the level that the water rises to in a borehole is the piezometric level. Contouring the piezometric levels creates a piezometric surface for the confined aquifer. This is similar to the water table for an unconfined aquifer. The piezometric surface provides an indication of the level to which water will rise in a borehole screened in a confined aquifer. The piezometric surface indicates the groundwater flow direction. The aquifer in the conceptual model corresponds to the network of fractures that are the most permeable and provide most of the flow to the pumped well. The piezometric surface can be used to identify areas of the aquifer under stress from pumping.

3.1.3 Transmissivity

Transmissivity is the rate of flow of water under a unit hydraulic gradient through a cross-section of unit width across the entire saturated section of an aquifer. Scientifically, transmissivity (T) should be determined from the analysis of a well test, but the figures given have been determined from past studies using Logan's method. (Logan, 1964) developed a relationship between specific capacity (Q/Δs) and T, 1.22 x Q/s, based on a reworking of Thiem's seminal steady-state groundwater flow equation (Thiem, 1906).

The product of (K) and thickness (d) is defined as the transmissivity (T) of an aquifer system (Kd=T). This property can be derived from the commonly applied Jacobs formula (Driscoll, 1986):

$$T=1.22Q/\Delta s \quad \text{(3.18)}$$

Where,

T=Transmissivity.

Q=borehole specific capacity per day.

Δs= drawdown.

Low-permeability parts of the aquifer system, for example, large blocks of compacted rock, are not explicitly included in the model. Furthermore, wells that are isolated from the pumped aquifer by low-permeability barriers to flow are not included in the model as well. For example, a well may be open to productive fractures, but those fractures may be isolated from the pumped aquifer by intervening beds of relatively compacted low-permeability beds.

3.2 Data Quality Control

Quality of the data is important for better and confident data analysis and interpretation, therefore, there is need to ensure that the electrodes are well connected to maximize precision of the data. When noise to signal ratio is high, the potential is shifted to increase signal quality. For this research, potential shifting was done at 32m and 80m respectively. Generally, response reduces with vertical increase in probing depth due to declining signal strength. For profiling data, the data are put in three distinct columns x, y and z, where x and y are the positions and z is the resistivity values. The data is fed into excel spreadsheet. In horizontal electrical profiling, the current and potential electrodes separation distances are kept constant. This measures the electrical response of the subsurface at a constant depth. The most severe limitation of the resistivity sounding method is that horizontal (or lateral) changes in the subsurface resistivity are not commonly found (Lowrie, 2007). The ideal situation is rarely found in practice; lateral changes in the subsurface resistivity will cause changes in the apparent resistivity values that might be misinterpreted as changes with depth in the subsurface resistivity (Telford *et al*., 1990). Some of the parameters that were verified for transmissivity and piezometric surface were WRL, total drilled depth, coordinates of the existing boreholes. These were then compared with the existing borehole data which showed some disparity.

3.3 Assumptions in Hydrogeological Data Analysis

The electrical properties of rocks in the upper part of the earth's crust are dependent upon the lithology, porosity, degree of pore space saturation and the salinity of the water. It is imperative to note that: (i) Saturated rocks have lower resistivities than unsaturated dry rocks (ii) the higher the porosity and or salinity of the saturated rock, the lower its resistivity (iii) Clays and conductive minerals reduce the resistivity of the rock (Chow *et al*., 1998).

For VES the assumptions is that ground consists of horizontal parallel layers with distinct resistivity and distinct thickness (Irshad, 1976). Interpretation of vertical electrical resistivity field data is usually done with an assumption that the earth's subsurface layers have uniform and parallel layers (Lowrie, 2007; Irshad, 1976). Theis (1935) assumes that all wells fully penetrate a confined aquifer in which the transmissivity (T) is independent of direction. The model parameters are T and storage coefficient (S). Simulated drawdown depends on the radial distance from the pumped well (r) and time elapsed since pumping began (t).

3.4 Methods

3.4.1 Desk Top Study

The source documents used for the project were journal papers, geological reports and maps, academic thesis and dissertations, topographical maps, aerial photographs and satellite images. In addition, geological reports of Kitale, Broderick Falls, Suk-Sekerr, Kakamega areas and geographical data, borehole and well data files from Water Resources Management Authority (WRMA) were used.

3.4.2 Field methods

Field data acquisition was done between October-November 2014 and March 2015 using SSR-MP-ATS Resistivity meter model (Plate 3.1). A total of thirty three (33) VES and three (3) HEP were carried out in the study area. Seventeen VES were executed in the metamorphic terrain; eleven on the volcanic terrain while five were at the transition zone between metamorphic and volcanic rocks. The VES were conducted in N-S orientation. Three HEP were also carried out to deduce lateral variation of the rocks at a depth of 100m. The first was on the northern section, second to the central part and third to the southern end of the study area (Figure 3.6).

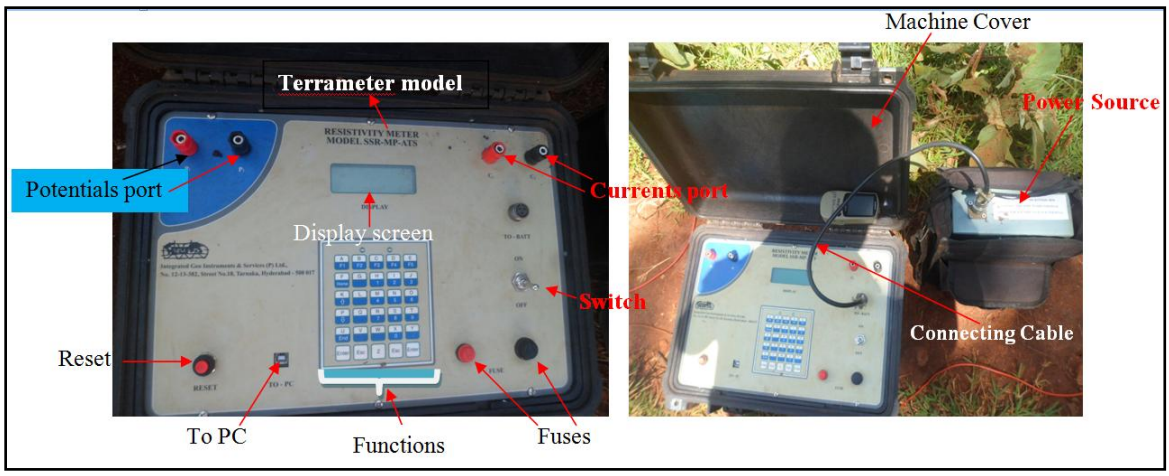

Plate 3.1: Photo showing the terrameter model, power source and function parts.

The available borehole data showed that the deepest borehole was 201m and the shallowest was 15m.The highest yielding borehole is C-1785 with a total yield of 11.34m^3/h. It is worth noting that the highest yielding borehole was in a volcanic terrain north of Saboti area.

3.4.2.1 Vertical Electrical Sounding (VES)

Current was propagated into the ground by means of two current electrodes (A and B). With two other potential electrodes (M and N), situated near the centre of the array, the potential field generated by the current was measured (Lowrie, 2007; Hersir and Bjornsson, 1991). From the current strength and the potential difference, and taking into account the electrode separations, the ground resistivity was determined. The separation between the electrodes was increased step-wise, thereby increasing current propagation to greater depths. At certain stage, AB/2 = 32m and 80m, potential drop got closer to detection limit hence the potential electrodes were shifted to MN/2=10m and 25m respectively to boost potential difference. (Hersir and Bjornsson, 1991). This was done to increase signal quality and reduce noise levels in the resistivity data.

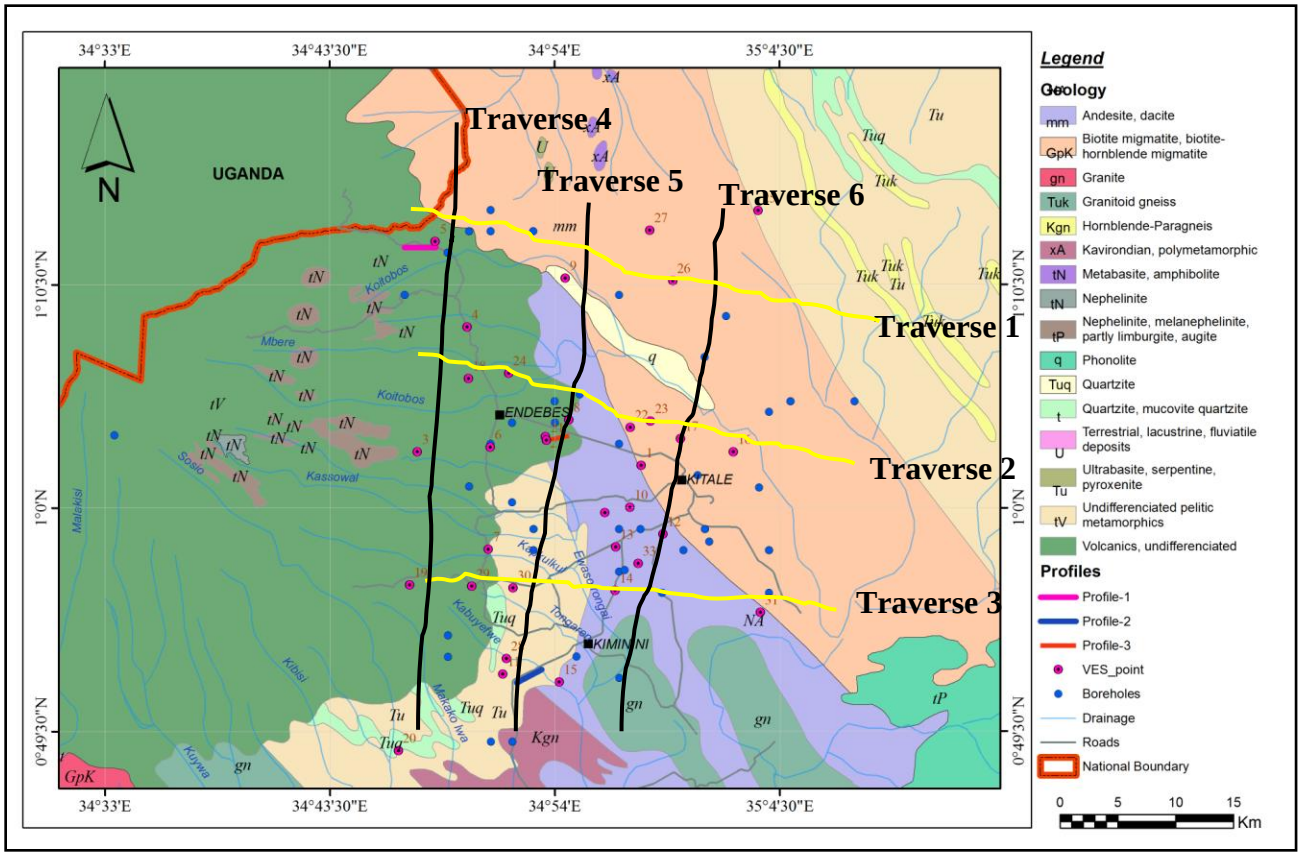

Figure 3.6: VES points, HEP lines and existing boreholes in the study area

Direct Current (DC) was introduced into the ground by means of two electrodes connected to the terminals to a portable source of Electromotive Force. The resulting potential distribution in the ground, mapped by two probes of non polarizing electrodes yielded distribution of electrical resistivity in the subsurface.

Plate 3.2: Data collection process in the field.

3.4.2.2 Horizontal Electrical Profiling (HEP)

In horizontal Electrical Profile, lateral changes in resistivity were measured at a given depth depending on the values of AB and MN. The profile was taken in east-west orientation transverse to geological structures. The spacing between the electrodes remained fixed, but the entire array was moved along a straight line. HEP gave information about lateral changes in the subsurface resistivity and detected vertical structures (Hersir and Bjornsson, 1991).

Three lines of geo-electrical profiling were conducted in the study area. HEP 1 was done to the North of study area around Andersen/Mt. Elgon Flowers along Endebess-Suam road. The profile length was 2321m. The second HEP was to the South around Muungano, Nabiswa Area along Kiminini-Webuye Road in a metamorphic terrain. The length of the profile line was 1998m.The third HEP was along KWS Road at Sabwani ADC farm. The profile length was 1665m. The results are shown qualitatively in Figures 4.10, 4.11 and 4.12 respectively. The resistivity values were interpreted according to Telford *et al.* (1990) (Figure 3.5). Depth of penetration was deduced using the relation below (Telford *et al*., 1990).

$$\left(\frac{2}{3}AB/_2\right) + \left(\frac{MN}{2}\right) \quad \text{(3.19)}$$

Where:

AB is the distance between the current electrodes.

MN is the distance between the potential electrodes.

The current electrode separation was 100m, while potential electrode separation was 33.3 from the array centre. Therefore, the penetration depth that was probed was

66.6+33.3 = 99.9, approximately 100m.

3.4.2.3 Piezometric levels

The piezometric levels were then computed to establish the aquifer potential yields in different geological units. Total drilled depth of existing boreholes and Water Rest Level (WRL) were verified using a water dipper. Water Rest levels (WRL) were obtained from existing borehole data. Ground elevation was taken using GPS Etrex model with an error of ±2.4m. WRL was subtracted from ground elevation to give the piezometric surfaces above mean sea level. The piezometric surface map was compared with the regional structural patterns to show the influence of structural features to groundwater potential and flow directions.

3.4.2.4 Transmissivity

Transmissivity is the rate of flow of water under a unit hydraulic gradient through a cross-section of unit width across the entire saturated section of an aquifer. Scientifically, transmissivity (T) should be determined from the analysis of a well test, but the figures given have been determined from past studies as reported in the National Water Waster Plan (1992) using Logan (1964) method and WRMA groundwater data base.

3.4.3 Data Processing

For VES data, the graph was first identified as of K, H, A or Q type. The next step was one-dimensional inversion of the field data. The technique involves iterative procedures that would be very time-consuming without a fast computer (Lowrie, 2007). For this study, the resistivity data were interpreted using IPI2Win inversion software package, which iterates the resistivity data and constructs pseudo-sections and resistivity profiles (Bobachev, 2002). A first estimate of layer thickness and resistivity was made for each layer and the predicted curve of apparent resistivity versus electrode spacing was computed. The discrepancies between the observed and synthetic curves were then determined. The layer parameters used in the governing equations were then adjusted, and the calculation was repeated with the corrected values, giving a new predicted curve to compare with the field data.

Using modern computers the procedure can be iterated rapidly until the discrepancies are smaller than a pre-determined value, that is, lower root mean square values (Hugh and Roger, 1996). The inversion method is equivalent to matching automatically the observed and theoretical curves. A one-dimensional analysis accommodates only the variations of resistivity and layer thickness with depth or two dimensional where the resistivity also varies along one horizontal direction (Hersir and Bjornsson, 1991). The response of a vertically layered structure has an analytical solution, so efficient inversion algorithms can be established (Hugh and Roger, 1996).

Although characteristic curves can also be computed for the interpretation of structures with multiple horizontal layers, modern VES analyses take advantage of the flexibility offered by small computers with graphic outputs on which the apparent resistivity curves can be assessed visually (Moon *et al.,* 2006). Interpretation of data from profiling surveys was mainly qualitative

(Loke, 2004), therefore showed visually with line graphs of station distance against resistivity.

Existing borehole data were examined. The coordinates, water rest levels, water strike levels, drawdown and yield of the boreholes were noted. The parameters of interest are then extracted with the corresponding coordinates which were then run in surfer 9 and Arc GIS programs to give visual variation and distribution of the Transmissivity and borehole potential yields.

4 CHAPTER FOUR: RESULTS AND INTEPRETATION

4.1 Aquifer Geometry

A total of thirty three (33) VES and three HEP were executed. Seventeen VES were executed in the metamorphic terrain; eleven on the volcanic terrain while five at the transition zone. The analyzed borehole data were distributed in the study area as follows: Eight boreholes were on the undifferentiated volcanics, eight in the andesites/dacites, eight in the metamorphic zone, and one on the granite. The geo-electric models have been grouped into three categories: volcanics, metamorphic and transition.

4.1.1 Geoelectric models within the volcanics

Eleven VES were executed on the volcanic terrain and the results of the geo-electrical sounding curves are presented in Figure 4.1

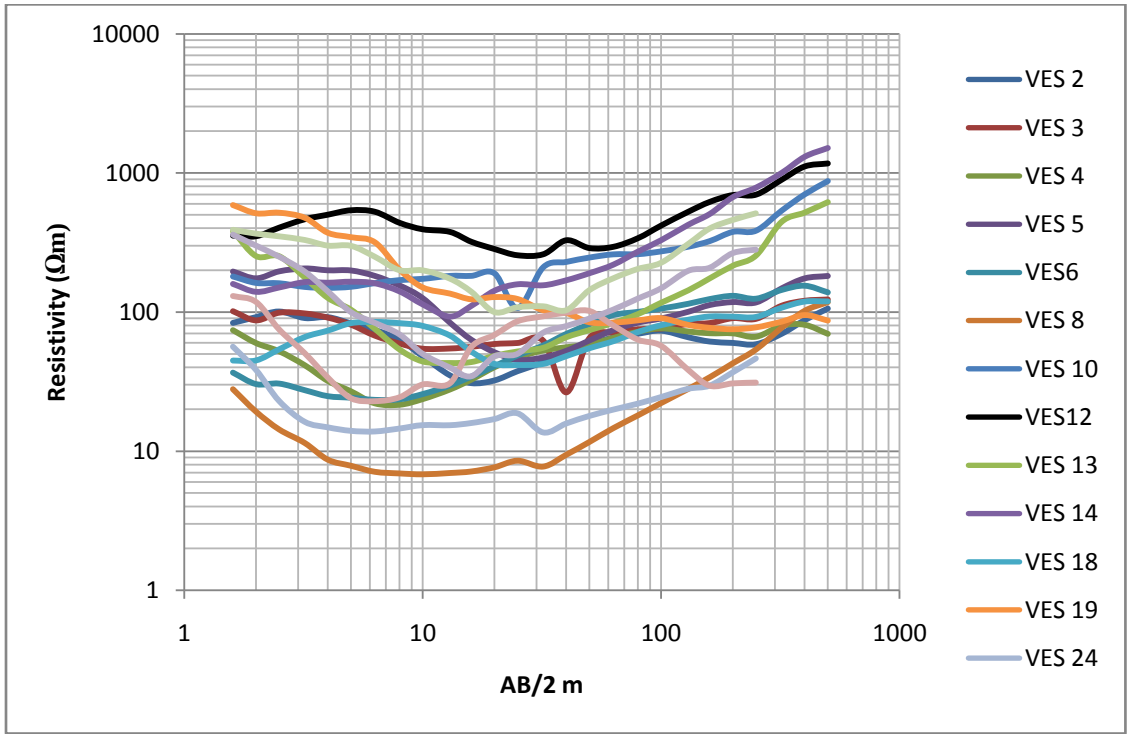

Figure 4.1: Geo-electric sounding curves for volcanic terrain

Generally, the geoelectric curves indicate a descending branch followed by a gentle ascending branch which correspond to upper weathered flowwhose intensity of weathering decrease with depth.

- VES 14, VES 2, VES 13, VES 19, VES 24 indicate thick volcanic sequence with probably deeper aquifers beyond the probbed depth.
- All the other VES indicate a very gentle ascending branch with a descending portion of the curve which depicts a deeper aquiferous zones.

4.1.2 Geoelectirc models within the Metamorphic terrain.

Figure 4.2 shows geo-electric curves that were executed in a metamorphic terrain. Except for VES 9, all the VES indicate a descending limb followed by variably increasing resistivity values. VES 30, VES 27 indicate deep weathering with minor aquifers. VES 2, VES 23, VES 16 indicate deep fractional aquifer represented by a saddle-shaped structure along the ascending branch. VES 25 has the deepest fractional zone.

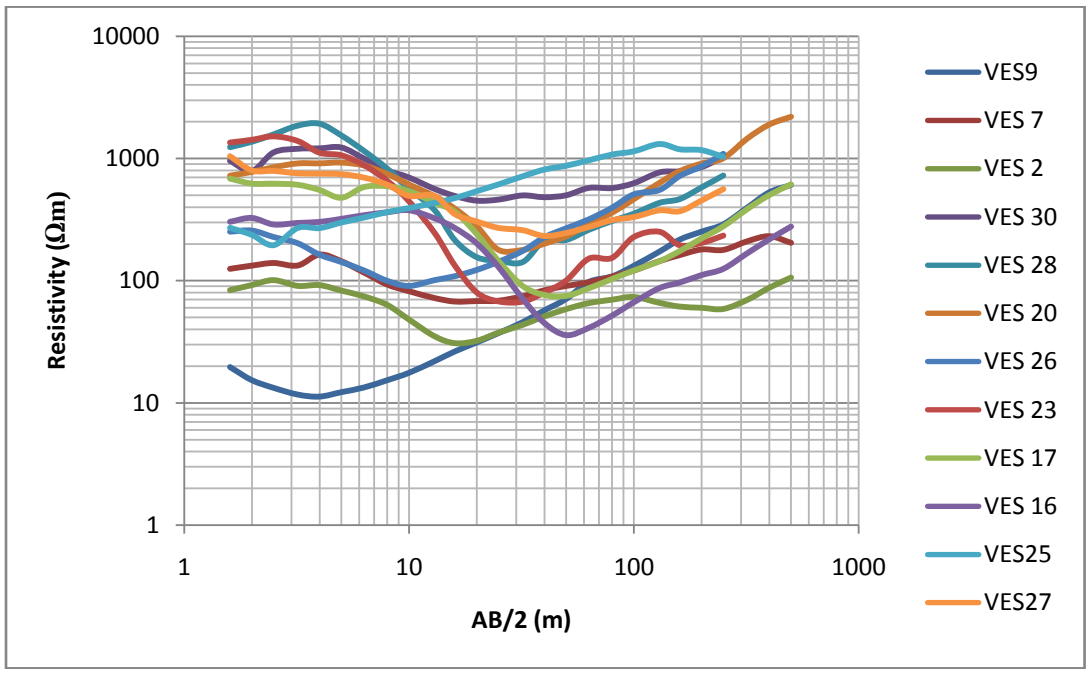

Figure 4.2: Geo-electric sounding curves for metamorphic terrain.

4.1.3 Geoelectirc models within the transitionzone.

The soundings that were executed in the transition zone showed good groundwater potential. The aquifers lie between 20m-150m except for VES 22 shows a thick underlying volcanic sequence followed by fractured metamorphics. The contact zone generally is at 150m beneath which metamorphic rocks are encountered.

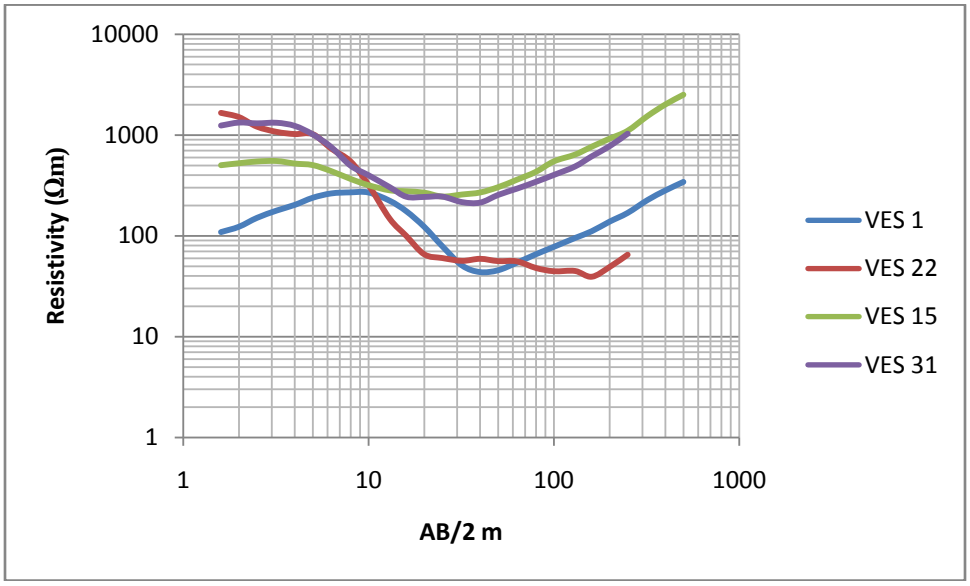

Figure 4.3: Geo-electric sounding curves for transition zone

The geo-electrical sounding curves (Traverse 1 to 6) depicted three to six different geo electric layers. A thick volcanic layer, over 500m bgl was deduced at the Mt. Elgon slopes. Pronounced borehole failure observed within the thick pyroclastics. The volcanic layer became shallower away towards Kitale Plains and Suk Lowlands. At the transition zone, the volcanic layer was about 70m. Groundwater occurrence was highly localised at the volcanic-metamorphic junction and good groundwater potential was expected. In the plains and lowlands, the curves showed three to four layers within the MMB rocks. Groundwater occurrence expected at the weathered zones and within the fractures.

4.1.4 Resistivity pseudo-sections and cross-sections

The depth to the bedrock was determined geo-electrically. A total of six traverses were made: three in the north-south and the other three in east-west directions. The resistivity pseudo sections and resistivity cross sections showed the visual variations of resistivity in the sub surface. Interpretations of the traverse lines are presented as follows:

4.1.4.1 West – East VES

These were the VES points that ran from Mt. Elgon to the east. The VES points were averagely 2 km from each other.

a) Traverse 1

This traverse was made in west-east orientation and represented in Figure 4.4. The VES points that are along the traverse are VES 18, 8, 22, 23, 17 and 16. This was due north of the study area. From Figure 4.4, the volcanic succession was thicker as observed in VES 18. Metamorphic rocks characteristics were not encountered in the whole probed depth. A metamorphic ridge was observed in VES point 8. The ridge was due to higher resistive sequence of the metamorphic rocks. Troughs and depressions bordered these ridges and were deduced to be the highly weathered metamorphic zones or the volcanic sequence. The metamorphics in this zone were weathered with resistivity of 693Ωm and overlain by highly weathered metamorphics. At the location of VES 22, the volcanic layer was approximately 100m bgl. There is compact soil layer followed by two episodes of volcanic flows with resistivities of 50 Ωm and 12Ωm. Good groundwater potential is expected at this volcanic-metamorphic boundary. At VES 23, there exists highly weathered metamorphics to a depth of 150m after which a compact metamorphic layer was encountered. A shallow aquifer expected at 20m bgl and it is unconfined. A compact metamorphic layer of 20m with resistivity of 2900 Ωm is underlain by the main confined aquifer. This aquifer is a highly weathered metamorphic and penetrates up to 150m bgl. In VES 17, weathered MMB rocks were approximately 45m and underlain by a compact MMB rocks. Potential aquifer expected at this weathered zones. At VES 16, the MMB top soil was compact with relatively high resistivity. There was highly weathered subsurface surface of about 20m bgl, which was aquiferous. This layer was sandwiched between MMB rocks and the aquifer is said to be confined. It is worth noting that boreholes drilled at the metamorphic ridge are likely to fail since the ridge acts as water divide hence no appreciable recharge zones to nourish these aquifers.

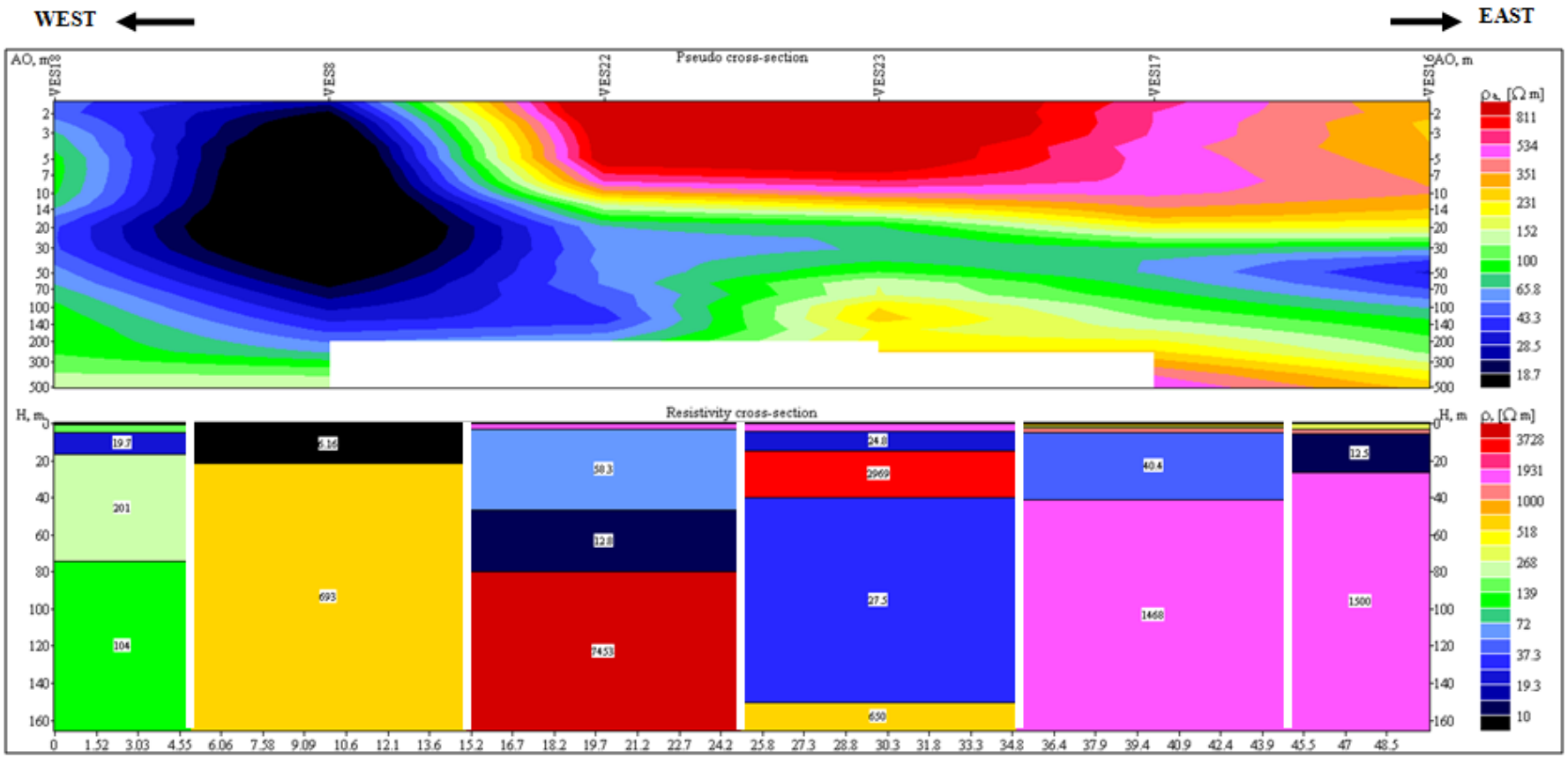

Figure 4.4: Resistivity pseudo section and cross of VES 18, 8, 22, 23, 17 and 16: traverse 1

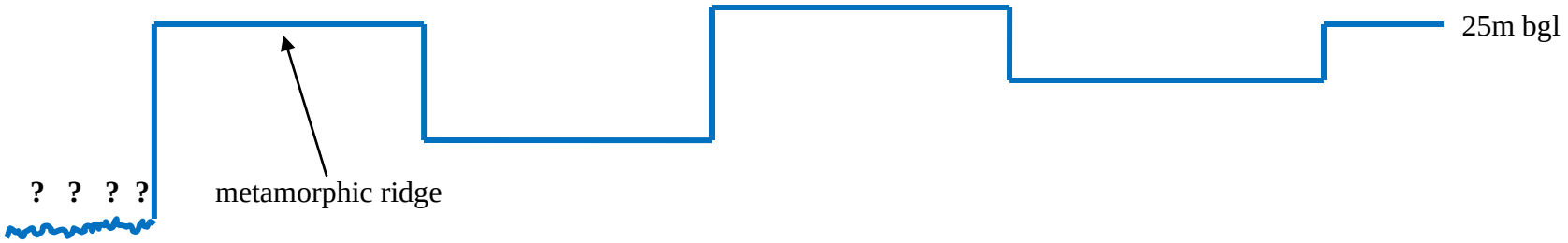

b) Traverse 2

The traverse was in the central part of the study area. From the pseudo-section and resistivity cross section in Figure 4.5, the number of geo-electric layers reduced systematically eastwards. At VES 3, there were six geo-electric layers that represented different phases of volcanic eruptions. The whole probed depth did not show any electrical characteristics of MMB rock. VES 32 had highly weathered volcanic rocks up to 20m bgl with electrical resistivity of 44.2 Ωm. This was succeeded by a highly compact layer of metamorphic rocks to a depth beyond 500m bgl with resistivity value of 3698Ωm. This coincided with the metamorphic ridge that had poor groundwater transmissivity. The ridge was bordered by a lower resistive layer of volcanic materials to the west and a weathered metamorphic layer to the right. The ridge causes a damming effect on both sides of the profile line. At VES 10, there were loose metamorphic soils with lower electrical resistivity. This was underlain by a highly weathered metamorphic rock layer to a depth of 120m bgl with electrical resistivity value of 426Ωm. This layer was further underlain by a compact and highly resistive MMB rocks with resistivity value of 3391Ωm. At VES 12, there were top soils derived from MMB rocks with lower resistivity to a depth of approximately 5m bgl. This was underlain by highly weathered MMB rocks to a depth of 50 bgl with resistivity of 332Ωm. A compact MMB rocks with resistivity of 2360Ωm underlay this layer to a depth exceeding 500m bgl probed depth. Groundwater was expected at the contact between the MMB and the volcanic rocks. Boreholes drilled at the basement ridge are likely to fail since the area has no water recharge.

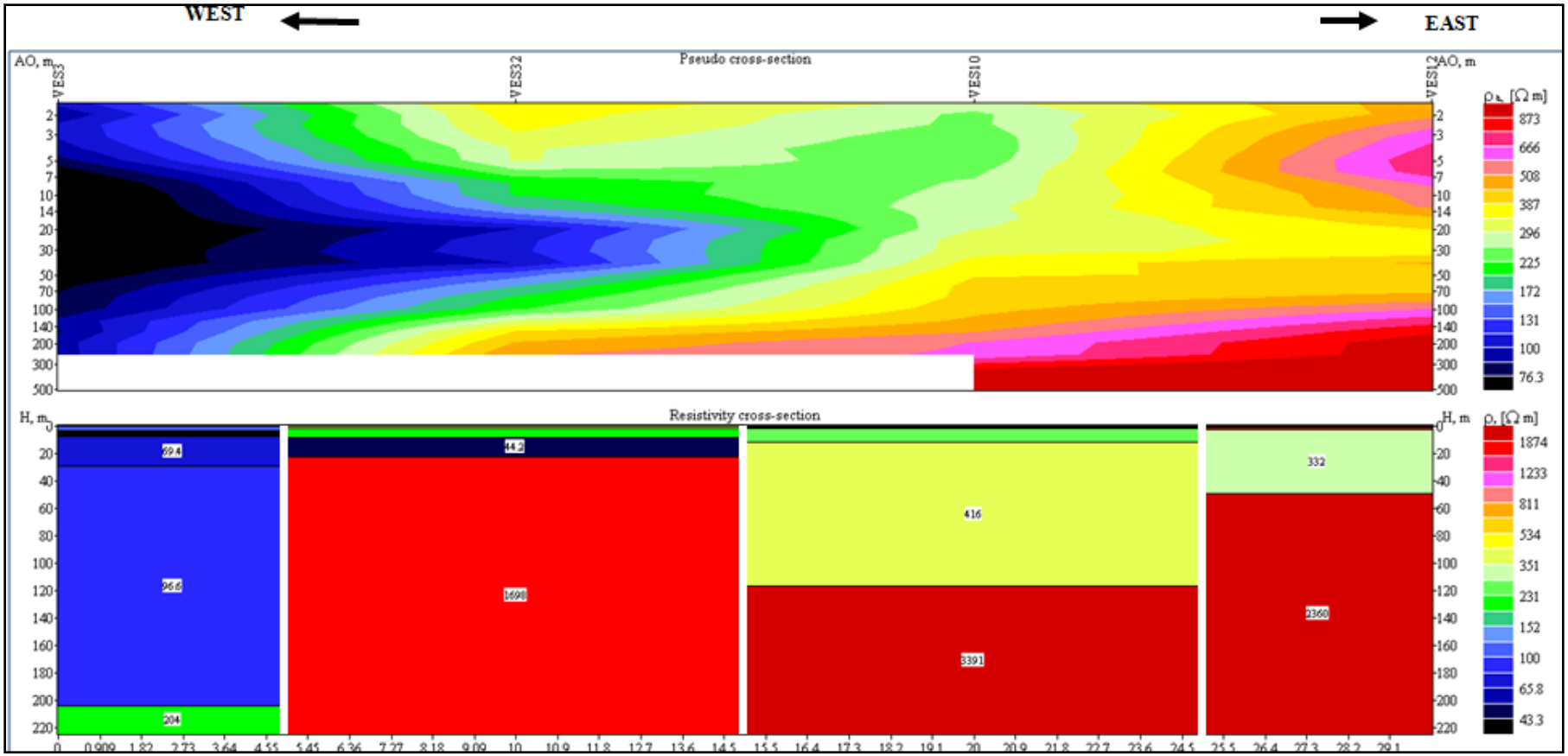

Figure 4.5: Resistivity pseudo-section and resistivity cross section of VES 3, 32, 10, and 12: traverse

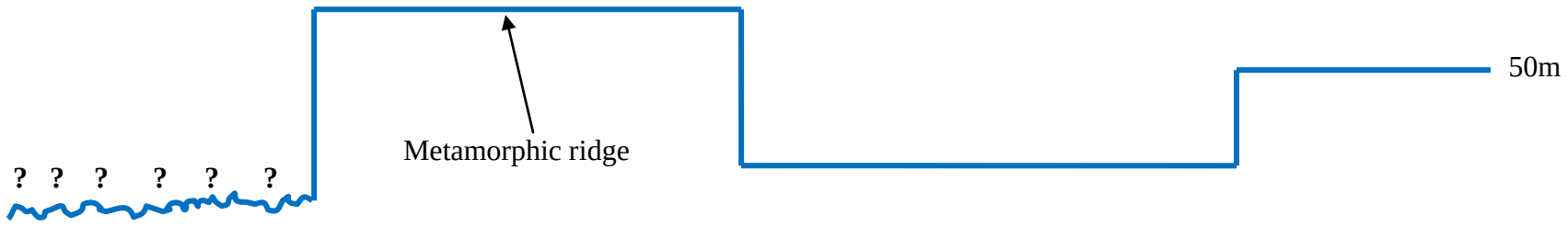

c) Traverse 3

From the resistivity cross section in Figure 4.6 running in east-west direction, there is a thick volcanic layer evident in VES 19 and 29. The layers show a thick volcanic succession with two distinct eruption episodes. In VES 19, a hard volcanic layer with resistivity of about 300Ωm comprising of agglomerates and welded tuffs penetrated up to 15m bgl. Thick volcanic flow then penetrates up to 175m bgl which is subsequently underlain by a different volcanic layer beyond 300m bgl. VES 29, compact volcanic soils are evident to a depth of 5m bgl which is underlain by thicker volcanic flow with resistivity of 30.9Ωm to a depth of 290m bgl. This was envisaged as the first episode of volcanic eruption. Beyond this point is a different volcanic succession layer. At VES 30 and 14, a thin layer of highly weathered MMB rocks of approximately 25m were observed. The remaining depth was a compact MMB rocks with resistivity values of 79729Ωm. VES 30 exhibits highly weathered MMB rocks characteristics. This point coincides with the NE-SW fault whose boreholes failed due to the 'open' nature of the fault. VES 31 had a thicker weathered MMB layer with resistivity of about 3029Ωm up to 60m bgl which was underlain by the compact MMB rocks with resistivity of about 41099Ωm. The metamorphic ridge observed in this traverse acts as water divide.

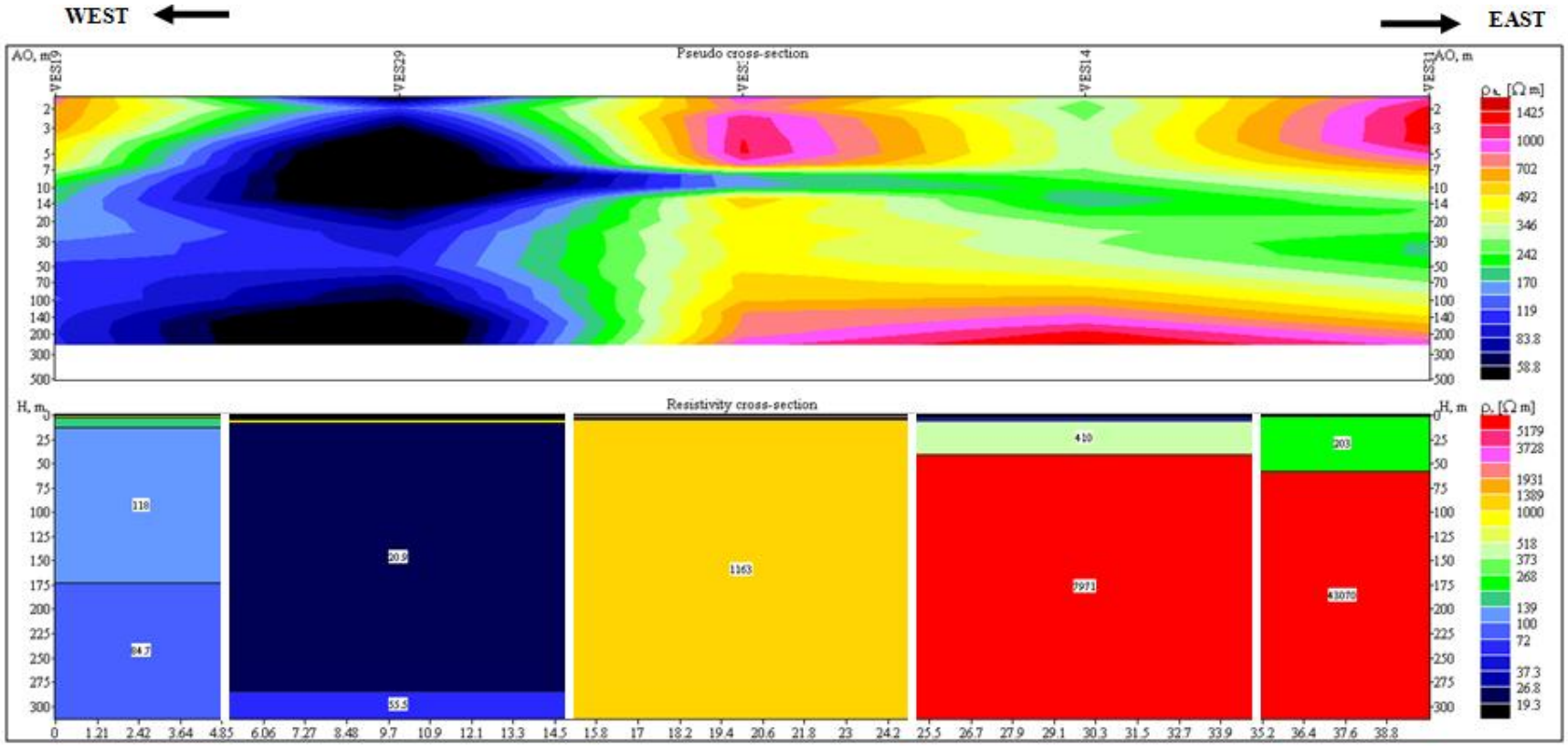

Figure 4.5: Resistivity pseudo-section and resistivity cross section of VES 19, 29, 30, 14, 31: traverse 3

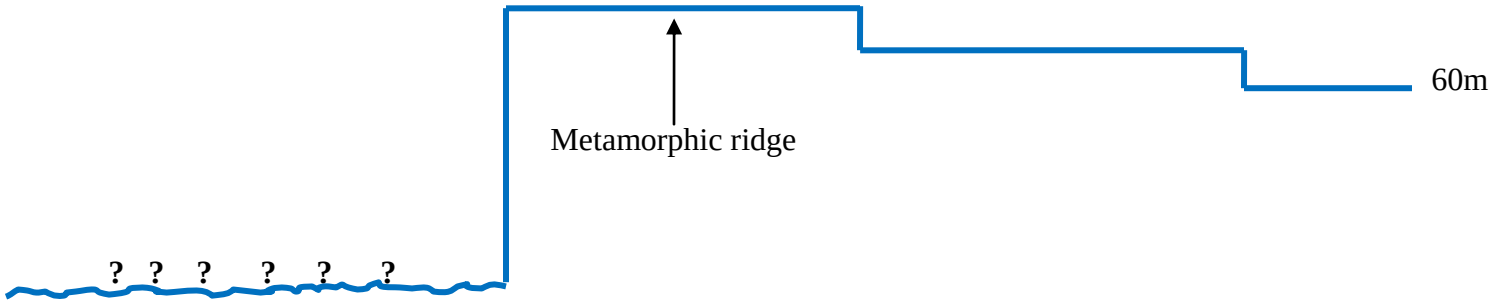

4.1.4.2 North-South VES

a) Traverse 4

The resistivity cross section in Figure 4.7 ran from Chechoina at the north through Mt. Elgon National Park's gate, through Gituamba, Saboti and southwards to Bungoma County. A thick volcanic layer along the profile in VES 5, 3 and 19 was encountered. VES 5 had three distinct volcanic layers with varying resistivity. The first layer penetrates to a depth of 65m bgl with resistivity of 102Ωm underlain by a thicker volcanic layer with resistivity of 144Ωm to a depth of 215m bgl. VES 3 has similar characteristics as VES 5 but with less resistive volcanic flows. The first layer penetrates to a depth of 30m bgl with resistivity of 69.9Ωm underlain by a thicker volcanic layer with resistivity of 96.6Ωm to a depth of 200m bgl. Below this layer is a more compact volcanic layer to with resistivity of 204Ωm. In VES 19, a thin top soil of volcanic origin observed. This is underlain by a very thick volcanic layer with resistivity of 108Ωm to a depth of 180m bgl. Beyond this depth is a highly weathered volcanic layer with resistivity of 64.7Ωm. Boreholes drilled in this area failed since there was infiltration of groundwater into the deeper confining layers. This area coincided with the volcanic window where no metamorphic characteristic was observed. At VES 20 which was further south in Bungoma County, there is highly weathered metamorphic layer with resistivity of 34.2Ωm to a depth of 20m bgl. Most aquifers were expected within the weathered zones and fractures within the MMB rocks.

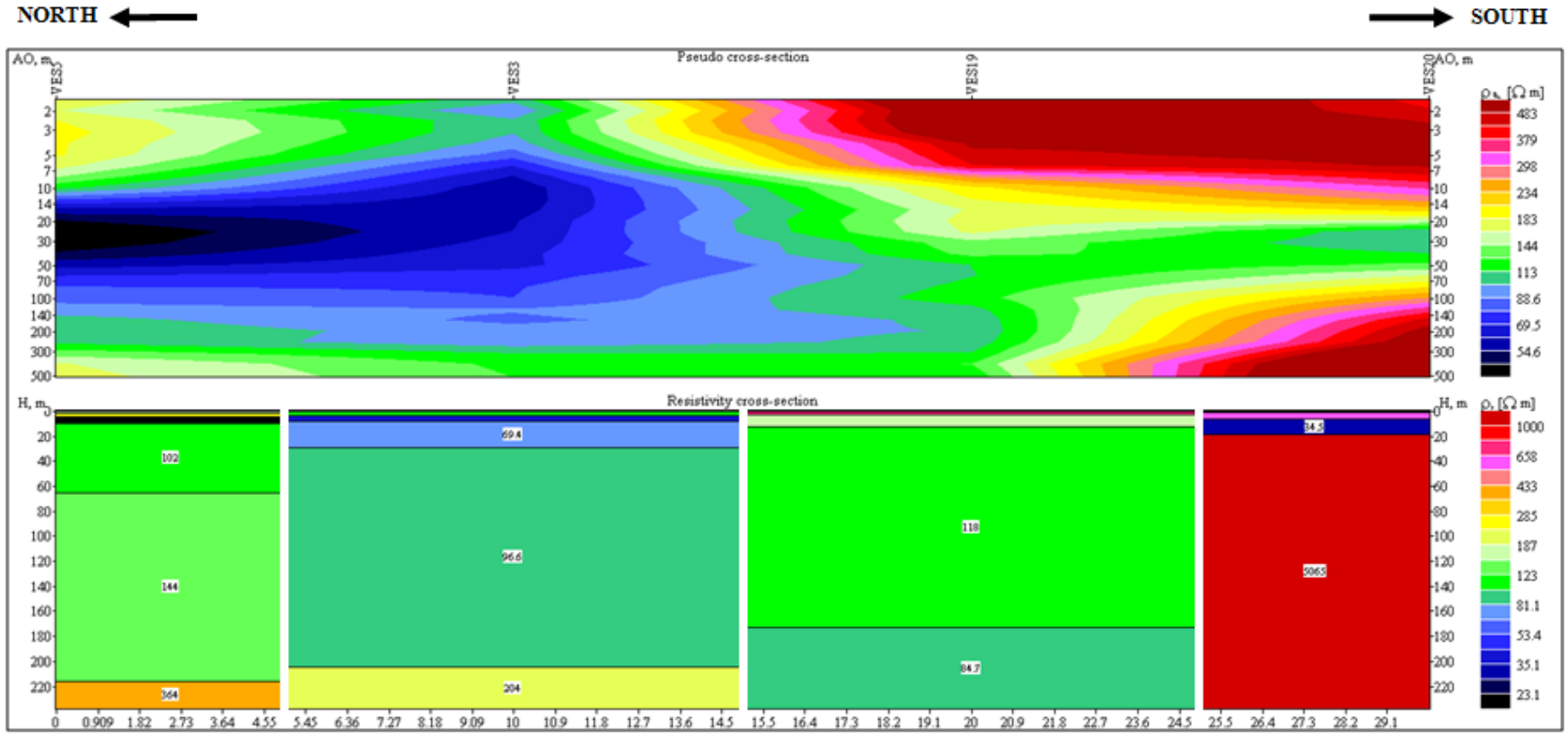

Figure 4.6: Resistivity tomograph and pseudo-section of VES 5, 3, 19, 20: traverse 4

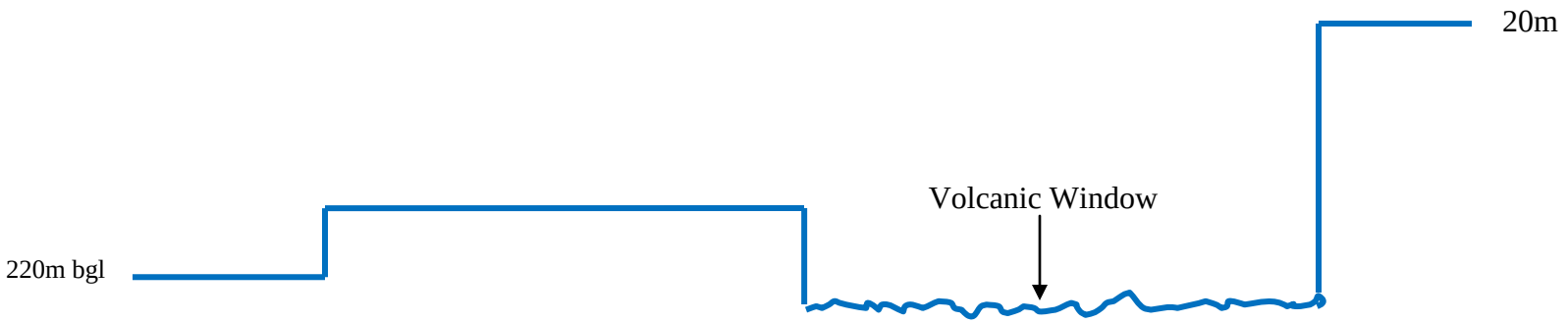

b) Traverse 5

In Figure 4.8, VES 9 shows two distinct metamorphic layers. A highly weathered metamorphic layer with resistivity of 25Ωm is observed from the surface to a depth of 12m bgl. Beyond this depth is a compact metamorphic rock that penetrates the entire probed depth. In VES 8, there is a highly weathered metamorphic rock with resistivity of 6.16Ωm to a depth of 25m bgl. This resistivity has clayey characteristics with poor groundwater Transmissivity. Beyond 25m bgl is weathered metamorphic rocks with resistivity of 693Ωm. VES 21 shows different episodes of volcanic eruptions. There is top weathered volcanic layer with resistivity of 21.2Ωm to a depth of 5m bgl. This is underlain by a resistive volcanic layer to a depth of 50m. Beyond this depth is a highly weathered volcanic layer with resistivity of 37.3Ωm. A volcanic widow is deduced at this zone and pronounced borehole failure due to infiltration of groundwater to the impermeable deeper layers. VES 30 has a highly weathered zone with resistivity of 100Ωm, between 3m to 5m sandwiched between the MMB systems. Beyond this depth is a compact metamorphic rock with resistivity of 2163Ωm. In VES 28, a weathered MMB layer, with resistivity of 109Ωm penetrates to a depth of 25m followed by a compact metamorphic layer with resistivity of 1232Ωm. Potential aquifers in this traverse are expected either at the deeper volcanic layers, fractures or weathered zones within the MMB rocks.

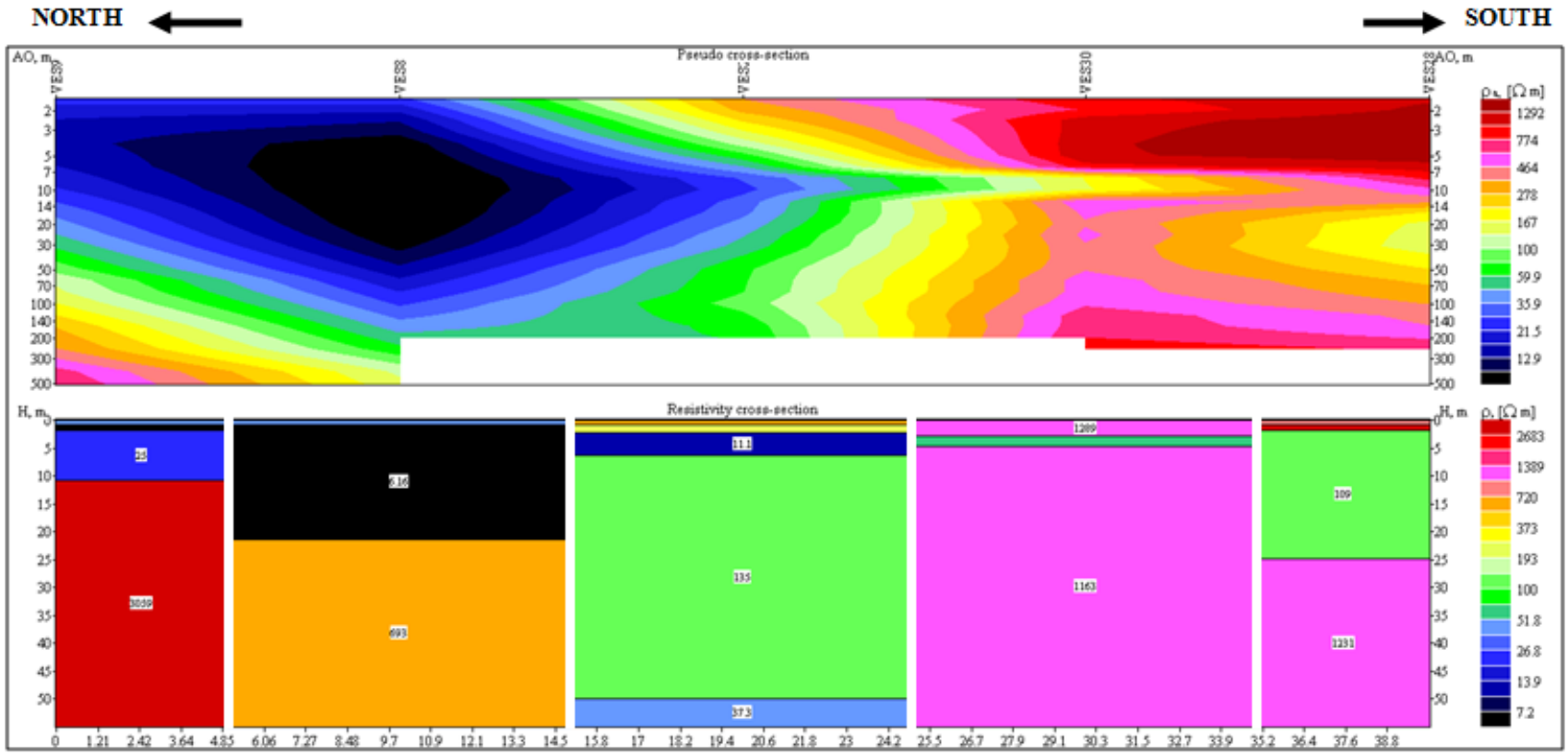

Figure 4.7: Resistivity tomograph and pseudo-section of VES 9, 8, 21, 30, 28: traverse 5

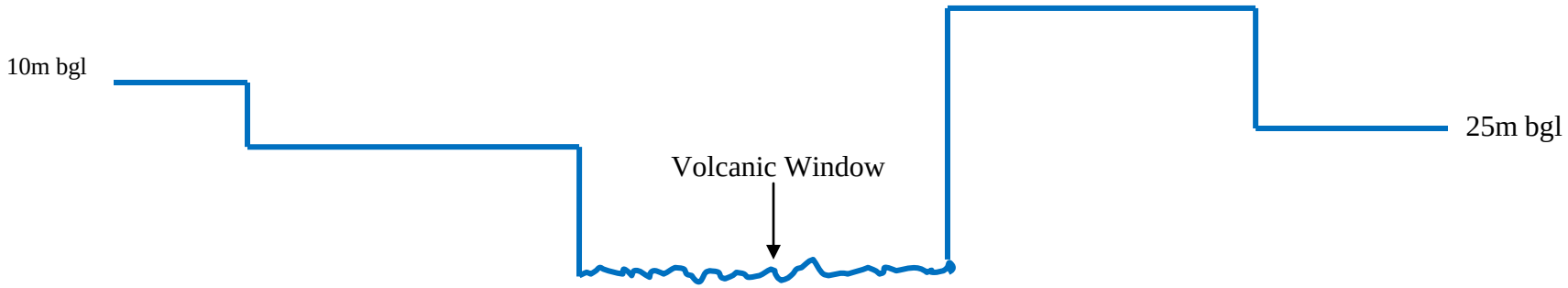

c) Traverse 6

From Figure 4.9, the traverse ran in north-south west of Kitale through Kiminini to the south. VES 16 had four geo-electric layers of volcanic soils followed by highly weathered volcanics up to 20m bgl. Shallow aquifer was expected at this zone which was a contact zone between volcanic formations and the metamorphic rocks. In VES 23, metamorphic rocks were not observed in the probed depth. There were clayey materials sandwiched between weathered metamorphic rocks to about 15 metres bgl. In VES 10, the metamorphic rocks were highly weathered to a depth of 15 metres bgl. A slightly weathered zone of up to 120 meters bgl that was aquiferous and underlain by compact MMB rocks. In VES 13, clayey materials between depths of 5m to 10m bgl, followed by a highly weathered MMB rocks to a depth of 60m bgl. Beyond this layer was a slightly weathered metamorphic zone that depicted an aquiferous zone. In VES 14 and 15, highly weathered MMB rocks up to 40m and 50m bgl respectively were evident in the traverse line. Beyond this depth was a compact basement layer which was relatively thicker. A shallow aquifer between 5m-8m was expected in VES 14.

NORTH ← → SOUTH

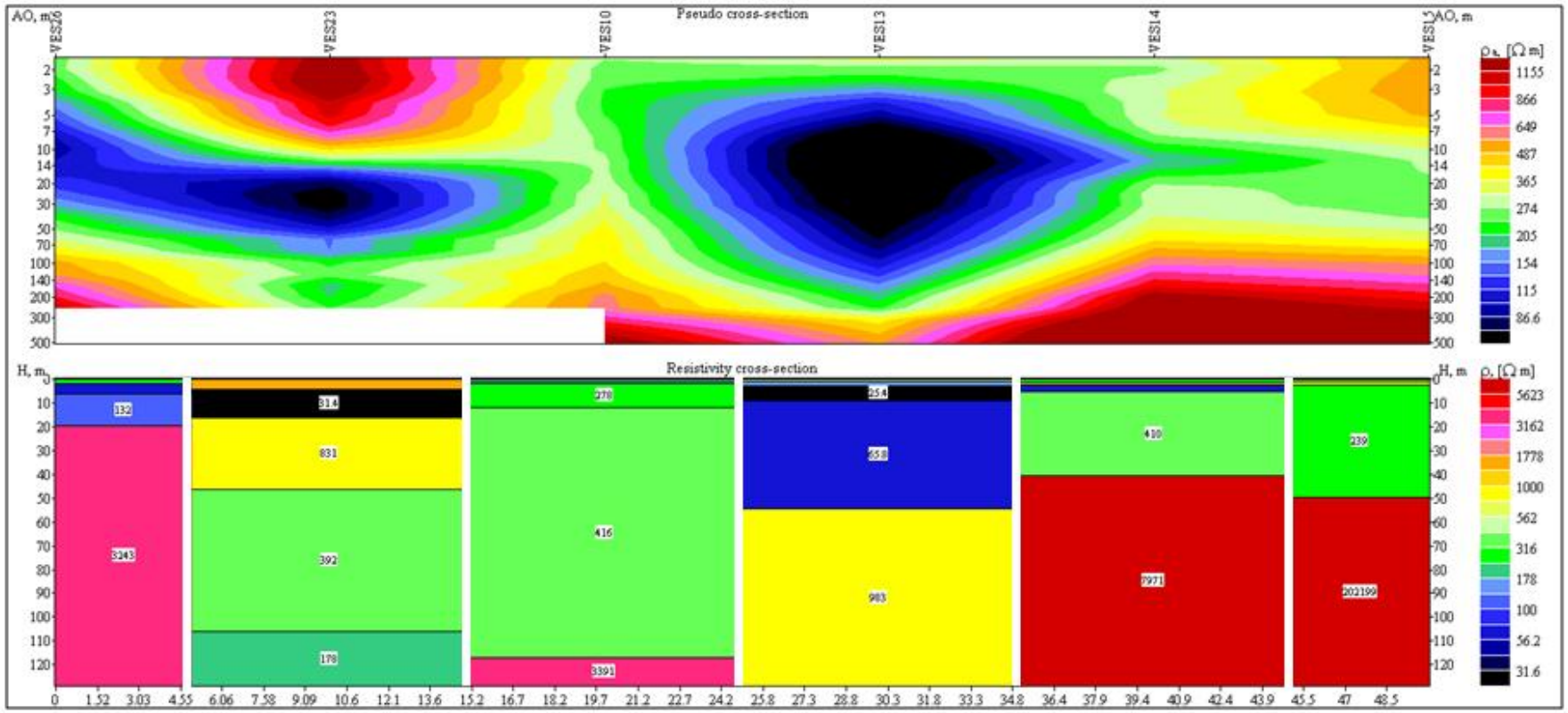

Figure 4.8: Resistivity tomograph and pseudo-section of VES 26, 23, 10, 13, 14, 15: traverse 6

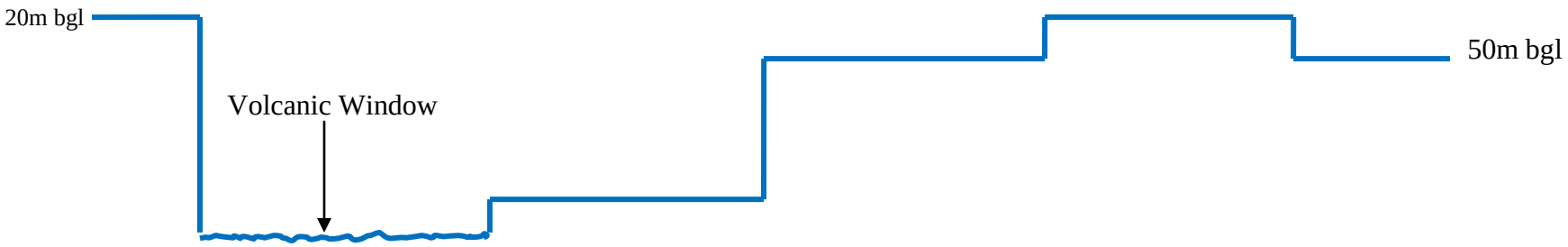

4.2 Groundwater Potential and Structural Influence of Groundwater Flow

In order to determine groundwater potential yield and structural influence on flow direction, groundwater potentiometric map was constructed in meters above mean sea level (masl). The piezometric levels i.e. the flow directions in response to declining hydraulic head indicate the regional groundwater network. The potentiometric values in surfer software were used to contour the grid map by displaying the vector indicating the flow directions. Figure 4.13 shows that re-charge zones are in the slopes of the Mt. Elgon. The discharge zones are around Saboti, Kiminini and Kitale Plains.

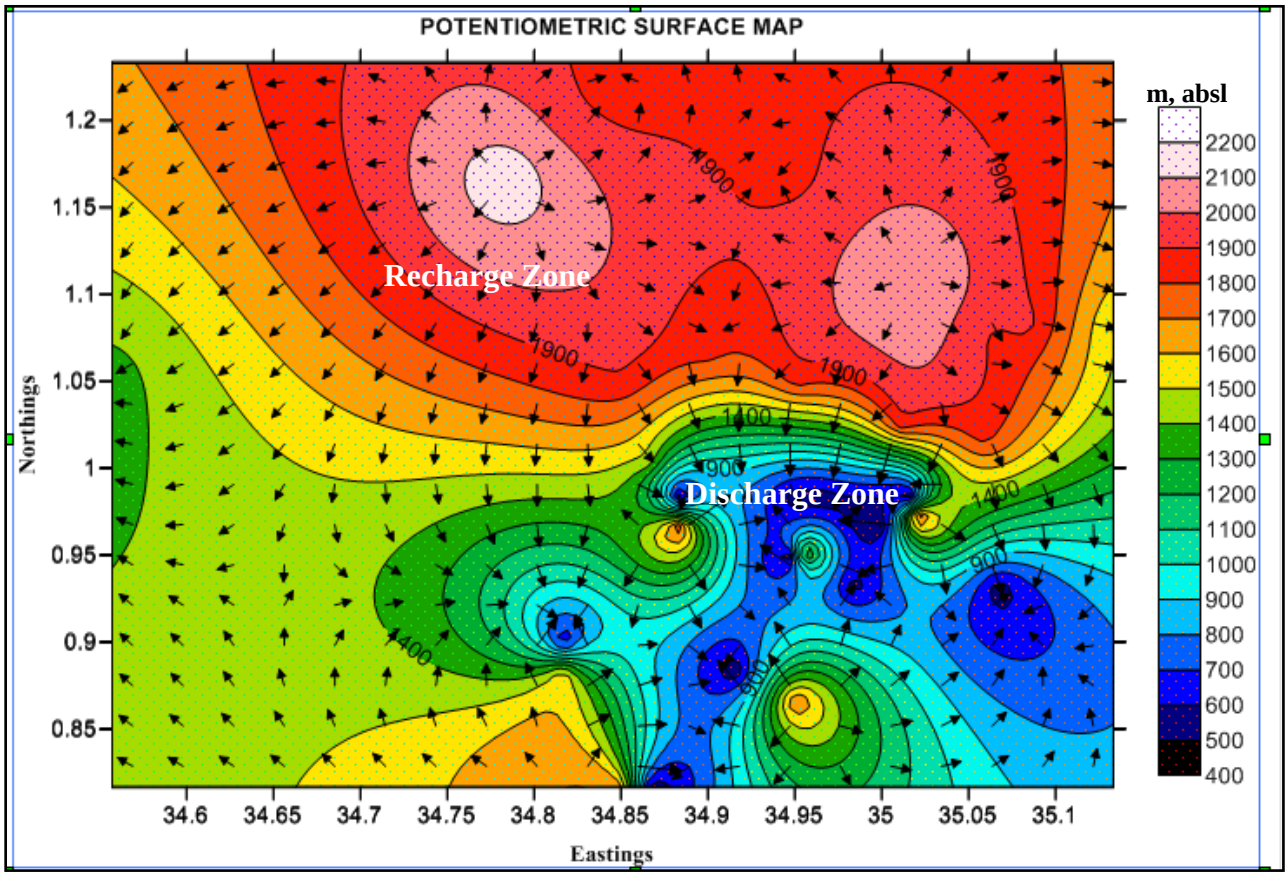

Figure 4.9: Potentiometric surface map of the study area and its environs

From the borehole potential map above, the higher potential boreholes with piezometric surfaces between 1400m to 2200m are to the north and southwestern quarters. This coincides with Mt. Elgon slopes. This is a volcanic zone and a bluff was observable around Koykoy area at Kahoya Farm. Minor fractures were inferred from Saboti towards Kiminini in a NE-SW direction. There

was a major fracture trending slightly in the same direction to the north which had medium yielding boreholes. In the NE quarter towards Kacheliba, SE quarter towards Kwanza had lower yielding aquifers with some failing completely. Groundwater recharge was from an area of higher hydraulic head to the area of lower hydraulic head.

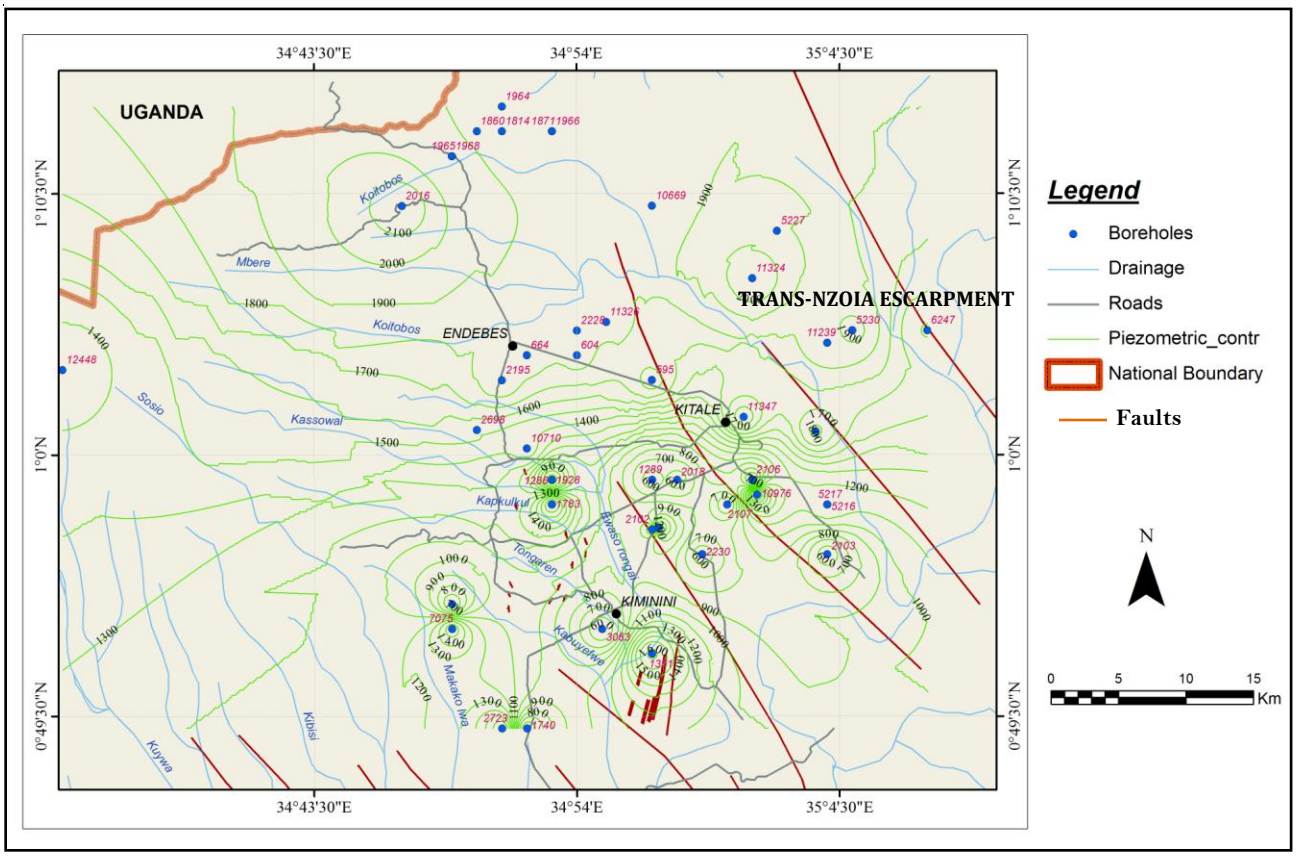

Figure 4.10: Map show relationship between the piezometric surface and structures

From Figure 4.11, there is structural influence of groundwater flow. NW-SE fault passing above Kiminini have a greater influence to the groundwater flow. From the piezometric surface map, this coincides with the aquiferous zones where groundwater from the elevated grounds of Mt. Elgon and Cherangany is discharged. Other minor fractures passing through Saboti are observed be discharge zones with good potential. The other major faults that pass through Kitale and Kwanza are not corresponding to the groundwater networks. These faults are on the MMB rocks. They are probably open faults without recharge. It is worth noting that the resistivity values are considerably lower to support groundwater occurrence but numerous borehole failure are exhibited in this area.

HEP 1: Mt. Elgon Flowers-Suam road

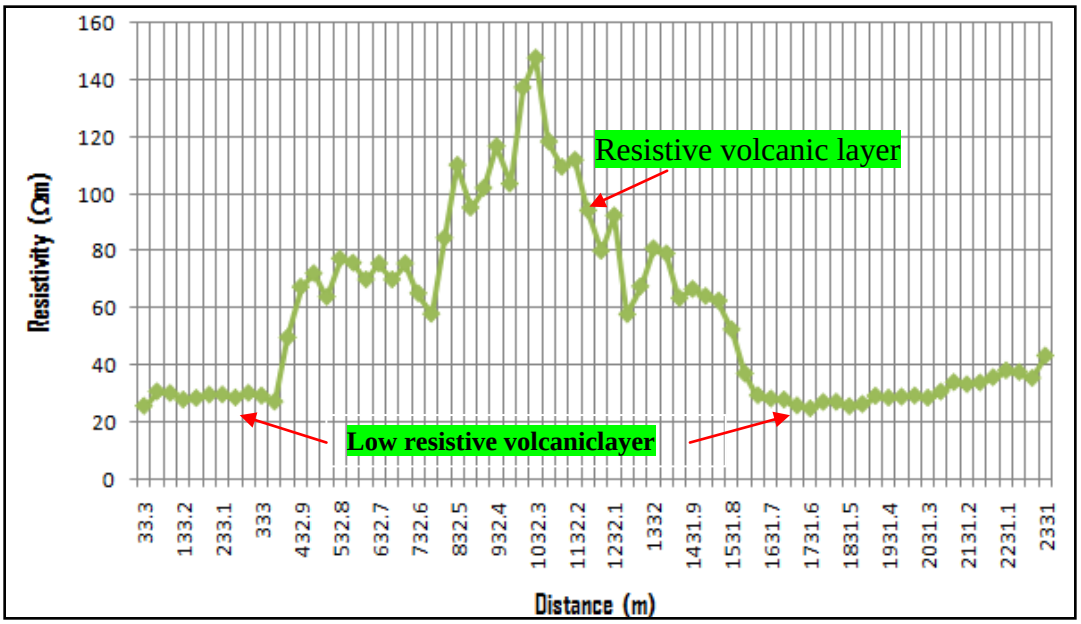

Figure 4.11: Resistivity variation at 100m depth for HEP 1

Figure 4.14 shows a qualitative representation for profile 1 that was carried out along Endebess-Suam Road at Andesen/Mt. Elgon flowers. The area has volcanic boulders. The profile confirmed compact volcanic at the central point with higher resistive layer. Lower resistive layer are at the edges of the profile. The results conform to the VES 4 results that had a thick volcanic overburden beyond 100m.

HEP 2

The profile was done around Sabwani ADC farm. A volcanic layer is present at a depth of 100m. To the west, there exist a more resistive volcanics that were considerably heavier hence could not be blown far from the vent during the volcanic eruption. Volcanic ash was blown further eastwards along the profile. Pronounced borehole failure can be attributed to the thick pyroclastic rocks and the volcanic ash. These materials are porous and permeable hence groundwater infiltrates freely to percolate at the more confining layers.

Figure 4.12: Resistivity variation at 100m depth for HEP 2

HEP3

Figure 4.14 represents profile 2 that was done along Kiminini-Bungoma road at Muungano area of Nabiswa Ward in a MMB terrain. Figure 4.14 below shows four distinct fracture zone.

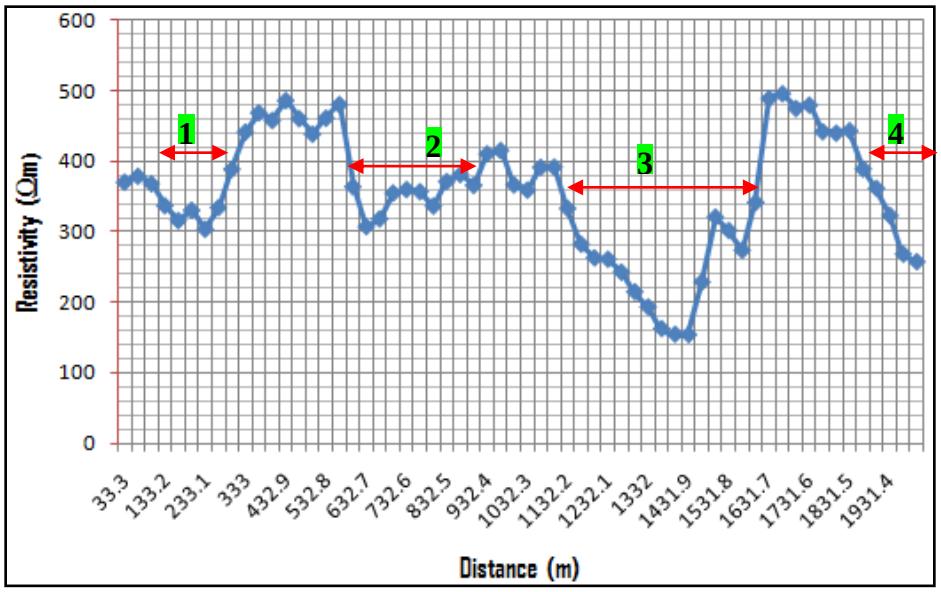

Figure 4.13: Resistivity variation at 100m depth for HEP 3

Fracture zone 1 is characterized by marginal fractures with resistivity above 300Ωm. Fracture zone 2 have resistivity values between 300Ωm-410Ωm. The faults are examples of open faults that are not aquiferous. Fault zones 3 and 4 have lower resistivities of below 250Ωm. Zone 3 can be aquiferous but since there was no groundwater recharge in the area, pronounced borehole failure was experienced.

4.3 Aquifer Transmissivity and Geology

From transmissivity map (Figure 4.15), the transmissivity of the aquifer is between 40m^2/day to 90m^2/day are to the SW quarter. The area lies in Ingavi Farm, Saboti District Hospital, Kisawai, Rafiki, Waumini and Tall tree areas within Saboti Sub County. This is a volcanic zone and a Koibotoss and Koykoy bluffs are very evident volcanic features around. The high transmissive aquifers are due to the contact zone between the volcanic and MMB rocks. There is a distinct contact zone trending north-south from Saboti northwards to Endebess area.

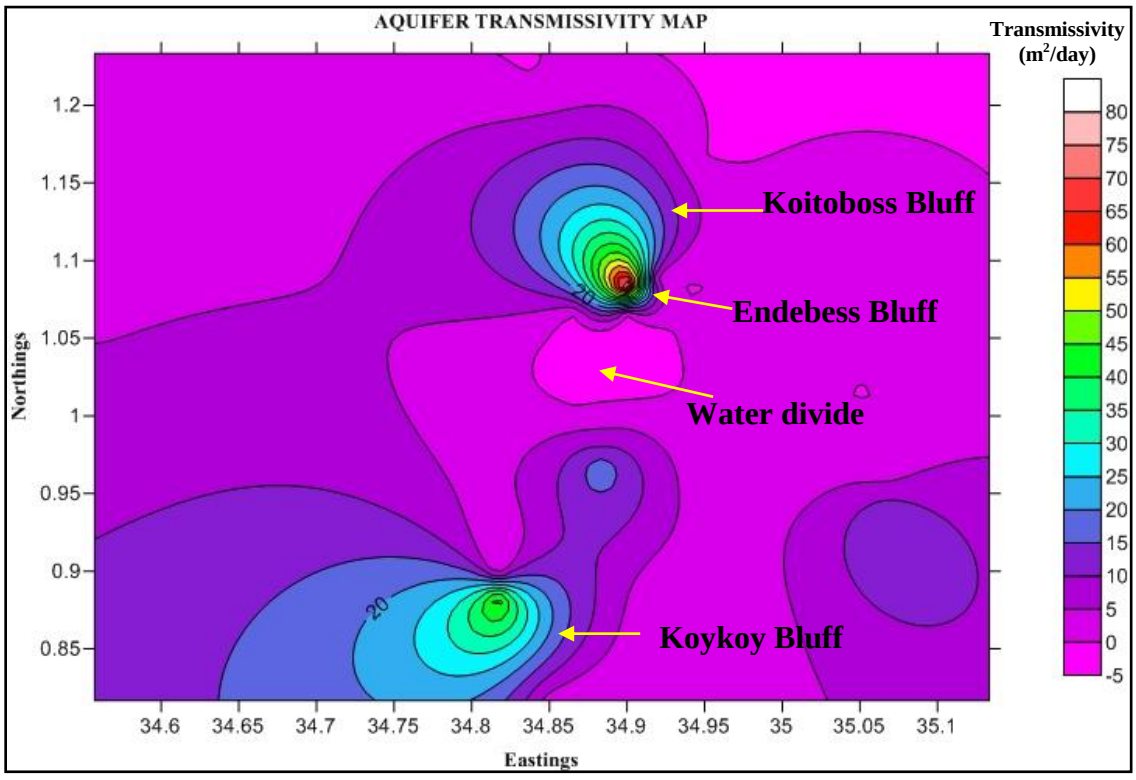

Figure 4.14: Transmissivity map of the existing boreholes.

(Dixey, 1948) noted that the Kitale plain, which forms part of the pre-Miocene peneplain of the Trans-Nzoia County, has a slight Southerly tilt, with the principal drainage system flowing to-

wards Lake Victoria. The maximum elevation appears to lie along an east-west line corresponding to latitude 1° 10' N (Dixey, 1948), which forms a watershed between the Nyanza drainage area and that of the Lake Turkana area. North of this line, the Kitale plain dips gently Northwards to the Trans-Nzoia escarpment. This maximum elevation marks the water divide of the area with no surface and groundwater resources potential. There is no recharge in the area as depicted by the transmissivity map (Figure 4.15).

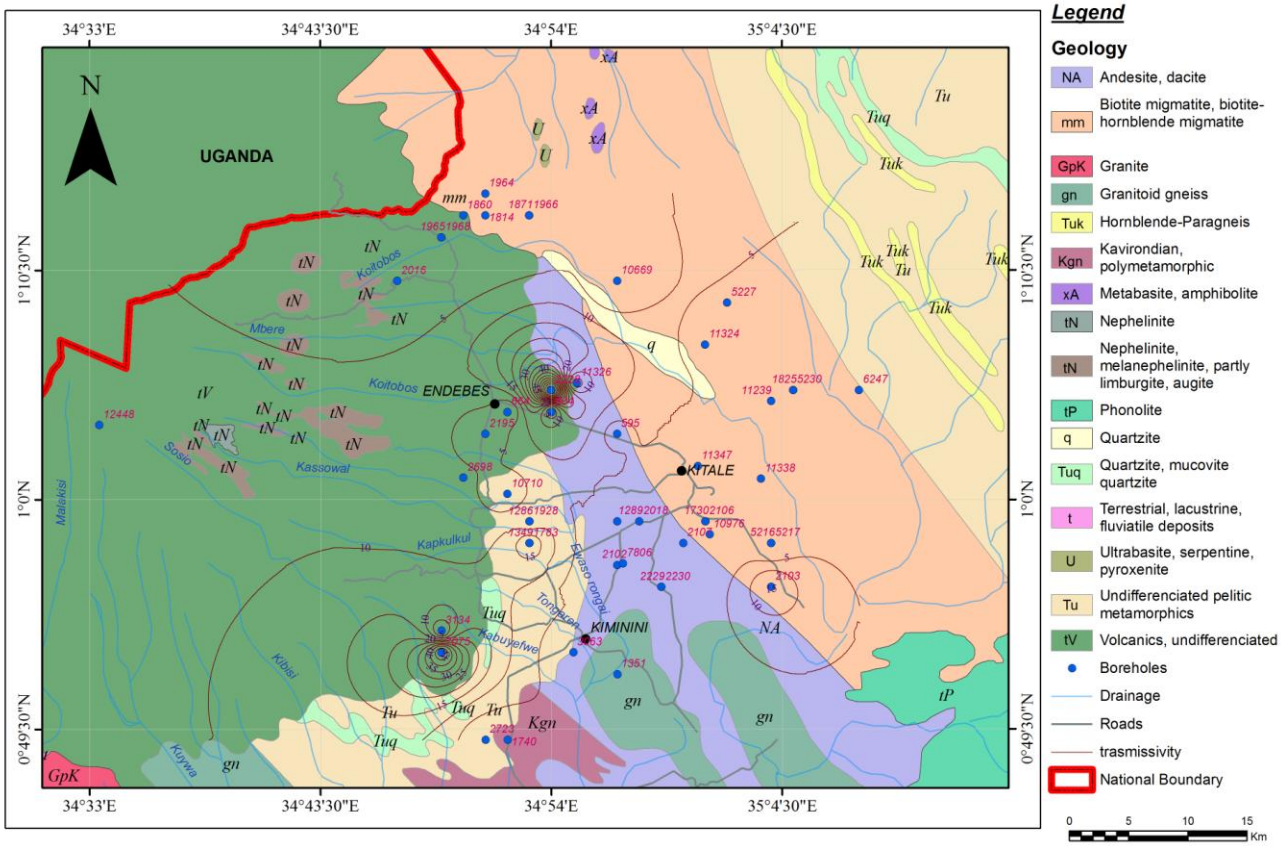

Figure 4.15: The relationship between geological formations and aquifer Transmissivity

The borehole data Table 5.1 indicates groundwater occurrence from a depth of 9m in some localities to as deep as 79m in others. The shallow aquifer is mainly from a shallow well-constructed to a depth of only 15 m. The main water strike within the deeper boreholes ranges from a depth of 24-79m. All these boreholes are located on the lower reaches of the Mt. Elgon pyroclastics. The water strike levels are very shallow i.e. from a depth of 3-46m bgl, which much higher than the corresponding water strike levels especially for the shallow borehole which stands at 76m. Consequently, it can be concluded that for all borehole with complete data the aquifer is confined.

These recorded specific capacities ranging from 0.01 m^3/hr (C10710) to 0.28 m^3/hr (C2229) translating to transmissivities of 0.14 and 6.72 m^3/day respectively. The average specific capacity for the 20 boreholes is 0.12 m^3/day and transmissivity of about 2.8 m^3/day. These values generally indicate low groundwater potential within the metamorphic rocks.

5 CHAPTER FIVE: DISCUSSION

5.1 Aquifer Geometry

From the geophysical survey conducted in the area, the east-west traverses show a thickened western block covering the entire foot of Mt. Elgon. The volcanic thickness at the mountain foot is more than 500m and this thickness reduces uniformly away from the mountain slopes towards the Suk Lowlands and Kitale plains. The three east-west traverses reveal a metamorphic ridge in the central region of the study areas can be observed from VES 22, 32 and 30 in traverses one, two and three respectively. Aquifer geometry is well defined in east-west direction with greater depth to bedrock at the mountain slope. The depth reduces and the bedrock topography becomes shallow eastwards to a depth of approximately 20m. There are weathered metamorphic zones in traverses 2 and 3 to a depth of approximately 50m.

The north-south traverses show defined bedrock topography. Traverse 4 shows a very thick volcanic exceeding the probed depth. The traverse passes from Molem/ Chepchoina to the north through Gituamba, Saboti area to Bungoma County southwards. The VES 20 data showed highly weathered metamorphic rocks to a depth of 20m. This depicts shallow bedrock topography to the south. Traverse 5 and 6 show similar aquifer geometry. VES 21 and 23 in traverse 6 and 5 denotes a narrow corridor of volcanic sequence. The VES points are situated to the east of Endebess Town. Traverse 5 shows highly weathered metamorphic rocks to a depth of 50m the south before fresh metamorphic rocks are encountered. Shallower bed rock topography with a depth of 25m is observed in traverse 6.

5.2 Groundwater Potential and Structural Influence on Groundwater Flow

From the resistivity measurements conducted, the analyzed models depicted dominantly a 3-6 geo electric layers within the volcanic and transitional zones. To the south of the study are, around Saboti, there were volcanic flows that penetrated to depths greater than 300m. The individual volcanic flow episodes accumulated significant amount of groundwater within the foliated volcanic layers. The uniformity and porosity of volcanic materials were the major contributors of successful boreholes in the area. Foliations surfaces acted as aquifers where the interface of the

successive layers had differing hydraulic characteristics. In this area, water bearing zones are found within the weathered volcanic layers, different depositional layers of volcanic materials and fractures within the compact volcanic as deduced from HEP 1 and HEP 2.

Along faulted or fissured rocks weathering can penetrate much deeper, thus creating sub-vertical zones filled with relatively coarse, weathered material. HEP 3 showed a fresh MMB rocks at 100m with unpredictable fracture zones along the profile. The fracture zones generally have a much higher transmissivity than their surroundings as observed in VES 27 and VES 33. Major faults may extend well beyond the surface catchment, thus intercepting adjacent aquifers or surface sources as depicted in VES 27. The sub vertical fault penetrates up to 146m below ground level. Scattered boreholes in the area occurred primarily along these weathered fractures and faults. The borehole had a relatively constant yield despite changes in precipitation. There are faults or fissure zones that, despite having all the properties of a water bearing zone, are not productive due to a lack of recharge. These were either dry faults or open fractures that did not have substantial recharge. Geo electrical survey conducted around Kwanza and north of Endebess exhibited this phenomenon despite presence of the presence of fault line. The area being relatively flat did not have sufficient recharge to replenish the underground water thereby resulting to either very low yields or no water.

Borehole yields in the volcanic terrain are moderately high and occur within the successive volcanic layers. Difference in mineralogy of the volcanic successions results in to contrasting transmissivity thereby influencing the recharge and percolation of the groundwater. At the transition zone between the MMB and the volcanic rocks, the yields are good and groundwater occurrence is mainly weathered MMB zones that were exposed before Mt. Elgon eruption (Miller, 1956).

5.3 Transmissivity and Geology

Three boreholes (C-1965, C-2016, and C-1968) drilled on the upper reaches of the Mt. Elgon struck no water despite being drilled to depth of 37, 32 and 72 m bgl. The main reason could largely be due prevalence on thick pyroclastics and limited recharge at those heights. The hydraulic conductivity is high within the primary pores of the volcanic. The groundwater therefore, infiltrates rapidly and percolates deep in the confining metamorphic zone. About sixteen (16)

boreholes were drilled within the volcanic series with specific capacities varying from 0.07 m^2/ day to 66.24 m^2/day, with an average of 33.16 m^2/day. The transmissivity values ranges from 1.76 to 80.81 m^2/day (Table 4.1), which indicates a huge disparity in aquifer characteristics despite the boreholes being on the same volcanic formation. See Appendix 4 for the existing boreholes within the study area and its environs.

ID/CODE	ALT(m)	T.DEPTH(m)	WSL(m)	WRL(m)	Q(m^3/day)	C (m^2/day)	T (m^2/day)
C-604	1840	88.000	76.000	3.000	3.120	1.026	1.251
C-664	1900	145.000	79.000	9.000	1.38	0.473	0.577
C-2018	2180	70.000	69.000	12.000	1.800	0.758	0.925
C-2195	1900	171.000	24.000	18.000	DRY	-	-
C-2228	1840	15.000	9.000	8.000	2.760	1.840	44.160
C-2698	1910	131.000	100.000	46.000	1.560	0.070	1.760
C-2228	1880	15.000	9.000	8.000	2.760	66.240	80.810
Range	**1840-2180**	**15.000-171.000**	**9.000-79.000**	**3.000-46.000**	**0-3.120**	**0.473-66.240**	**0.5772-80.810**

Table 5.1: Specific capacity, transmissivity of boreholes in volcanic terrain

Where:

ALT is the altitude above mean sea level taken by GPS

T.DEPTH is the total drilled depth of the borehole

WSL is the water strike level in metres below mean ground level

WRL is the water rest level below mean ground level

Q is the aquifer yield per day

C is the specific capacity of the borehole

T is the aquifer transmissivity

The aquifer transmissivity is higher on the volcanic bluffs: Endebess and Koibotoss to the north, Koykoy Bluff to the south. A distinct contact zone is evident with better aquifer transmissivity. Groundwater from the Mt. Elgon slopes travel at the volcanic-metamorphic contacts. Groundwater at these zones travel in a direction with reducing hydraulic head, since the bedrock topography becomes shallower with distance from the mountain. Aquifers are well recharged and springs are observed flowing freely between the rocks.

In the metamorphic terrain, a total of 9 boreholes have been drilled. The boreholes are relatively

shallower i.e. less than 100m which denotes shallow occurrence of the groundwater. The shallowest groundwater was struck at a depth of 18m for a borehole drilled to a depth of 26m while the deepest boreholes was drilled to a depth of 100m and struck water at 50m. The average strike is at 39m. Two boreholes (C-10976 and C11326) struck aquifers at two levels two aquifer i.e. 33 – 76m and 44-60m respectively. This would largely indicate a shallow water strike within the weathered horizon while the deeper strike is confined within the fracture system.

ID/CODE	ALT(m)	T.DEPTH(m)	WSL(m)	WRL(m)	Q(m^3/day)	C (m^2/day)	T (m^2/day)
C-2229	567	26.000	18.000		18.0000	0.840	0.280
C-10976	1840	84.000	76.000	33	16.600	3.000	0.070
C-1286	552	40.000	27.000		20.000	1.920	
C-1928	549	79.000	76.000		32.000	3.600	0.120
C-10710	1465	100.000	50.000		16.800	0.430	0.010
C-595	1850	40.000	33.000		12.000	2.280	
C-11326	1848	85.000	60.000	44	14.500	4.600	0.180
Range		**26.000-100.000**	**18.000-76.000**	**33.000-44.000**	**12.000-32.000**	**0.430-4.600**	**0.01-0.18**

Table 5.2: Specific capacity, transmissivity of boreholes in metamorphic terrain

Where:

ALT is the altitude above mean sea level taken by GPS

T.DEPTH is the total drilled depth of the borehole

WSL is the water strike level in metres below mean ground level

WRL is the water rest level below mean ground level

Q is the aquifer yield per day

C is the specific capacity of the borehole

T is the aquifer Transmissivity

Groundwater in the basement terrains is found mainly in the fractures and faults. This was observed in H.E.P. 2 (Muungano area, Nabiswa) to the south. The aquifer transmissivity of these wells and boreholes were fairly good and are mainly influenced by fractures and weathered crystalline MMB rocks. The poor transmissivity of the confining MMB system ensured better perco-

lation with little or no seepage both laterally and vertically. This was evident in the boreholes around Misanga, Kabomboi, Kolongolo and Lunyu areas of Kwanza Sub County that had clear water.

Dixey (1948) observed that a maximum elevation appears to lie along east-west line corresponding to latitude 1° 10´ N and runs in an east-west direction, which forms a watershed between the Nyanza drainage area and that of the Lake Turkana area. This zone is important for both surface and groundwater flow patterns. The aquifer transmissivity between 1° S to 34.8°E and 1.05° N to 34.95° (Figure 4.14) is less than 1. This zone is a water divide that influences both surface and groundwater flow. Undifferentiated pelitic metamorphic rocks are the geological rocks in this zone. Kitale Plains that form pre-Miocene peneplain has a slight southerly tilt with the principal drainage pattern flowing to Lake Victoria.

6 CHAPTER SIX: CONCLUSION AND RECOMMENDATIONS

6.1 Conclusions

From the discussion, the research concluded that:

a) There is a thick layer of volcanic materials at the Mt. Elgon slopes and this layer reduces progressively away from the mountain until the MMB rocks dominate. The geometry is well defined. There is a metamorphic ridge between 1° S to 34.8°E and 1.05° N to 34.95° which acts as water divide between Turkana and Lake Victoria drainage basins.

b) Structural orientations are predominantly north west- south east. Other minor structures are north-south as can be observed in surface water flows. A volcanic window is observed at the end of the volcanic flows and the contact zones at these points have been exposed to the surface. Groundwater discharges at these contact zones as springs.

c) Boreholes in the volcanic terrain are high yielding than those in the MMB terrain. The contact zones have good borehole potential yields.

6.2 Recommendations

From the geophysical and geological observations in Mt. Elgon area, it is recommended that siting a borehole in Saboti and Gituamba areas require thorough knowledge of the geo electric behavior of agglomerates. This is because resistivity of cementing matrix and that of boulders/clasts differs. One can easily confuse subsurface matrix as an aquifer.

In Koykoy area, Kahoya farm North of Saboti town, there are very productive springs which are yielding even during dry periods. The locals are advised to harvest this water since most of the shallow boreholes in the area dry up during dry seasons.

In Endebess area, the geophysical data reveal that boreholes should be drilled to a depth of 100m for sustainable water. Shallow wells should penetrate to a depth of 40m.This is a confining layer that represents a new episode of volcanic eruptions. Most of the shallow wells drilled dried up during dry seasons. The residents drilled deeper to tap the groundwater that seeped and percolated in the lower confining volcanic layers.

Groundwater in the area is mainly recharged through the regional faults and fractures. The north-south trending faults are responsible for groundwater flow. The main recharge zone is Mt. Elgon which has numerous rivers flowing through the slopes. There is reduced groundwater recharge during dry seasons hence shallow wells should be dug deeper to exploit the potentially viable aquifers.

It is further recommended that siting of boreholes should be done at the fault lines or fissures in the MMB terrains. At the transition zones, the geophysical investigation should try to map the contact zones between the MMB and the volcanic rocks. These zones have better recharge due to better transmissivity hence higher yielding boreholes.

From comprehensive aquifer geometry mapping, more geophysical methods should be used to validate the results obtained by DC resistivity method. Seismic reflection and gravity methods should be carried out by future researchers to map the bedrock topography (aquifer geometry). Core drilling should be enhanced since it is a direct method of getting subsurface information.

REFERENCES

ACCESS/IUCN (2006) *An Overview of Climate Change and Adaptation in Tropical Mountain Ecosystems*. Prepared by African Collaborative Centre for Earth System Science (ACCESS). Authors: Daniel O. Olago, Eric O. Odada, Washington Ochola and Lydia Olaka, iii+11p, pp.2-3

Adiat, K.A.N., Olayanju, G.M., Omosuyi, G.O. and Ako, B.D. (2009) Electromagnetic profiling and electrical resistivity soundings in groundwater investigation of a typical basement complex, A case study of Oda town, southwestern Nigeria, *Ozean J. Social Sci*., **2**: 333-359.

Batte, A.G., Muwanga, A., Sigrist, P.W., and Owor, M. (2008) Vertical electrical sounding as an exploration technique to improve on the certainty of groundwater yield in the fractured crystalline basement aquifers of eastern Uganda, *Hydrogeology Journal*, **16**: 1683–1693.

Bobachev, A. (2002) IPI2win: A window software of an automatic interpretation of resistivity sounding data, *Moscow State University*.

Burger, H.R. (1992) *Exploration Geophysics of the Shallow Subsurface*, Prentice Hall, Englewood Cliffs, NJ: pp. 53-133.

Chorowicz, J. (1992) The role of Ancient Structures in the genesis and evolution of the East African Rift, *Bull. Soc. Geol. Fr*., **163 (3):** 217–227.

Chow, V., Maidment, D. and Mays, L. (1988) *Applied Hydrology*, 2nd Edition, Longman Group, UK.

Combe, A. D.(1950) *The Kaptumet River Asbestos Deposits, Western Kenya*, Unp. Report, Geol. Surv. Uganda, pp. 30-35.

Cooper, P. J. M. and Law, R. (1978) Enhanced soil temperature during very early growth and its association with maize development and yield in the Highlands of Kenya, *The Journal of Agricultural Science*, **91**: 569-577.

Dixey, F. (1948) The relation of main Peneplain of Central Africa to the sediments of Lower Miocene Age. *Quart. Journ. Geol*. Soc., **101**: 243-253.

Dobrin, M.B. and Savit, C.H. (1988) *Introduction to Geophysical Prospecting*, McGraw-Hill Inc., New York.

Domenico, S. N. (1977) Elastic properties of unconsolidated porous sand, *Reservoir Geophysics*, **42**: 1339-1349.

Driscoll, E. G. (1986) *Groundwater and Wells*, 2nd Edition, Johnson Division, St. Paul pp 1089.

Flathe, H. (1963) Five-layer master curvets for the hydrogeological interpretation of geoelectric

resistivity measurements in an aquifer, *Geophys. Prosp.*, **11**: 471–508.

Fetcher, C.W. (1988) *Applied Hydrogeology: Groundwater flow patterns in Homogenous Aquifers,* CBS Publishers and Distributers, London, pp. 215-222.

Fletcher, N.J.C. (1978) *Structures in Folded Rocks, An illustrated Guide Book to Structural Geology*, Institute of Geological Sciences, Reedprint Limited, London.

Fuchs, V.E. (1939) *The Geological History of Lake Rudolph Basin*, Phil. Trans. Royal Soc. London, Series B, **229**: 219-279.

Ghosh, D. P. (1971) Inverse filter coefficients for the computation of apparent resistivity standard curves for a horizontally stratified earth. *Geophysical Prospecting,* **19**: 769-775.

Gibson, A.B. (1954) *Geology of the Broderick Falls Area*, Ministry of Environment and Natural Resources, Mines & Geol Dept., Kenya, Report No. 26.

Glenday, V.G., Parkinson J. (1926) Geology of Suk Hills, *Quart. Journ. Geol. Soc.,* **83**: 586-614.

GOK & UNESCO (2012) Kenya Man and Biosphere National Committee, Government of Kenya. Kenya National Commission for UNESCO, National Report, 5 pp.

Grant, F.S. and West, G.F. (1965) *Interpretation Theory in Applied Geophysics*, McGraw Hill Inc., New York.

Greenhalgh, M. S. (2009) *DC Resistivity Modeling and Sensitivity Analysis in Anisotropic Media*, PhD thesis, Department of Physics, University of Australia.

Griffiths, D.H. and Barker, R. D. (1993) Two-dimensional resistivity imaging and modeling in areas of complex geology, *Jour. Appl. Geophysics*, **29**: 211-226.

Griffiths, D.H., and King, R.F. (1981) *Applied Geophysics for Geologists and Engineers*. Pergamon Press, England.

Hersir, P. G., and Bjornsson, A. (1991) *Geophysical Exploration for Geothermal Resources,Principles and Application: Geoelectrical properties of rocks*, UNU Geothermal Training Programme, Reykjavik, Iceland, Report No. **15**: 28-40.

Hess, D. (2010) *Physical Geography, A Landscape Appreciation*, Tenth Edition. Upper Saddle River, Prentice Hall.

Hetzel, R. and Strecker, R.M. (1993) Late Mozambique Belt structures in Western Kenya Colony and their influence on the evolution of Cenozoic Kenya Rift, *Journal of Strucural Geol*., **16(2):** 189-201.

Huddleston, A. (1946) *The Occurrence of Ground Water in Boreholes in Kenya Colony with Notes on the Geology of the Chief Formations*, Durham PhD thesis (with five plates and a geological map), Durham University.

Hugh, D.Y. and Rodger A.F., (1996) *Current, Resistance and Electromotive Force*, 9th Edition, University Physics, Addison Wesley Publishing Co. Inc., pp. 798-853.

Irshad, R.M., (1976) *Finite-Difference Resistivity Modelling for Arbitrarily Shaped Two Dimensional Structures*, Proceedings in the 44th Annual International S.E.G. Meeting,Dallas, November 12, 1974, Society of Exploration Geophysicists, **41**(1): 62-78.

Jones, M.J. (1985) The weathered zone aquifers of the Basement Complex Areas of Africa, *Quart. Journal Engineering Geol. London*, **18**: 34-46.

Kagai, K. K. (2011) Assessment of public perception, awareness and knowledge on genetically engineered food crops and their products in Trans-Nzoia County, Kenya, *Journal of Development in Sustainable Agriculture,* **6**: 164-180.

Keary P. and Brooks M. (1991) *An Introduction of Geophysical Prospecting*, Blackwell Scientific Publ., London.

Kipkorir, E.C., Raes D., Bargerei R. J., and Mugalavai E. M. (2007) Evaluation of two risk assessment methods for sowing maize in Kenya, *Agricultural and Forest Meteorology*, **144:** 193-199. DOI: 10.1016/j.agrformet.2007.02.008.

Kipkorir, J. L., and Towett, J. (2013) Towards ensuring a supply of sufficient and quality water in the Logam Escarpment and Kerio Valley in Marakwet District, Kenya, *International Journal of Humanities and Social Sciences*, **3(3):** 1-5

Kitutu M. G., Muwanga A., Poesen J., and Deckers J. A. (2009) Influence of soil properties on landslide occurrences in Bududa district, Eastern Uganda, *African Journal of Agricultural Research*, **4 (7)**: 611-620.

Knapen, A., Kitutu, M.G., Poesen, J. Breugelmans, W., Deckers, J. and Muwanga, A. (2006) Landslides in a densely populated county at the foot slopes of Mount Elgon, Uganda: Characteristics and causal factors, *Geomorphology*, **73**: 149–165.

Kuria, Z.N. (2013) Groundwater distribution and aquifer characteristics in Kenya, *Development in Earth surface processes,***16**: 83-107.

Larsen, S.T., Kamugasha, N. and Karani, I. (2008) Mid-term Review of Mt. Elgon Regional Ecosystem Conservation Programme (MERECP), *Norwegian University of Life Sciences*, Noragric Report No.**44**.

Logan, J. (1964) Estimating transmissivity from routine production tests of water wells, *Groundwater journal*, **2**: 35-37.

Loke, M.H. (2004) 2D and 3D electrical imaging survey, *Geotomo Software*, Malaysia.

Lowrie, W. (2007) *Fundamentals of Geophysics, Geoelectricity, Earths Age, Thermal and Electrical Properties, Geoelectricity*, Cambridge University Press, Second Edition, pp. 252-268.

Miller, J. L. (1956) *The Geology of Kitale-Cherangani Hills*, Report No. **35**, Geol. Survey of Kenya.

Moon, C. J., Whateley, G.E.M., and Evans, M.A. (2006) *Introduction to Mineral Exploration, Geophysical Methods, Resistivity*. Second Edition, Blackwell Publishing, pp. 136-138.

Mugagga, F. and Bunyinza, M. (2013) Land Tenure and soil conservation practices on the slopes of Mt. Elgon National Park, Eastern Uganda. *Journ. of Geography and Regional Planning*, **6 (7):** 4-8

Murray-Hughes, R. (1933) *Geological Successions, Tectonics and Economic Geology of the Western half of Kenya Colony*, Report No **3**, Geol. Surv. Kenya.

National Water Master Plan (1992) Ministry of Water and Irrigation

NEMA (2009) *Tran- Nzoia District Environmental Action Plan 2009-2013*. Nairobi, National Environment Management Authority. Retrieved 20th, September, 2014, from. http://www.nema.go.ke

Nilsson E. (1940) Ancient changes of Climate in British East Africa and Abyssinia, *Middelanden Fran Stockholms Hogskolass Geologiska Institut*, **50:** 4-18

Odong, O.P. (2013) Groundwater potential evaluation and aquifer characterization using resistivity method in Southern Obubra, Southeastern Nigeria, *International Journal of Environmental Sciences*, **4(1):** 96-104.

Overmereen, R.A. (1981) A combination of electrical resistivity, seismic refraction, and gravity measurements for groundwater exploration in Sudan, *Geophysics Journal*, **46**: 1304-1313.

Paransis, D. (1997) *Principles of Applied Geophysics*, Chapman and Hall, London Press, United Kingdom.

Petursson, J.G. (2006) Transboundary Biodiversity Management Challenges: The case of Mount Elgon, Uganda and Kenya, Phd Thesis.

Rannveig K. F. and Bernardas P. (2012) *Feasibility Study Report, Mt. Elgon Information Needs*.

Reynold, J.M. (1997) *An Introduction to Applied and Environmental Geophysics*. Wiley (Eds) Press, England.

Robinson, E.S. and Coruh, C. (1988) *Basic Exploration Geophysics*, John Wiley and Sons, NewYork pp. 43-57.

Rift Valley Water Services Board (2007) RVWSB Strategic Plan (2006-2015). GOK, Ministry of Water and Irrigation.

Searle, D.L. (1952) *Geology of the Area North-West of Kitale Township*, Ministry of Environment and Natural Resources, Mines & Geol Dept., Kenya, Report No. **19**.

Sombroek, W. G., Braun, H.M.H. Pouw Van Der, B.J.A. (1982) *Exploratory Soil Map and Agro-climatic Zone Map of Kenya*, Kenya Soil Survey, pp. 17-37.

Telford, W.M., Geldart, L.P. and Sheriff, R.E. (1990) *Applied Geophysics: Electrical properties of Minerals and Rocks*. 2nd Edition, Cambridge University Press, pp. 535-538.

Theis, C.V. (1935) The relation between the lowering of the piezometric surface and the rate and duration of discharge of a well using groundwater storage, Am. Geophys. Union Trans. **16**: 519-524.

Thiem, G. (1906) Hydrogeologic Methods, Gebhardt, Leipzig.

White, F. (1983) The Vegetation of Africa, UNESCO, Paris.

APPENDIX I: Electrical resistivity data

a)VES Data

VES 1
Elevation 1861 36N 0718915 UTM 0114252

MN/2	AB/2	Constant, K	Resistivity
0.5	1.6	7.26	89.33
0.5	2.0	11.8	101.74
0.5	2.5	18.8	124.50
0.5	3.2	31.4	147.18
0.5	4.0	49.5	167.33
0.5	5.0	77.8	196.91
0.5	6.3	124	217.42
0.5	8.0	200	222.76
0.5	10.0	313	222.02
0.5	13.0	530	184.04
0.5	16.0	803	144.77
0.5	20.0	1260	101.37
0.5	25.0	1960	65.31
0.5	32.0	3220	41.97
10	**32.0**	**145**	**45.42**
10	40.0	236	39.14
10	50.0	377	40.81
10	63.0	608	48.38
10	80.0	990	58.73
10	100.0	1560	69.61
10	130.0	2640	85.1
10	160.0	4010	99.34
10	200.0	6270	123.69
10	250.0	9800	150.86
25	**250.0**	**3890**	**168.67**
25	320.0	6370	226.06
25	400.0	10000	281.65
25	500	15700	341.85

VES 2
Elevation 1880 36N 0718915 UTM 0114252

MN/2	AB/2	Constant, K	Resistivity
0.5	1.6	7.26	108.85
0.5	2	11.8	119.73
0.5	2.5	18.8	131.40
0.5	3.2	31.4	117.91
0.5	4.0	49.5	119.66
0.5	5.0	77.8	107.97
0.5	6.3	124	96.83
0.5	8.0	200	82.43
0.5	10.0	313	62.59
0.5	13.0	530	45.64
0.5	16.0	803	40.11
0.5	20.0	1260	41.95
0.5	25.0	1960	48.92
0.5	32.0	3220	56.59
10	**32.0**	**145**	**48.21**
10	40.0	236	56.58
10	50.0	377	64.89
10	63.0	608	72.65
10	80.0	990	77.47
10	100.0	1560	81.51
10	130.0	2640	73.01
10	160.0	4010	68.03
10	200.0	6270	66.53
10	250.0	9800	65.10
25	**250.0**	**3890**	**58.80**
25	320.0	6370	69.90
25	400.0	10000	87.72
25	500	15700	106.23

VES 3
Elevation 2147 36N 0718915 UTM 0114252
Mt. Elgon National Park's Gate

MN/2	AB/2	Constant, K	Resistivity
0.5	1.6	7.26	104.50
0.5	2	11.8	89.77
0.5	2.5	18.8	101.92
0.5	3.2	31.4	100.71
0.5	4.0	49.5	94.00
0.5	5.0	77.8	83.62
0.5	6.3	124	69.70
0.5	8.0	200	61.16
0.5	10.0	313	56.14
0.5	13.0	530	56.33
0.5	16.0	803	57.89
0.5	20.0	1260	60.72
0.5	25.0	1960	61.75
0.5	32.0	3220	64.21
10	**32.0**	**145**	**63.39**
10	40.0	236	26.90
10	50.0	377	66.10
10	63.0	608	72.86
10	80.0	990	76.43
10	100.0	1560	77.39
10	130.0	2640	83.49
10	160.0	4010	84.81
10	200.0	6270	91.96
10	250.0	9800	90.91
25	**250.0**	**3890**	**89.48**
25	320.0	6370	111.14
25	400.0	10000	120.74
25	500	15700	123.31

VES 4
Elevation 1938m 36N 0703823 UTM 0126247
Molem Area, Chepchoina Ward, Endebess.

MN/2	AB/2	Constant, K	Resistivity
0.5	1.6	7.26	78.10
0.5	2	11.8	63.11
0.5	2.5	18.8	55.10
0.5	3.2	31.4	43.77
0.5	4.0	49.5	33.76
0.5	5.0	77.8	28.44
0.5	6.3	124	23.31
0.5	8.0	200	22.78
0.5	10.0	313	25.01
0.5	13.0	530	29.29
0.5	16.0	803	34.52
0.5	20.0	1260	42.35
0.5	25.0	1960	49.77
0.5	32.0	3220	55.83
10	**32.0**	**145**	**49.32**
10	40.0	236	52.05
10	50.0	377	54.62
10	63.0	608	60.73
10	80.0	990	67.24
10	100.0	1560	71.07
10	130.0	2640	67.47
10	160.0	4010	65.56
10	200.0	6270	65.44
10	250.0	9800	61.90
25	**250.0**	**3890**	**66.38**
25	320.0	6370	79.58
25	400.0	10000	80.82
25	500	15700	69.60

VES 21
Elevation 2703m 36N 0710695 UTM 116446
Endebess Sub County

MN/2	AB/2	Constant, K	Resistivity
0.5	1.6	7.26	363.41
0.5	2	11.8	305.23
0.5	2.5	18.8	226.69
0.5	3.2	31.4	158.01
0.5	4.0	49.5	110.94
0.5	5.0	77.8	71.07
0.5	6.3	124	46.00
0.5	8.0	200	28.77
0.5	10.0	313	25.64
0.5	13.0	530	30.06
0.5	16.0	803	33.49
0.5	20.0	1260	38.89
0.5	25.0	1960	45.30
0.5	32.0	3220	50.83
10	**32.0**	**145**	**42.51**
10	40.0	236	52.02
10	50.0	377	61.11
10	63.0	608	62.84
10	80.0	990	64.90
10	100.0	1560	72.16
10	130.0	2640	61.40
10	160.0	4010	53.94
10	200.0	6270	50.78
10	250.0	9800	63.49

VES 22
Elevation 1880m 36N 717965 UTM 0117566
Kapsitwet, Endebess Sub County

MN/2	AB/2	Constant, K	Resistivity
0.5	1.6	7.26	1663.12
0.5	2	11.8	1508.97
0.5	2.5	18.8	1213.44
0.5	3.2	31.4	1076.02
0.5	4.0	49.5	1023.88
0.5	5.0	77.8	1022.4
0.5	6.3	124	733.43
0.5	8.0	200	547.86
0.5	10.0	313	319.72
0.5	13.0	530	147.96
0.5	16.0	803	99.53
0.5	20.0	1260	65.38
0.5	25.0	1960	60.12
0.5	32.0	3220	56.40
10	**32.0**	**145**	**57.49**
10	40.0	236	59.06
10	50.0	377	56.02
10	63.0	608	55.79
10	80.0	990	47.90
10	100.0	1560	44.45
10	130.0	2640	44.72
10	160.0	4010	39.21
10	200.0	6270	49.04
10	250.0	9800	64.94

b) RESISTIVITY CURVES AND MODELS

VES1

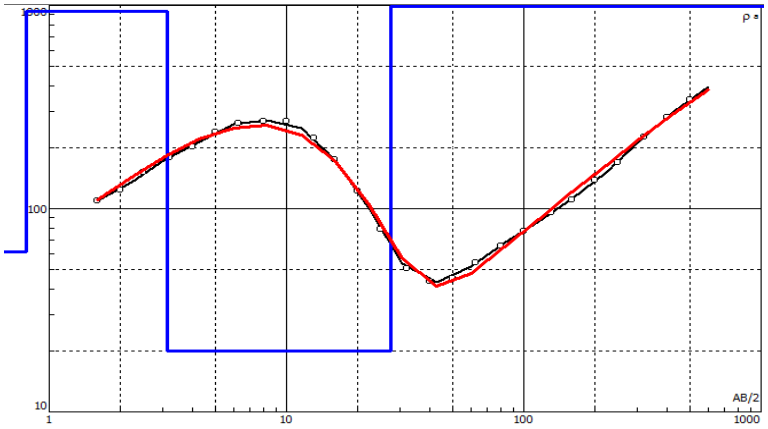

N	ρ	h	d	Alt
1	61.2	0.8	0.8	-0.8
2	933	2.33	3.13	-3.13
3	19.9	24.4	27.5	-27.53
4	1724			

VES2

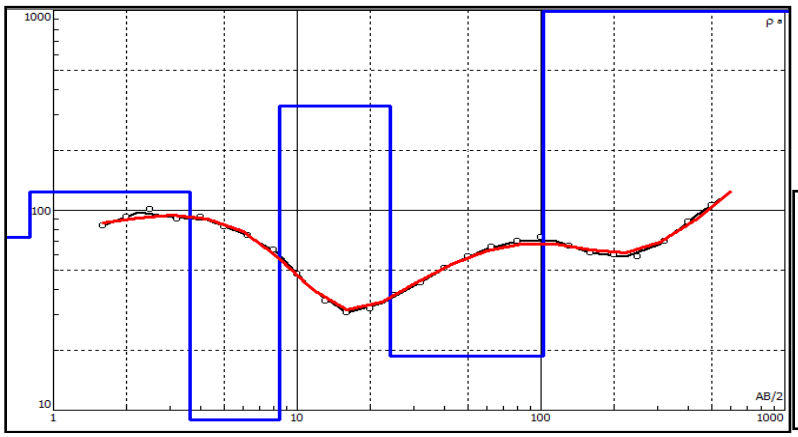

N	ρ	h	d	Alt
1	73.3	0.8	0.8	-0.8
2	124	2.84	3.64	-3.64
3	8.97	4.78	8.42	-8.42
4	334	15.6	24	-24.02
5	18.7	77.8	102	-101.8
6	7413			

VES3

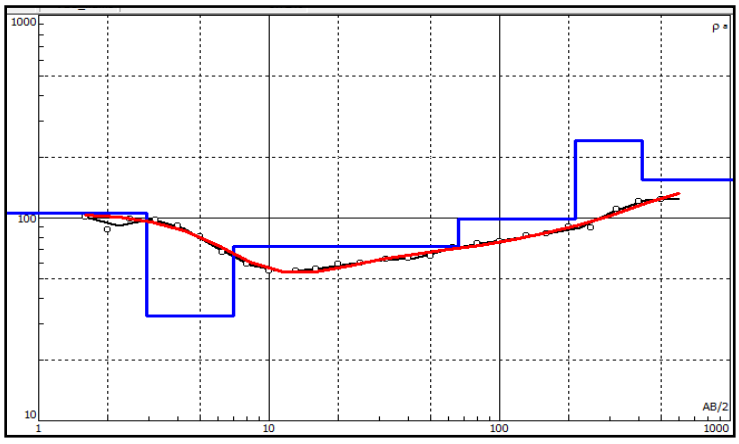

RMS=3.72%

N	ρ	h	d	Alt
1	106	2.94	2.94	-2.942
2	32.9	4.06	7.01	-7.005
3	72.4	59.3	66.3	-66.26
4	98.9	147	213	-213.1
5	241	202	415	-415.3
6	154			

VES 4

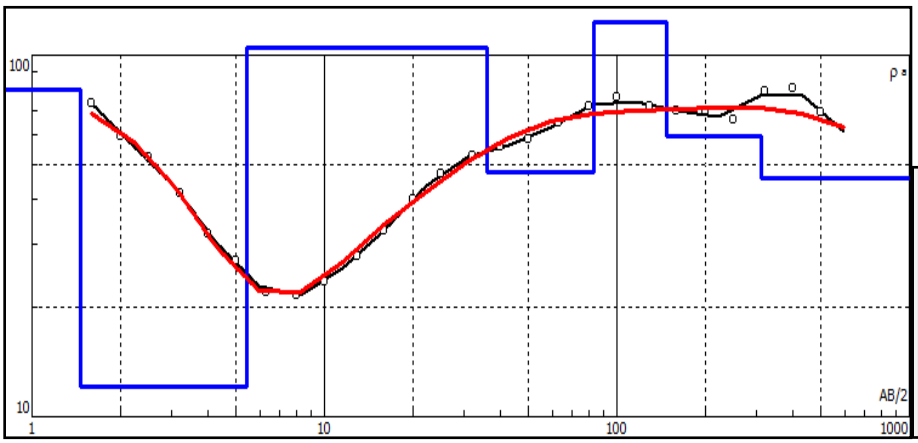

RMS=5.1%

N	ρ	h	d	Alt
1	80.3	1.47	1.47	-1.47
2	12.1	3.96	5.43	-5.426
3	105	30.6	36	-35.98
4	47.5	47.4	83.4	-83.4
5	123	64.6	148	-148
6	59.7	164	312	-311.7
7	45.7			

VES20

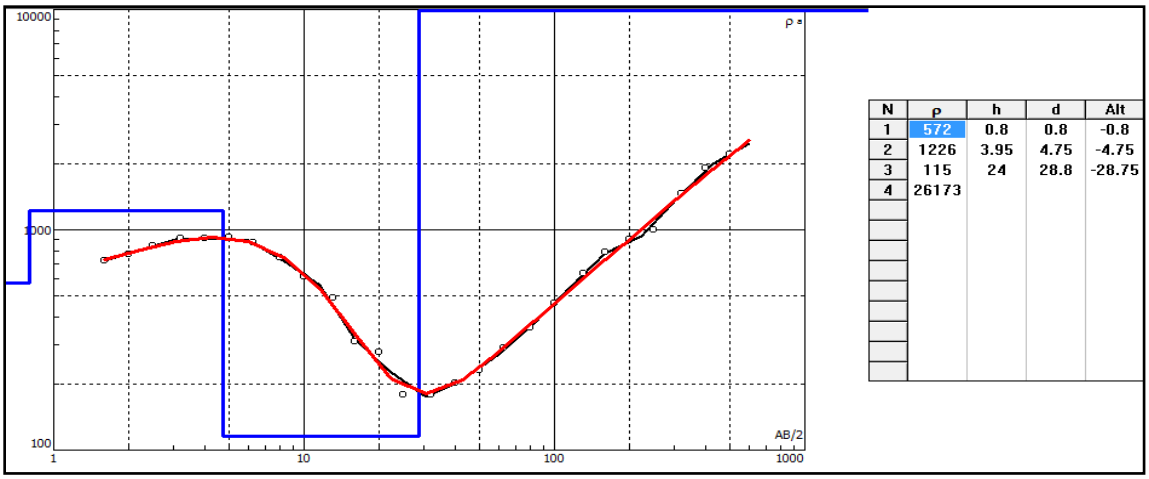

N	ρ	h	d	Alt
1	572	0.8	0.8	-0.8
2	1226	3.95	4.75	-4.75
3	115	24	28.8	-28.75
4	26173			

VES23

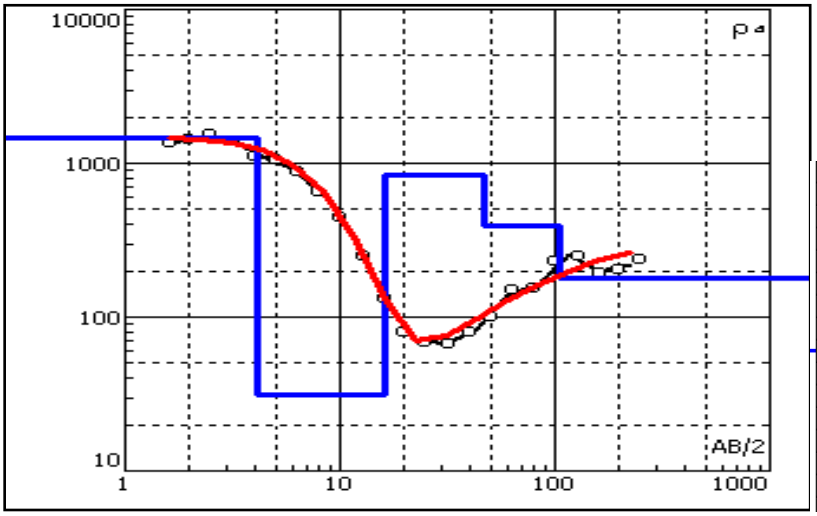

N	ρ	h	d	Alt
1	1465	4.12	4.12	-4.12
2	31.4	12	16.1	-16.12
3	831	30.4	46.5	-46.52
4	392	59.7	106	-106.2
5	178			

APPENDIX II: HEP DATA

	PROFILE 1:ANDESEN/MT.ELGON FLOWERS		
EASTING	**NORTHNG**	**ELEVATION**	**RESISTIVITY**
698662	133160	1992	25.58
698695	133171	1992	30.65
698725	133183	1991	30.11
698756	133194	1991	27.81
698787	133207	1990	28.36
698818	133219	1989	29.53
698848	133231	1990	29.59
698878	133245	1989	28.54
698909	133256	1988	30.15
698939	133270	1987	29.19
698968	133280	1987	27.12
698999	133290	1986	49.65
699029	133304	1985	67.36
699061	133315	1985	72.17
699091	133328	1984	63.9
699124	133336	1984	77.32
699154	133342	1984	75.86
699188	133353	1984	69.97
699220	133356	1983	75.6
699252	133361	1984	69.97
699284	133366	1984	75.6
699321	133371	1983	65.16
699351	133369	1983	57.89
699384	133367	1982	84.58
699417	133359	1982	110.21
699447	133351	1983	95.23
699481	133345	1983	102.1
699514	133342	1982	116.8
699546	133337	1982	103.6
699577	133326	1981	137.37
699609	133320	1982	147.8
699641	133313	1982	118.38
699671	133306	1980	109.49
699701	133293	1980	111.93
699732	133280	1979	94.23
699757	133259	1978	80.06
699786	133239	1977	92.44

699809	133216	1976	57.74
699839	133200	1976	67.56
699865	133184	1975	80.9
699896	133166	1974	79.13
699925	133155	1975	63.43
699954	133140	1974	66.6
699984	133127	1972	64.16
700017	133112	1970	62.51
700045	133098	1968	52.45
700072	133083	1964	36.98
700103	133070	1964	29.32
700136	133063	1962	28.16
700168	133060	1961	27.82
700200	133064	1960	25.73
700235	133068	1960	24.71
700268	133071	1961	26.96
700297	133075	1959	27.04
700332	133077	1959	25.5
700365	133084	1959	26.23
700399	133088	1958	29.13
700430	133091	1958	28.5
700467	133088	1957	28.8
700500	133091	1956	29.2
700530	133094	1956	28.48
700561	133096	1955	30.61
700594	133096	1955	33.92
700629	133097	1954	33.17
700664	133098	1953	33.82
700694	133099	1953	35.65
700724	133099	1952	38.05
700759	133098	1951	37.48
700791	133098	1950	35.38
700827	133096	1950	43.23

PROFILE 2:MUUNGANO AREA,NABISWA WARD

EASTING	NORTHING	ELEVATION	RESISTIVITY
708348	95561	1799	370.15
708380	95576	1797	378.77
708409	95590	1796	368.07

708436	95602	1794	336.75
708469	95621	1793	315.69
708496	95635	1791	330.25
708529	95649	1789	303.29
708558	95666	1788	334.02
708588	95683	1787	388.83
708616	95697	1784	441.63
708646	95713	1783	469.11
708676	95727	1781	458.22
708705	95742	1780	486.66
708735	95757	1778	460.84
708765	95773	1777	438.75
708796	95789	1775	461.47
708826	95804	1774	480.89
708854	95818	1772	363.81
708885	95831	1770	307
708915	95844	1769	318.13
708945	95860	1767	354.79
708974	95874	1766	359.86
709005	95888	1764	356.73
709035	95906	1763	336.3
709065	95920	1761	371.22
709094	95935	1760	381.12
709123	95951	1759	365.9
709152	95966	1756	410.61
709183	95982	1753	415.46
709212	95995	1752	366.63
709242	96012	1750	359.01
709273	96028	1749	391.45
709301	96043	1749	391.82
709330	96058	1748	332.95
709363	96073	1747	282.02
709390	96088	1746	262.56
709421	96104	1745	260.55
709451	96117	1744	242.19
709482	96132	1743	214.27
709511	96145	1742	192.63
709543	96159	1741	161.74
709572	96177	1740	153.68
709604	96188	1739	153.06
709633	96202	1737	228.27

709665	96216	1736	320.7
709692	96231	1738	301.48
709718	96252	1741	273.31
709746	96267	1742	341.64
709777	96284	1744	489.47
709805	96299	1745	496.43
709835	96313	1747	475.33
709865	96330	1750	480.23
709892	96348	1752	442.24
709922	96364	1754	440.19
709952	96378	1756	443.63
709982	96395	1758	389.17
710011	96412	1760	361.68
710043	96426	1760	322.82
710068	96444	1764	267.75
710092	96463	1765	257.03

PROFILE 3:SABWANI ADC AREA

EASTING	NORTHING	ELAVATION	RESISTIVITY
710697	116467	1888	82.12
710732	116477	1888	72.42
710764	116484	1888	71.02
710797	116488	1889	82.71
710829	116493	1886	87.58
710862	116498	1887	89.17
710894	116504	1888	79.67
710927	116509	1888	76.88
710958	116514	1888	79.19
710992	116519	1886	82.74
711026	116525	1888	78.44
711059	116531	1886	63.05
711094	116536	1888	66.03
711125	116542	1888	70.78
711156	116547	1888	69.19
711190	116553	1890	57.77
711223	116556	1890	49.07
711257	116564	1890	48.05
711290	116569	1890	44.71
711322	116574	1890	58.17
711356	116579	1890	55.71

711389	116584	1890	55.64
711421	116589	1890	58.26
711454	116596	1889	55.64
711488	116600	1890	58.26
711521	116607	1890	55.64
711552	116611	1890	53.21
711587	116617	1890	51.61
711618	116624	1890	47.15
711650	116627	1890	46.68
711685	116636	1889	47.37
711715	116639	1889	45.45
711751	116646	1888	42.51
711784	116652	1888	42.4
711817	116655	1888	41.72
711849	116664	1887	40.68
711881	116666	1887	39.67
711915	116673	1887	41.01
711948	116681	1887	36.6
711984	116686	1886	33.87
712015	116688	1885	34.77
712047	116694	1885	50.23
712079	116698	1885	31.32
712112	116703	1885	30.2
712145	116709	1885	27.62
712178	116717	1884	24.23
712220	116721	1884	23.84
712243	116723	1883	25.01
712278	116735	1883	35.44
712310	116737	1881	35.99

APPENDIX III: EXISTING BOREHOLE DATA

CODE/ID	ALT(m)	TD (m)	WSL(m)	WRL(m)	Q(m2/h)	PIEZO(m)	C(m2/day)	T(m2/day)
C-595	1850	40	33	12	2.28	1838	2.6057	3.1790
C-604	1840	88	76	3	3.12	1837	1.0258	1.2514
C-664	1900	145	79	9	1.38	1891	0.4731	0.5772
C-1286	552	40	27	20	1.92	532	6.5829	8.0311
C-1288	536	55	37	30	0.24	506	0.8229	1.0039
C-1289	552	37	29	11	0.9	541	1.2000	1.4640
C-1349	1820	40	26	23	1.92	1797	15.360	18.739
C-1351	1730	35	25	12	0	1718	0	0
C-1730	579	79	70	23	0.54	556	0.2757	0.3364

C-1740	532	46	35	9	0.9	523	0.8308	1.0135
C-1783	549	40	34	8	11.34	541	10.4677	12.77
C-1814	1900	110	109	55	0.66	1845	0.2933	0.3579
C-1825	1951	49	26	15	1.14	1936	2.4873	3.0345
C-1860	1890	201	24	9	0.12	1881	0.1920	0.2342
C-1871	1880	83	0	0	0.06	1880	-	-
C-1928	549	79	76	32	3.6	517	1.9636	2.3956
C-1964	1880	55	52	27	0.24	1853	0.2304	0.2811
C-1965	1960	37	0	0	0	1960	-	-
C-1966	1880	59	0	0	0	1880	-	-
C-1968	1960	72	0	0	0	1960	-	-
C-2016	2180	32	0	0	0	2180	-	-
C-2018	555	70	69	12	1.8	543	0.7579	0.9246
C-2102	561	26	23	15	0.66	546	1.9800	2.4156
C-2103	567	21	17	14	1.56	553	12.4800	15.226
C-2106	579	41	31	27	0.66	552	3.9600	4.8312
C-2107	506	25	18	9	0.72	497	1.92	2.3424
C-2195	1900	171	24	18	0	1882	0	0
C-2228	1840	15	9	8	2.76	1832	66.240	80.81
C-2229	567	26	18	18	0.84	549	-	-
C-2230	567	36	0	0	0	567	-	-
C-2723	1707	38	30	18	1.08	1689	2.1600	2.6352
C-3063	536	61	46	12	1.62	524	1.1435	1.3951
C-3134	613	195	35	0	0.12	613	0.0823	0.1004
C-5216	1200	76	72	35	1.68	1165	1.0897	1.3295
C-5217	1200	84	80	24	3.6	1176	1.5429	1.8822
C-5230	1500	69	48	31	0.72	1469	1.0164	1.2401
C-6247	1495	90	57	0	0	1495	0	0
C-7075	1565	37	16	7	15	1558	40.00	48.80
C-7806	1447	0	0	0	0	1447	-	-
C-10669	1885	80	40	10.4	0	1874.6	0	0
C-10710	1465	100	50	16.8	0.43	1448.2	0.3108	0.3792
C-10976	1840	84	76	16.6	3	1823.4	1.2121	1.4788
C-11239	1880	80	56	9.7	1.2	1870.3	0.6220	0.7589
C-11324	2100	87.4	68	24.4	5.5	2075.6	3.0275	3.6936
C-11326	1848	85	60	14.5	4.6	1833.5	2.4264	2.9602
C-11338	1840	66	48	21	0	1819	0	0
C-11347	1860	65	0	0	0	1860	-	-
C-12448	1370	54	32	7.1	3.9	1362.9	3.7590	4.5860